

**A LOAD-DEFLECTION STUDY OF FIBER REINFORCED
PLASTICS AS REINFORCEMENT IN CONCRETE BRIDGE
DECKS**

by

Curtis Barton Boyd

Thesis submitted to the Faculty of the

Virginia Polytechnic Institute and State University

in partial fulfillment of the requirements for the degree of

MASTER OF SCIENCE

in

Civil Engineering

APPROVED:

Richard M. Barker, Chairman

Richard E. Weyers

Thomas M. Murray

May, 1997

Blacksburg, Virginia

Keywords: bridge, bridge design, fiber reinforced plastics, FRP, reinforced concrete

A LOAD-DEFLECTION STUDY OF FIBER REINFORCED PLASTICS AS REINFORCEMENT IN CONCRETE BRIDGE DECKS

by

Curtis Barton Boyd

Richard M. Barker, Chairman

Civil Engineering

ABSTRACT

Approximately fifty percent of the bridges in the United States are considered deficient. The deterioration of the concrete components is a leading cause of the problem. The deterioration of concrete bridge decks is due primarily to corrosion of the reinforcing steel in the concrete. A promising solution to the problem is the use of fiber reinforced plastics (FRP) as a replacement for reinforcing steel. The use of FRP as reinforcement has the following advantages of lightweight, high tensile strength, corrosion resistance, flexibility, and electromagnetic resistance. This paper looks at the use of FRP as reinforcement in concrete beams and compares the information from deflection measurements of different configurations. Also, a material cost comparison is made to determine the cost of using the FRP reinforcement over standard steel reinforcement. Concrete bridge deck systems are designed using steel and fiber-reinforced plastics and allowable stress and load resistance factor methods. Recommendations for further study and uses of FRP are made.

ACKNOWLEDGEMENTS

I would like to thank Dr. Richard Barker and Dr. Richard Weyers for providing the focus of this study. In addition, I would like to thank Dr. Thomas Murray for serving on my thesis committee. Also, I thank the entire committee for providing me the time to complete this thesis.

I give special thanks to the other structures students, Joe Howard, John Harmis, and Debra Vazquez for their assistance in the equipment setup and testing. All the structure graduates at the lab that provided assistance in the fabrication of the concrete test beams, and lab technicians, Brett Farmer and Dennis Huffman for their aid are hereby noted.

An extra thanks goes to the Pauley family, Dana, Sonora, Stephen, and Christopher, for their friendship and support during some rough times.

I would like to acknowledge the Virginia Department of Transportation (VDOT) for providing me the opportunity, support and resources to attend the graduate program.

And thanks to my parents and family for their devotion, support, encouragement and love for without, none of this would have been possible.

TABLE OF CONTENTS

ABSTRACT	ii
ACKNOWLEDGEMENTS	iii
TABLE OF CONTENTS	iv
LIST OF FIGURES	ix
LIST OF TABLES	xii
NOTATION	xiii
CHAPTER 1	
INTRODUCTION	1
1.1 Background	1
1.2 Objectives	4
1.3 Scope of Study	4
CHAPTER 2	
LITERATURE REVIEW	6
2.1 Introduction	6
2.2 Mechanical Properties	7
2.3 Material Properties	8
2.4 Experimental Results	9
2.5 Summary	10

CHAPTER 3

MATERIAL PROPERTIES	13
3.1 Introduction	13
3.2 Fiber Reinforced Plastic Reinforcement	14
3.2.1 FRP Rebar	14
3.3.3 Duradek Fiberglass Grating	16
3.3 Steel Reinforcement	18
3.4 Polypropylene Fiber	21
3.5 Carpet Fiber	22
3.6 Concrete	23
3.7 Cost Comparison	24

CHAPTER 4

EXPERIMENTAL SETUP	28
4.1 Introduction	28
4.2 Beam Configuration	28
4.2.1 Formwork	28
4.2.2 Beam Reinforcement Setup	31
4.2.2.1 Control Beams	32
4.2.2.2 FRP Bars	33
4.2.2.3 FRP Grids	33
4.2.2.4 Fibers	33
4.3 Beam Setup	35

CHAPTER 5

EXPERIMENTAL RESULTS	39
5.1 Introduction	39
5.2 Crack Patterns	39
5.2.1 TD Series	40
5.2.2 KS Series	41
5.2.3 KD Series	43
5.2.4 DK Series	44
5.2.5 NS Series	45
5.2.6 FC Series	46
5.2.7 CC Series	47
5.3 Load-Deflection	48
5.3.1 TD Series	55
5.3.2 KS Series	57
5.3.3 KD Series	59
5.3.4 DK Series	61
5.3.5 NS Series	63
5.3.6 FC Series	65
5.3.7 CC Series	67

CHAPTER 6

DESIGN OF BRIDGE DECKS	76
6.1 Introduction	76

6.2 Design of a Bridge Deck	76
6.2.1 Steel Reinforcement	77
6.2.1.1 Allowable Stress Design Method (ASD)	77
6.2.1.2 Load Resistance Factor Design Method (LRFD)	91
6.2.2 FRP Reinforcement	94
6.2.1.1 Allowable Stress Design Method (ASD)	94
6.2.1.2 Load Resistance Factor Design Method (LRFD)	97
6.3 Comparison of Designs	101
CHAPTER 7	
CONCLUSIONS AND RECOMMENDATIONS	103
7.1 Conclusions	103
7.2 Recommendations	106
7.2.1 General Recommendations	106
7.2.2 Specific Recommendations	107
REFERENCES	110
APPENDICES	
RECORDED LOAD-DEFLECTIONS	115
A.1 Beam TD1	115
A.2 Beam TD2	116
A.3 Beam TD3	117
A.4 Beam KS1	118
A.5 Beam KS2	119

A.6 Beam KD1	120
A.7 Beam KD2	121
A.8 Beam DK1	122
A.9 Beam DK2	123
A.10 Beam NS1	124
A.11 Beam NS2	125
A.12 Beam FC1	126
A.13 Beam FC2	127
A.14 Beam CC1	128
A.15 Beam CC2	129
VITA	130

LIST OF FIGURES

Figure 1.1 Bridge Deck Reinforcement Layout – a) VDOT typical layout, b) alternative VDOT layout, and c) proposed FRP layout.	3
Figure 3.1 Reinforcement bars used in this study. a) Kodiak #3 FRP rebar, b) Duradek I-6000 grid, c) non-coated steel reinforcement bar, and d) epoxy-coated steel reinforcement bar.	13
Figure 3.2 Stress-Strain curve for Non-Epoxy Coated Reinforcement.	20
Figure 3.3 Stress-Strain curve for Epoxy Coated Reinforcement.	21
Figure 4.1 Photo showing forms for the beams ready for concrete.	29
Figure 4.2 Photo showing three forms for beams, NS, TD, and KD series of beams.	30
Figure 4.3 Photo showing three forms for beams, KS, and DK series of beams.	30
Figure 4.4 Cross Section of Beams.	34
Figure 4.5 Side view of different beam configurations.	35
Figure 4.6 Test setup with beam in position.	36
Figure 4.7 Beam load testing setup.	37
Figure 5.1 Schematic of crack patterns in the TD beam series.	41
Figure 5.2 Schematic of crack patterns in the KS beam series.	42
Figure 5.3 Schematic of crack patterns in the KD beam series.	43
Figure 5.4 Schematic of crack patterns in the DK beam series.	44

Figure 5.5 Schematic of crack patterns in the NS beam series.	45
Figure 5.6 Schematic of crack patterns in the FC beam series.	46
Figure 5.7 Schematic of crack patterns in the CC beam series.	47
Figure 5.8 Typical Cyclic Load-Deflection Diagram.	51
Figure 5.9 Load versus deflection for beams with top reinforcement, TD, KS, KD, and DK.	53
Figure 5.10 Load versus deflection for control beams and beams without top reinforcement, TD, NS, FC, and CC.	54
Figure 5.11.1 Chart of average and predicted load-deflection values for the minimum and maximum applied loads at each cycle for the TD beams.	56
Figure 5.11.2 Chart of average load-deflection values for the minimum and maximum applied loads at each cycle for the KS beams.	58
Figure 5.11.3 Chart of average load-deflection values for the minimum and maximum applied loads at each cycle for the KD beams.	60
Figure 5.11.4 Chart of average load-deflection values for the minimum and maximum applied loads at each cycle for the DK beams.	62
Figure 5.11.5 Chart of average load-deflection values for the minimum and maximum applied loads at each cycle for	

the NS beams.	64
Figure 5.11.6 Chart of average load-deflection values for the minimum and maximum applied loads at each cycle for the FC beams.	66
Figure 5.11.7 Chart of average load-deflection values for the minimum and maximum applied loads at each cycle for the CC beams.	68
Figure 5.12.1 Load cycle 1 deflection of all beams.	69
Figure 5.12.2 Load cycle 2 deflection of all beams.	70
Figure 5.12.3 Load cycle 3 deflection of all beams.	71
Figure 5.12.4 Load cycle 4 deflection of all beams.	72
Figure 5.12.5 Load cycle 5 deflection of all beams.	73
Figure 5.12.6 Load cycle 6 deflection of all beams.	74
Figure 5.12.7 Load cycle 7 deflection of all beams.	75
Figure 6.1 Proposed transverse section of bridge design.	77
Figure 6.2 Section of deck design a) over support and b) at midspan.	81
Figure 6.3 Stress diagram for a) negative and b) positive moment region.	84

LIST OF TABLES

Table 3.1 FRP Reinforcement Properties.	16
Table 3.2 Properties of EXTREN Series Fiberglass.	17
Table 3.3 Steel Reinforcement Properties.	19
Table 3.4 VDOT A4 Post and Rail Concrete Mix.	23
Table 3.5 Properties of Concrete in Test Beams.	24
Table 3.6 Cost Comparison of Reinforcement Material.	25
Table 3.7 Cost Comparison of Beams.	27
Table 4.1 Reinforcement Layout.	32
Table 4.2 Cyclic tests load steps.	38
Table 5.1 Non-Load Related Terms for Equations.	50
Table 5.2 Maximum Load Capacity and Percentage of Applied Load.	50
Table 6.1 Comparison of Concrete Bridge Design Methods.	102

NOTATION

A = area

A_b = area of reinforcing bar.

A_{FRP} = area of FRP bar.

A_s = area of steel reinforcement.

a = depth of equivalent rectangular stress block.

b = width of beam.

C_{FRP} = compression strength of FRP reinforcement.

C_s = compression strength of steel reinforcement.

d = distance from compression surface to centroid of tension reinforcement.

d' = distance from compression surface to closest layer of reinforcement.

E = modulus of elasticity

E_c = concrete modulus of elasticity.

E_s = steel modulus of elasticity.

E_{FRP} = FRP modulus of elasticity.

f'_c = compressive strength of concrete.

f_c = allowable compressive strength of concrete.

f_{FRP} = stress in FRP reinforcement.

f_r = modulus of rupture.

f_{ult} = ultimate stress in reinforcement.

f_y = yield strength of reinforcement.

I = moment of inertia.

I_e = effective moment of inertia.

I_{cr} = cracked moment of inertia.

I_{gt} = moment of inertia, transformed section.

j, k = design constants.

M = moment in beam.

M_a = applied moment.

M_{cr} = moment causing first cracking.

M_D = dead load moment.

M_{LL+I} = live load plus impact moment.

M_n = nominal moment capacity of a section.

M_T = total moment.

M_u = Ultimate moment capacity of a section.

P = applied load.

P_{cr} = load which causes first cracking.

P_u = ultimate load.

S = effective span length.

T_{FRP} = tension strength of FRP reinforcement.

T_s = tension strength of steel reinforcement at d .

T'_s = tension strength of steel reinforcement at d' .

t_s = thickness of deck slab.

y_t = distance from top of section.

Δ_{\max} = maximum deflection.

Δ_{LL+I} = live load deflection.

Δ_D = dead load deflection.

Δ_T = total deflection.

Δ_M = deflection due to moment.

ρ = steel ratio due to bottom (tensile) reinforcement.

ρ' = steel ratio due to top (compressive) reinforcement.

CHAPTER 1

INTRODUCTION

1.1 BACKGROUND

In the United States, there are somewhere between 560,000 and 600,000 highway bridges. Bridges comprise a portion of the infrastructure that has been reported in need of rehabilitation. Approximately forty percent of these structures require work due to structural deficiency.

Bridges with steel-reinforced concrete decks represent a large portion of the structures that are disintegrating. A common cause for this breakdown is that the steel reinforcement used to strengthen the flexural capacity of the structures is susceptible to corrosion. Reinforcing steel corrodes when contact is made with humid or salty environments. When steel corrodes, the rust by-products expand and create tensile forces in the concrete. As the concrete reaches its limit in tension it begins to crack and spall. This creates an environment for the corrosion to propagate even further (Bedard, 1992).

The deterioration of concrete bridges, due primarily to corrosion of the reinforcing steel in the concrete, is a major concern today (Khalifa, 1993). The costs to rehabilitate and repair the bridges in the United States are estimated at nearly fifty billion dollars. The primary cause of the deterioration is the corrosive action of steel in concrete due to deicing chemicals and harsh saltwater environment (Bedard, 1992).

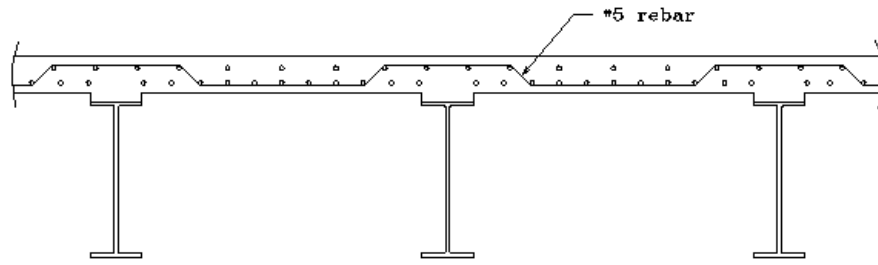
Epoxy-coated steel reinforcement was once believed to be a solution. It has not worked as well as expected. Additional methods to extend the longevity or to provide protections for

bridges are to apply sealers, to increase cover depth, to increase concrete density, and to use additives to retard the chemical process (Bedard, 1992).

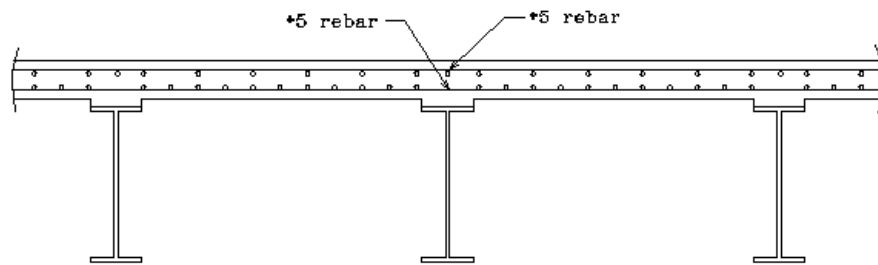
A promising solution to the problem is the use of fiber reinforced plastics (FRP) as a replacement for reinforcing steel. FRP is composed of high strength fibers bonded in a polymer matrix. FRP can be made of carbon, aramid, or glass fibers. The use of FRP as reinforcement has the advantages of light weight, high tensile strength, corrosion resistance, flexibility, and electromagnetic resistance. The disadvantages of FRP are high cost, low modulus of elasticity, low failure strain, difficult anchorage methods, low bond to concrete, and ultraviolet light sensitivity (Khalifa, 1993).

John Allen (ENR, 1994) has proposed the theory that the top mat of reinforcement is not needed. Due to deflection of the beam, the negative moment is not as great as once believed. If Allen's theory of no top reinforcement required for strength is adhered, then any top reinforcement would be primarily for temperature and shrinkage control. In a bridge structure, replacing only the top layer of reinforcing steel with FRP provides approximately the same strength as the steel; while at the same time provides for protection against corrosion effects. The FRP also provides for shrinkage and temperature control. The bottom mat of steel reinforcement provides the stiffness and strength required.

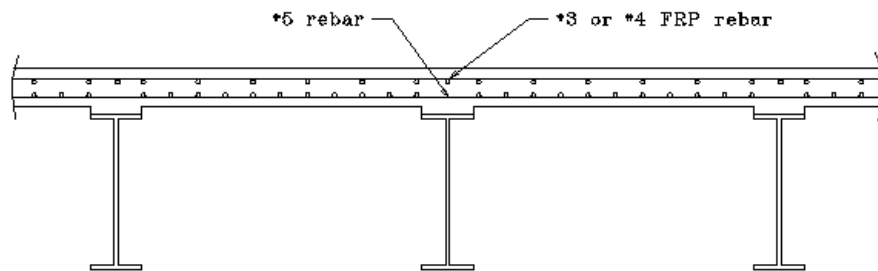
In Virginia, the current practice is to design bent bar reinforcement over the beams. An alternative design is to allow straight reinforcement to be substituted at no additional cost. Figure 1.1 shows the current reinforcement layout in use in Virginia. Also, the figure presents a proposed FRP reinforcement layout.



a) Typical VDOT deck reinforcement layout



b) Typical VDOT alternative deck reinforcement layout



c) Proposed FRP deck reinforcement layout

Figure 1.1 Bridge Deck Reinforcement Layout -- a) VDOT typical layout, b) alternative VDOT layout, and c) proposed FRP layout.

Projects that have used FRP are bridges in Germany, Japan, China, and the United States (Bedard, 1992). These bridges have been designed for pedestrian and highway traffic. Additional projects are in the process of being designed and awaiting approval. A short-span bridge with FRP beams and timber decking is planned for a site near Virginia Tech and Blacksburg, Virginia.

1.2 OBJECTIVES

The focus of this study is to determine the behavior of fiberglass-reinforced plastic reinforcement for possible use in concrete bridge decks.

The types of FRP materials used were recommended from previous work of Peter Allen (1995). Two types of FRP materials are examined in different reinforcement layout patterns. Also polypropylene and discarded carpet (polypropylene) fibers are incorporated in some additional beams for comparison. Criteria examined are the load-deflection response and cracking patterns under cyclic loading. Recommendations for additional study are also made.

1.3 SCOPE OF STUDY

The objective of this study is to analyze load-deflection behavior of different concrete beams containing FRP as reinforcement and fiber strand in concrete. Concrete beams with seven layouts and materials were constructed and tested.

A literature review of FRP studies is presented in Chapter 2. This review includes the recent proposal of a bridge in the District of Columbia using FRP grating in the bridge deck. The materials used for this study are described in Chapter 3. The concrete was Virginia Department

of Transportation's A4 Post and Rail mix ($f'_c = 4000$ psi). The reinforcements are: epoxy-coated steel bars, non-coated steel bars, FRP bars (two different bar layouts), Duragrid pultruded FRP grating, polypropylene fibers (from concrete supplier), and carpet fibers (from local flooring supplier).

Chapter 4 contains data on the construction and testing of fifteen rectangular concrete beams, eight inches by twelve inches by eight feet. The bottom layer consisted of reinforcing steel in all beams constructed. The top reinforcement was the FRP bars in two layouts, the grating, and nothing. Additional beams consisted of either polypropylene or carpet fibers added to the concrete mix. All beams are tested under progressively increasing cyclic loading up to eighty percent of the moment capacity of the currently used epoxy-coated reinforcement.

Experimental test data and observations from the experiments are presented in Chapter 5. The design of a concrete bridge deck using the standard steel reinforcement and Kodiak FRP reinforcement is made in Chapter 6 and comparison is made between the two designs. Chapter 7 contains conclusions and recommendations for further work..

CHAPTER 2

LITERATURE REVIEW

2.1 INTRODUCTION

Concrete structures in the United States regardless of their purpose are disintegrating. A common link for this breakdown is that steel reinforcement is being used to strengthen the flexural capacity of the structures. Reinforcing steel will corrode when contact is made with humid or salty environments. When steel corrodes, it is expanding which creates tensile forces in the concrete. As the concrete reaches its limit in tension it begins to crack and spall. This spalling creates an even better environment for the corrosion to propagate even further (Bedard, 1992).

The deterioration of concrete bridges due primarily to corrosion of the reinforcing steel in the concrete is a major concern today (Khalifa, 1993). The cost to rehabilitate and repair the bridges in the United States is estimated at nearly fifty billion dollars. The cost to bring the entire infrastructure up to par is many times the original bridge cost. The primary cause of the deterioration is the corrosive action of steel on concrete cause by deicing chemicals and saltwater harsh environment (Bedard, 1992).

Methods used to extend the longevity or protection of bridges are the use of sealers, increase cover depth, increase concrete density, and additives to retard the chemical process (Bedard, 1992). A promising solution to the problem is the use of fiber reinforced plastics (FRP) as a replacement for reinforcing steel. The use of FRP as reinforcement has the following advantages of lightweight, high tensile strength, corrosion resistance, flexibility, and

electromagnetic resistance. FRP is comprised of high strength fibers bonded in a polymer matrix. It has been used by the aerospace and automotive industry for quite some time. FRP reinforcement can be used for marine and water exposed structures, piers, docks, suspension and cable-stayed bridges (Khalifa, 1993).

FRP reinforcing rods can be use to combat deicing salts in bridge decks, parapets, retaining walls, foundations, and curbs. FRP reinforcing can be use to combat saltwater for the same type of structures or components. Other areas where FRP can be used are wastewater and chemical corrosion areas and low electrical conductivity areas. Projects that have FRP used in them are bridges in Germany, Japan, China, and the United States (Bedard, 1992).

2.2 MECHANICAL PROPERTIES

The ultimate strength of FRP is stronger than steel for same diameter, however unlike steel the compression strength is less than the tensile strength. The strength is close to twice that of steel. The stress-strain diagrams for FRP show it is linearly elastic to rupture. The stresses in Glass FRP (GFRP) bars are well below ultimate when failure occurs. The modulus of elasticity is twenty to twenty-five percent of that of steel. The low modulus of elasticity of FRP may lead to the deflection limit state controlling designs due to it being one quarter that of steel. Lower stiffness produces load deflection that is almost linear. At ultimate load, deflection in GFRP is double that of steel, but due to the higher strength and ductility at failure, deflection of the steel reinforcing is greater (Saadatmanesh, 1994). The specific gravity of FRP material is a quarter of that of steel which makes it easier to handle. FRP and concrete have similar coefficients of

thermal expansion which will aid in its use. The bond strength of FRP reinforcing is not as high as steel reinforcing bars, but then again epoxy coated bars reduce bond strength (Bedard, 1992). The bond strength has been determine to be two-thirds that of steel reinforcement (Brown, 1993). The fatigue of GFRP reinforcing is good up to half their strength.

2.3 MATERIAL PROPERTIES

The use of FRP as reinforcement has the following advantages of light weight, high tensile strength, corrosion resistance, flexibility, and electromagnetic resistance (Khalifa, 1993). The disadvantages of FRP are low modulus of elasticity, higher cost, low failure strain, anchorage methods, bond to concrete, and ultraviolet light sensitivity. FRP can be made of carbon, aramid, or glass.

Fiber reinforced plastics are often made by the pultrusion process. The fibers are impregnated with a resin and pulled through a dye that forms the geometry of the section. The sections can be hollow tubes, I shape or round rods. The round rods are wrapped with additional fiber to form ribs which aids in the bonding to concrete (Saadatmanesh, 1994). Hooks and bends are difficult to make. It may be necessary to make connections like plumbing or use grids where straight sections will not work (Bedard,1992).

Carbon and aramid FRP can have high fatigue characteristics, three times more than steel, glass fatigue characteristics are generally less than steel. Of the three types of FRP, mentioned here, CFRP (Carbon Fiber Reinforced Concrete) has the highest tensile properties. Aramid FRP (AFRP) has the higher strain at failure, but also is most effected by water. Glass FRP (GFRP) is

the least expensive and is sand finished for better bonding properties (Erki, 1993). FRP material resists temperatures as high as 225°F. At temperatures in excess of 400°F, FRP reinforcement loses some of its flexural capacity. High temperature areas could prevent the use of FRP in bridges (Brown, 1993).

2.4 EXPERIMENTAL RESULTS

The Army Corps of Engineers found deflections to be two-three times steel and poor bond was typical in their work. In other tests, deflection and cracking greater than when steel was observed. However the computation of section capacity seems to be accurate using the formulas currently in use for steel. Ductile failure similar to steel. Deflection was found to be four times that of steel reinforced sections (Brown, 1993).

Since the Army Corps of Engineers study of FRP as reinforcement, there has been additional research. Most of the research has been done outside the United States and mostly it appears to have been done in Europe and Japan. Several tests have developed to measure the properties of FRP in concrete. The most popular test is the concentric pullout test. This test is to determine the bond strength of FRP and concrete. The test has determined that the ultimate bond is comparable to steel with greater slippage however. Also the temperature affects the bond by decreasing it for higher temperatures. The FRP rod surface pattern, shear strength, shear modulus, and surface area to diameter ratio affects the bonding mechanism (Nanni, Bakis, 1994).

Another test that is in use is the axial tension test that provides an indicator of the cracking width and spacing. The cantilever beam test is a good indicator of the flexural action in bridges.

The test shows bond, crack spacing and width. Additional tests are spliced-reinforcement beam test, notched beam test, hinged beam test, trussed beam test, reinforced and prestressed concrete beam flexural test.

Static and dynamic testing of FRP used in concrete is being done presently by several of those used in the referenced papers. Nanni (1994) does present some design criteria for the use of FRP reinforcing rods using LRFD and ASD. Currently, he recommends that a strength reduction factor of 0.7 be used for LRFD design. Also, the nominal moment capacity should be greater than the cracking moment, thus preventing the rupture of the FRP reinforcement. Deflection is considered more important because it stands a better chance of governing the design. The strain in the FRP reinforcement furthest from the neutral axis needs to be checked.

2.5 SUMMARY

There is a need to increase the use of alternative materials for reinforcing concrete structures (Brown, 1993). FRP is a promising material for use as concrete reinforcement. FRP is available as grids, rods, and ropes for prestressing. FRP initial cost is much greater but gets closer to steel once consideration is given to the preventive methods in use to prevent damage to the concrete. Possible cost saving could be found in thinner concrete sections due to less cover requirement. However, some sections may need to be increased due to tensile splitting of the concrete (Erki, 1993). The use of FRP could be a cost effective long term solution to the deterioration of concrete due to corrosion of reinforcing steel (Bedard, 1992).

Additional bond test needs to be performed to determine development lengths. The manufacturing process needs to be standardized, so that results are universally applicable from one manufacturer to another. The long-term performance of FRP as reinforcing needs to be studied. The durability and reliability need to be predictable (Saadatmanesh, 1994). The ACI current equation for effective moment of inertia, I_e , uses M_{cr}/M_s to the third power whereas going to the fifth power is a more accurate measure of I_e used in the deflection calculations (Brown, 1993).

ASTM standards for FRP need to be developed, so that the material is consistent and as reliable and predictable in use as steel. FRP will need more extensive testing to determine design parameters that will provide comparable safety factors as used in steel reinforced concrete. More research and work are needed to develop guidelines for the design of structures incorporating FRP materials (Bedard, 1992). Appropriate design procedures need to be developed and confirmed by test data. Acceleration of material testing such as cyclic loading needs to be increased to further studied FRP as reinforcement (Nanni, 1994). Nanni also suggests a greater benefit would be to use FRP as prestressing strands.

In 1996, the ACI produced the *State-of-the-Art Report on Fiber Reinforced Plastic Reinforcement for Concrete Structures*. The report presents material development, test methods, design guidelines, research summaries, recommendations, and research needs. It is recommended concrete sections incorporating FRP reinforcement use compression failure design due to higher ductility, deformability, and lower deflections and crack widths. The concrete strength governs the design rather than the reinforcement strength. Design parameters and problems using ASD and LRFD design methods are presented. There is a lack of research data to allow any specific

recommendations to be provided. Due to the variability in manufacturers of FRP products, the designs currently must be based on specific manufacturer's product line. It is recommended that actual test values be used for design when available.

CHAPTER 3

MATERIAL PROPERTIES

3.1 INTRODUCTION

This study is concerned with essentially seven different beam configurations. The concrete used was the same basic mix in all configurations. Epoxy-coated reinforcement was used in the control specimens. Non-coated reinforcement was used in the test specimens that contained FRP bars and grids and polypropylene-based fiber strands. Figure 3.1 is a photo of the various reinforcement bars of this study. The properties of material used are presented in the following sections.

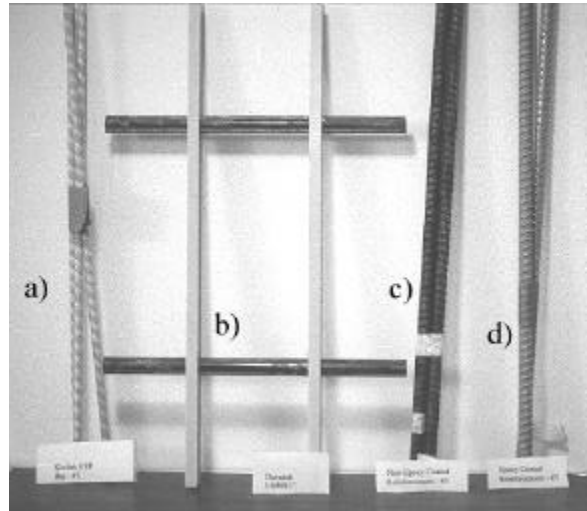


Figure 3.1 Reinforcement bars used in this study. a) Kodiak #3 FRP rebar, b) Duradek I-6000 grid, c) non-coated steel reinforcement bar, and d) epoxy-coated steel reinforcement bar

3.2 FIBER REINFORCED PLASTIC REINFORCEMENT

Fiberglass reinforced plastic is a composite material. It consists of a plastic resin array with glass fibers to reinforce it. The reinforcement strength is controlled by the type of fibers, the orientation of the fibers, the amount of fibers, and the placement of the fibers. A resin binds the reinforcing glass and provides rigidity. The resin material determines the degree of protection from corrosive action, fire, impact, and fatigue. The resin also determines the maximum operating temperature in which the reinforcement can be used. Fiber reinforced plastic is manufactured by the process of pultrusion.

Pultrusion is a manufacturing process for producing the lengths of reinforced plastic structural shapes. The raw materials are pulled through a heated steel die by pulling continuously on the material. The reinforcement materials are in rolls of fiberglass mats or balls of fiberglass roving. The reinforcements are encased in a resin bath and pulled through the die. Heat is applied which produces a gelatin of the resin that takes on the shape of the die.

3.2.1 FRP Rebar

The fiberglass-reinforced plastic rebar used in the beams was obtained from International Grating, Inc. (IGi). The trade name designated is KODIAK. Properties that IGi claim to be advantages of their product are non-magnetic and electrically nonconducting. The rebar has the ability to resist electrolytic corrosion and attack of acids, salts, and other chemicals that affect steel.

Kodiak rebar is made by the pultrusion process. The strands are soaked in resin and pulled through a die that removes excessive resin. Around these strands, additional bands of glass fibers are wrapped. This produces the deformed surface similar to that found on steel reinforcement rods. The final procedure is to heat cure the Kodiak rebar and cut it to length, twenty feet for IGi.

To obtain hooks and bends in the FRP rebar, they must be made at the plant. The placement in the field is the same as for steel reinforcement except for the use of plastic ties and bent reinforcement areas are not done in the field. The material is lighter than the same size steel reinforcement. The high strength to weight ratio is an advantage that makes it easier to handle in the field.

IGi presents some of the disadvantages of their product in their literature. The modulus of elasticity of FRP bars being much lower than steel bars affects strength, deflection, and crack width. Whereas low temperature does not seem to be a problem, high temperature ($>230^{\circ}\text{F}$) produces a loss in strength and flexural modulus. The ultimate tensile stress has a range of 100 to 200 ksi. The manufacturer recommends that 100 ksi be used. Also, they recommend that concrete should be 4,000 psi or greater. Table 3.1 contains properties of Kodiak FRP #3 rebar as measured or supplied by the manufacturer.

Table 3.1 FRP Reinforcement Properties

Material	f_y ksi	f_{ult} ksi	E ksi	Area in²	I in⁴
#3 FRP *	77	100	6,700	0.11	–
Duragrid **	--	70	4,880	2.50	0.328

Test information from * Dr. Weyers and ** Peter Allen thesis.

3.2.2 Duradek Fiberglass Grating

Morrison Molded Fiber Glass Company (MMFG) provided the FRP grating material used as reinforcement in the beams. The trade name that MMFG uses for its proprietary line of fiberglass shapes is EXTREN. EXTREN has the features of high strength, light weight, corrosion resistant, non-conductive, electro-magnetic transparency, and dimensional stability according to the manufacturer's literature. Three resin systems are available and their properties are summarized in Table 3.2.

The procedure for designing with EXTREN material is similar to designing with other materials. When designing with EXTREN material, the manufacturer recommends that the differences in material properties be considered. There is a low modulus of elasticity compared to steel, which leads to deformations being greater. The material is not homogeneous, thus the direction of strands makes a difference in the properties of the material. A low shear modulus exists which means that shear stresses must be examined carefully. High temperature can affect

pultruded fiberglass more than steel. Corrosive resistance is greater than steel thus the plastic material is more useful in harsh environments.

Table 3.2 Properties of EXTREN Series Fiberglass Shapes

	EXTREN SERIES 500	EXTREN SERIES 525	EXTREN SERIES 625
Resin	Isophthalic Polyester	Isophthalic Polyester with Flame Retardant Additive	Vinyl Polyester with Flame Retardant Additive
Standard Color	Olive Green	Haze Gray	Beige
UV Inhibitor	No	Yes	Yes
Purpose	General Use	General Use and Flame Retardant	Highly Corrosive Environment

The grating by MMFG is produced by the pultrusion process and incorporates a number of material improvements. The center of the grating is packed with dense glass fibers with a continuous glass mat wrapped on the outside. The center provides for longitudinal strength and stiffness. The glass mat provides for transverse strength. The surface of the grating is coated with a synthetic veil that protects the grating from ultraviolet light and corrosion.

The grating is connected by a rod system that is locked mechanically and chemically. The purpose is to provide strength to resist torsion, lateral movement, and to distribute the load

throughout the system. It has the advantage of large sections that are light and that can be cut to fit.

DURADEK fiberglass grating is a type produced by MMFG. It comes in “T” and “I” sections. It is available in gray (G) or yellow (Y). It consists of a fire retardant vinyl ester (FRVE) resin that also resists corrosion and ultraviolet exposure. It is coated with a skid resistant epoxy. Designation for the grating is GFRVE or YFRVE.

The DURADEK series used for study is the I-6000 1 inch, YFRVE. The grating is made similar to the FRP rebar except the strands are formed into an I-shape. This I-shape is used to provide the bond strength. The indentation that make the “I” shape provide an irregular surface for the concrete to mold around. This bond provides resistance to loads. The other main difference is that the grating is put together in a grid as specied when ordered. For this study, the I-shape was specified to be on six-inch centers with the transverse grid on twelve-inch centers, which correlated to the control beams steel layout. See Table 3.1 and Table 3.2 for properties of Duradek I-6000 grating as measured or supplied by the manufacturer.

3.3 STEEL REINFORCEMENT

The steel reinforcement is either epoxy-coated reinforcement bars or non-coated reinforcement bars. The non-coated steel reinforcement was obtained from a local supplier. The epoxy-coated steel reinforcement was obtained from stock on hand at the Virginia Tech Structures/Material Laboratory research facility. Table 3.3 describes the material properties as measured or obtained from manufacturer’s data.

Table 3.3 Steel Reinforcement Properties

Material	f_y ksi	f_{ult} ksi	E ksi	Area in²	I in⁴
#5 rebar	64	105	29,000 *	0.31	–
#5E rebar	67	108	29,000 *	0.31	–

E = Epoxy Coated Reinforcement * Assumed value

The stress-strain curves for non-coated steel reinforcement and epoxy-coated steel reinforcement are shown in Figures 3.2 and 3.3, respectively. From the curve in Figure 3.2, the non-coated steel reinforcement has a yield strength of 64 ksi. From the curve in Figure 3.3, the epoxy-coated steel reinforcement has a yield strength of 67 ksi.

Non-Epoxy Coated Reinforcement

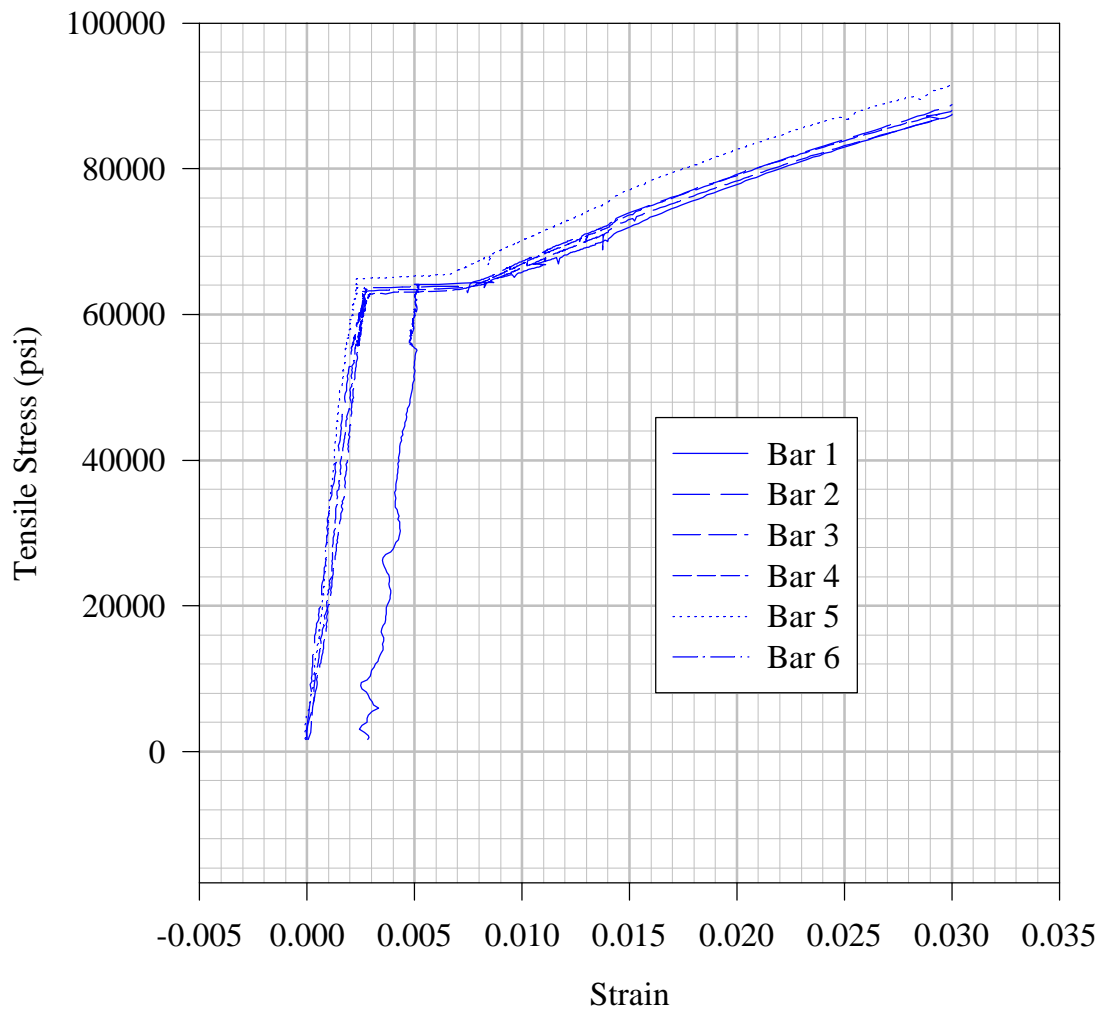


Figure 3.2 Stress-Strain curve for Non-Epoxy Coated Reinforcement

Epoxy Coated Reinforcement

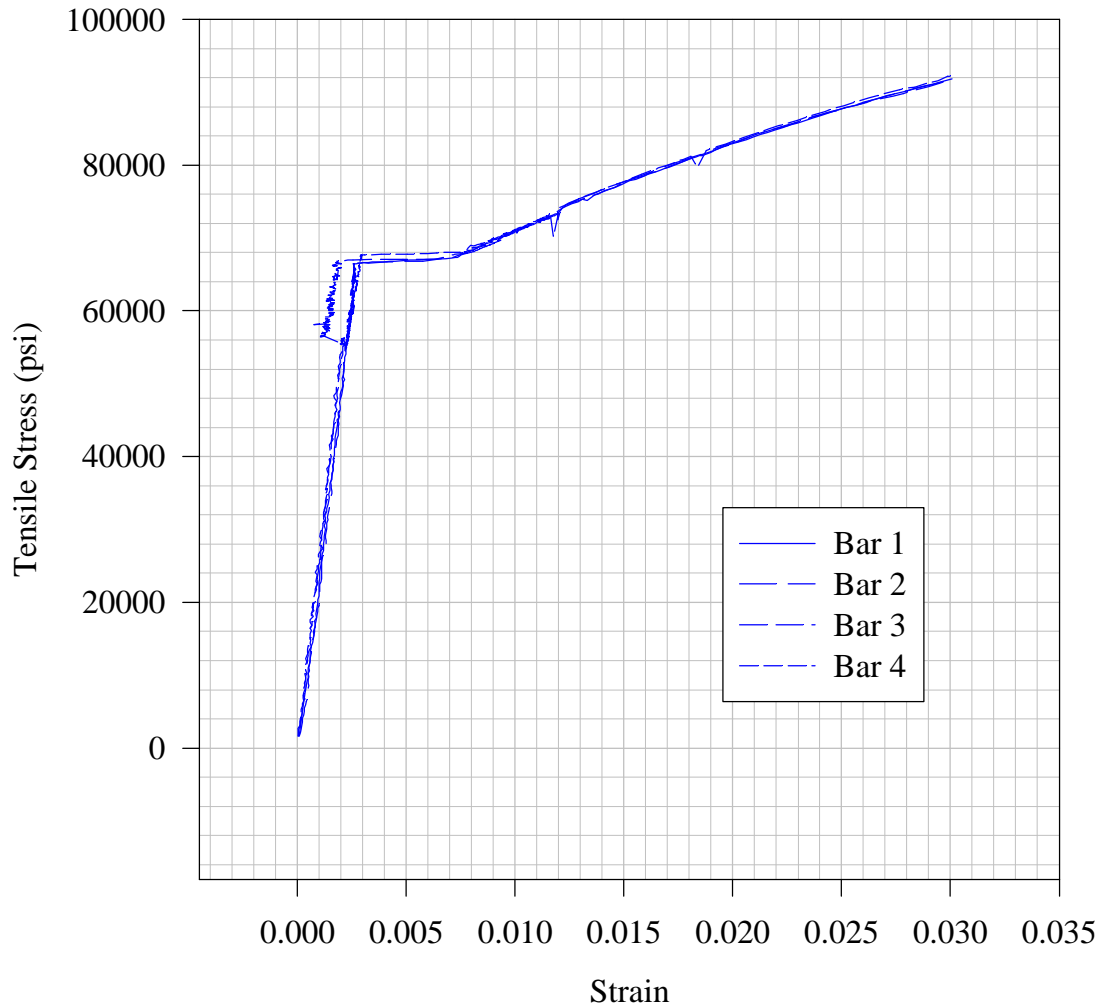


Figure 3.3 Stress-Strain curve for Epoxy Coated Reinforcement.

3.4 POLYPROPYLENE FIBER

Polypropylene fibers were obtained from a local concrete plant. The manufacturer of the fibers was W. R. Grace. The brand name was Microfibers. The typical volume mix is one and one-half pounds per cubic yard. The volume mix used for this study was one pound per cubic

yard. The addition of polypropylene fibers generally increases the cohesiveness of the mix which lowers the slump. The air content and unit weight is not significantly affected (Balaguru, 1992).

3.5 CARPET FIBER

Carpet scrap was obtained from a local flooring provider. According to the dealer, the carpet was olefin made with polypropylene fibers. Olefin can be composed of several different materials, polyester, polyethylene, and polypropylene. The dealer was certain that the carpet was polypropylene fibers; however, it was deemed necessary to perform a test to be certain. A simple test to determine whether the carpet consist of polypropylene fibers was made. Since each material has a distinct melting temperature: polyester's melting temperature is greater than 250°C; polyethylene's melting temperature is 135°C; and polypropylene's melting temperature is 170°C (AATCC Technical Manual). An oven was set below 135°C; every thirty minutes the temperature was increased until the fibers melted. The melting temperature observed was at 170°C. No additional melting occurred when temperature was raised above 170°C. A conclusion is that the carpet contained primarily polypropylene fibers.

Because the polypropylene fibers from the concrete plant were three-fourths of an inch long, the carpet was cut into similar pieces. The yarn and backing that made up the carpet were shredded. The carpet fibers were placed in bags and weighed.

3.6 CONCRETE

The concrete used in the beams was designated as Virginia Department of Transportation (VDOT) A4 Post and Rail mix. The concrete was obtained from a local supplier. The properties of the required mix are shown in Table 3.4. The half-inch maximum aggregate size was reduced to 3/8 of an inch.

The slump measured when concrete was delivered was less than three inches so one-third of a gallon of plastizer was added to the mix. This is designated as mix #1. When measured again after the first beams were placed, the slump was not much over three inches. The remaining plastizer was added to the mix that brought the slump to nearly four inches. This is designated as mix #2. Mix #3 is from the same truck with the carpet fibers added. Mix #4 is a separate truck with one pound of polypropylene fibers added at the concrete plant. Table 3.5 shows the properties of the concrete mix when beams were made.

Table 3.4 VDOT A4 Post and Rail Concrete Mix

Strength, f_c' (psi)	4,000
Slump (in)	2-4
Aggregate Size	7
Maximum	1/2 in. (3/8 in.)*
Air Content (%)	7 ± 2
Cement (lb/yd ³)	635
Water (water/lb)	0.45

* change from standard mix

Table 3.5 shows that the air content was lower than specified, however the mix was deemed usable. The concrete compressive strength, f'_c , determined at the time the beams were tested exceeded required strength by a considerable margin.

Table 3.5 Properties of Concrete in Test Beams

Mix	Air Content (%)	Slump (in)	Weight (lb/ ft ³)	Fiber Content (lb/ yd ³)	f'_c (psi)
#1	3.5	3.25	149.6	NA	7,026
#2	--	3.75	--	NA	6,448
#3	--	--	--	4.96	6,395
#4	4.3	3.75	146.7	1	6,156

When all concrete beams were finished being made, burlap sacks were placed over the beams and wetted down. Then a plastic sheet was placed over the beams. The burlap sacks were monitored and kept wet until the full twenty-eight days had past. Once the beams were cured, the beams were placed off to the side until they could be tested. The same procedures were performed on the concrete test cylinders.

3.7 COST COMPARISON

Table 3.6 contains the cost of the various reinforcement materials used in this study. From the table, it can be seen that the cost per pound of FRP reinforcement material is high compared

to steel reinforcement. However, the FRP reinforcement material being lighter offsets some of this cost. Table 3.7 shows the cost per beam.

Table 3.6 Cost Comparison of Reinforcement Material

Material	Cost \$/lb	Cost \$/foot
Epoxy Coated Steel	0.38	0.36
Non-Coated Steel	0.30	0.29
Kodiak #3 Rebar	4.58	0.44
Duradek I-6000	7.25	4.17
Microfiber	1.20	----
Carpet Fiber	0.60*	----

* Assume carpet shredding cost is one half production cost of new fibers

Table 3.7 is a cost comparison of the beams in this study. The individual reinforcement cost per beam is in bold font. The total is at the bottom of the table. From Table 3.7, the cost of the beam using Kodiak #3 rebar is more cost efficient than steel reinforcement. The use of non-epoxy coated steel reinforcement makes up the difference. The cost differential shows that the use of FRPs is becoming competitive with steel reinforcement.

The lower cost plus lighter weight that should decrease the cost of construction is a good indication that it will be an acceptable replacement. Lighter weight should increase speed of

placement and decrease the labor necessary to perform the job. The Duradek grating cost is slightly more than twice the cost of conventional steel reinforcement. The shipping of FRP would be less than steel due to its weight. The Duradek is assembled in large grids for placement. The construction in the field would be quicker and easier but the cost will probably still be higher than steel reinforcement.

Seven beam configurations are part of this study. The control test beam was the TD series. It contains epoxy-coated steel reinforcement top and bottom. The reinforcement in the beams are as tabulated below.

TD = Top and Bottom Steel #5 epoxy-coated

KS = Top – One Kodiak FRP and Bottom -- Steel #5 non-coated

KD = Top – Two Kodiak FRP and Bottom -- Steel #5 non-coated

DK = Top -- Duragrid 1 in. I-bar and Bottom -- Steel #5 non-coated

NS = Bottom Steel #5 epoxy-coated

FC = Polypropylene fibers concrete mix and Bottom -- Steel #5 non-coated

CC = Carpet fibers concrete mix and Bottom -- Steel #5 non-coated

Table 3.7 Cost Comparison of Beams

Beam Designation	TD	KS	KD	DK	NS	FC	CC
Epoxy-Coated Rebar							
Weight per beam (lbs)	48.67	----	----	----	24.33	----	----
Cost per beam (\$)	18.50	----	----	----	9.25	----	----
Non-Coated Rebar							
Weight per beam (lbs)	----	24.33	24.33	24.33	----	24.33	24.33
Cost per beam (\$)	----	7.30	7.30	7.30	----	7.30	7.30
Kodiak #3 Rebar							
Weight per beam (lbs)	----	1.50	2.24	----	----	----	----
Cost per beam (\$)	----	6.89	10.26	----	----	----	----
Duradek I-6000 Grating							
Weight per beam (lbs)	----	----	----	4.6	----	----	----
Cost per beam (\$)	----	----	----	33.35	----	----	----
Microfiber							
Weight per beam (lbs)	----	----	----	----	----	0.20	----
Cost per beam (\$)	----	----	----	----	----	0.24	----
Carpet fibers							
Weight per beam (lbs)	----	----	----	----	----	----	0.92
Cost per beam (\$)	----	----	----	----	----	----	0.55
Total Cost per beam (\$)	18.50	14.19	17.56	40.65	9.25	7.54	7.85

CHAPTER 4

EXPERIMENTAL SETUP

4.1 INTRODUCTION

The beam configurations and testing setup for this study are presented in this chapter. The beams are grouped in two categories, those with top reinforcement and those without top reinforcement.

4.2 BEAM CONFIGURATION

The description of the configurations is separated into those parts that are standard to all beams, then unique features of each beam type are discussed in subsections for that particular beam. The formwork, reinforcements and concrete details are outlined for each subsection. The experimental beam setup is then described with the use of photographs and schematics.

4.2.1 Formwork

The formwork for the test specimens consisted of a half-inch plywood bottom of the beam. Two by eight wood members with one by two furring strips on top are used to make the sides and ends for an eight inch deep beam. The plywood bottom had a ladder system of two by fours underneath for support and clearance for straps to lift the beams. The assembly is put together with screws with an inch embedment in the connected member. The eight foot length of

the plywood sheet controlled the length of the beams. The formed beam size was twelve inches by eight inches by seven feet nine inches.

Holes are drilled in the side members for the placement of steel reinforcement. The steel reinforcement is placed so that there is one inch cover at the bottom and two inches at the top. Nails are used for support of the fiber reinforcing bars and grids. The nails are driven on the inside of the form to provide an inch of cover on the fiber reinforcement.

Figures 4.1, 4.2, and 4.3 show the forms prior to being placed with concrete. Figures 4.2 and 4.3 identify some of the beam configurations.

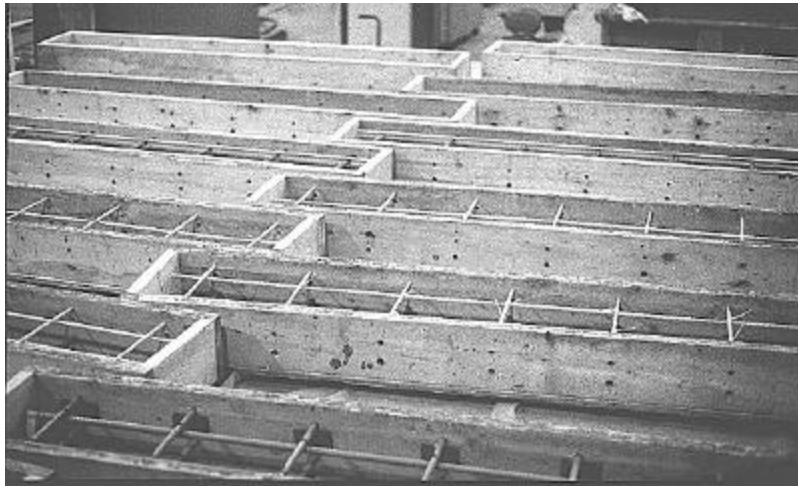


Figure 4.1 Photo showing forms for the beams ready for concrete.

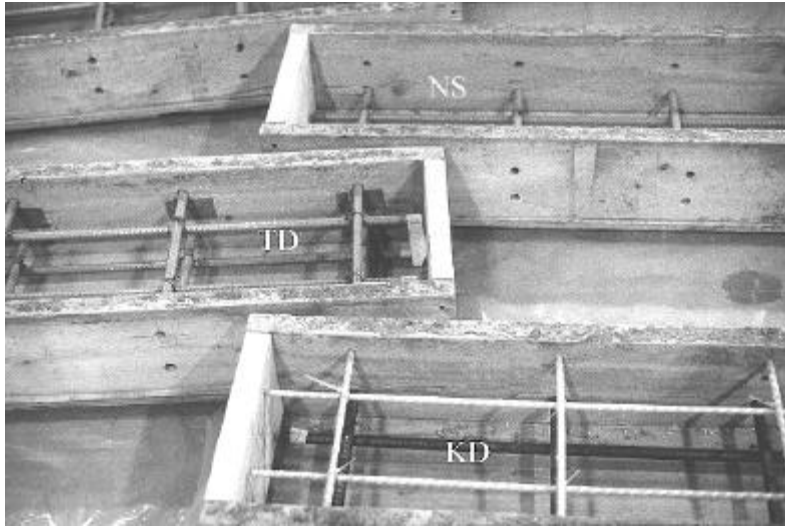


Figure 4.2 Photo showing three forms for beams, NS, TD, and KD series of beams.

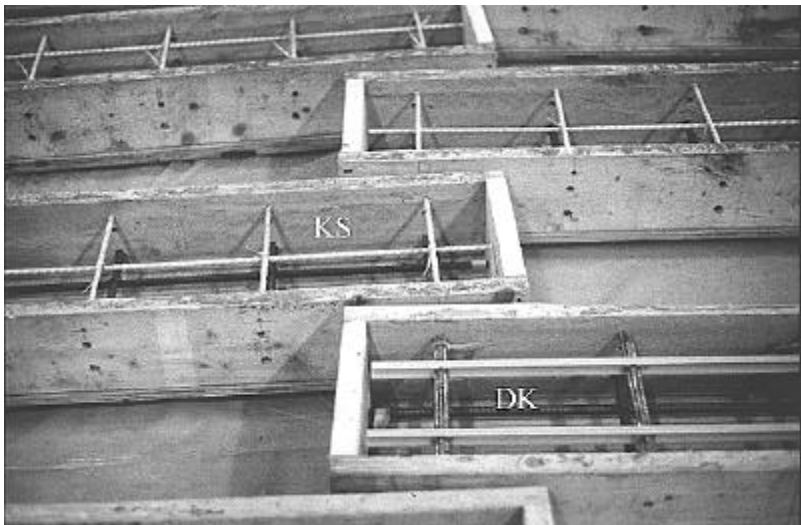


Figure 4.3 Photo showing three forms for beams, KS, and DK series of beams.

4.2.2 Beam Reinforcement Setup

Seven beam configurations with six different reinforcement material are part of this study. The control case, TD series, was epoxy-coated steel reinforcement top and bottom on six inch centers with transverse reinforcement on twelve inch centers. Additional pair of control beams without top reinforcement, NS series, were used for comparison with beams with fiber strands in their composition. Other beam designations are as follows:

TD = Top and Bottom Steel #5 epoxy-coated

KS = Top -- Kodiak FRP on twelve inch centers and Bottom -- Steel #5 non-coated

KD = Top -- Kodiak FRP on six inch centers and Bottom -- Steel #5 non-coated

DK = Top -- Duragrid 1 in. I-bar on six inch centers and Bottom -- Steel #5 non-coated

NS = Bottom Steel #5 epoxy-coated

FC = Polypropylene fibers in concrete mix and Bottom -- Steel #5 non-coated

CC = Carpet fibers in concrete mix and Bottom -- Steel #5 non-coated

Table 4.1 shows the reinforcement layout and cover for the different beams by designation name.

Table 4.1 Reinforcement Layout

Specimen	Bottom Bars	Top Bars	Bottom Cover	Top Cover
TD	#5 Epoxy	#5 Epoxy	1 in.	2 in.
KS	#5	Kodiak	1 in.	1 in.
KD	#5	Kodiak	1 in.	1 in.
DK	#5	Duradek	1 in.	1 in.
NS	#5 Epoxy	----	1 in.	----
FC	#5	----	1 in.	----
CC	#5	----	1 in.	----

The cover for the top steel reinforcement is two inches in accordance with ACI. The cover for the FRP material reinforcement was reduced to one inch because permeability and the closeness of the reinforcement to the deck surface is of lesser concern.

4.2.2.1 Control Beams -- The control beams for this study are TD1, TD2, and TD3. The extra beam is to evaluate the test setup and enable it to be evaluated and refined. Additional beams, NS1 and NS2, are for comparison of the concrete with fiber strands included in the mix. These beams also provide a basis for verifying the assumption that no reinforcement is needed in the top of a bridge deck.

Figure 4.4 shows the cross section of the control beams. Figure 4.5c and 4.5b shows the side view of the TD and NS beams, respectively.

4.2.2.2 FRP Bars -- The beams which use Kodiak #3 FRP rebar are designated KS and KD. These beams represent top reinforcement twelve inches and six inches on center respectively. The cross section for these beams are shown in Figure 4.4. The side view of these beams are shown in Figure 4.5a.

4.2.2.3 FRP Grids -- Duradek I-6000 grid represents reinforcement on six inches on center spacing. Figure 4.4 shows a cross section of these beams. Figure 4.5d shows the side view of the Duradek beams.

4.2.2.4 Fibers -- Cross sections of beams with carpet and polypropylene fibers are shown in Figure 4.4. The side view of these beams are shown in Figure 4.5b.

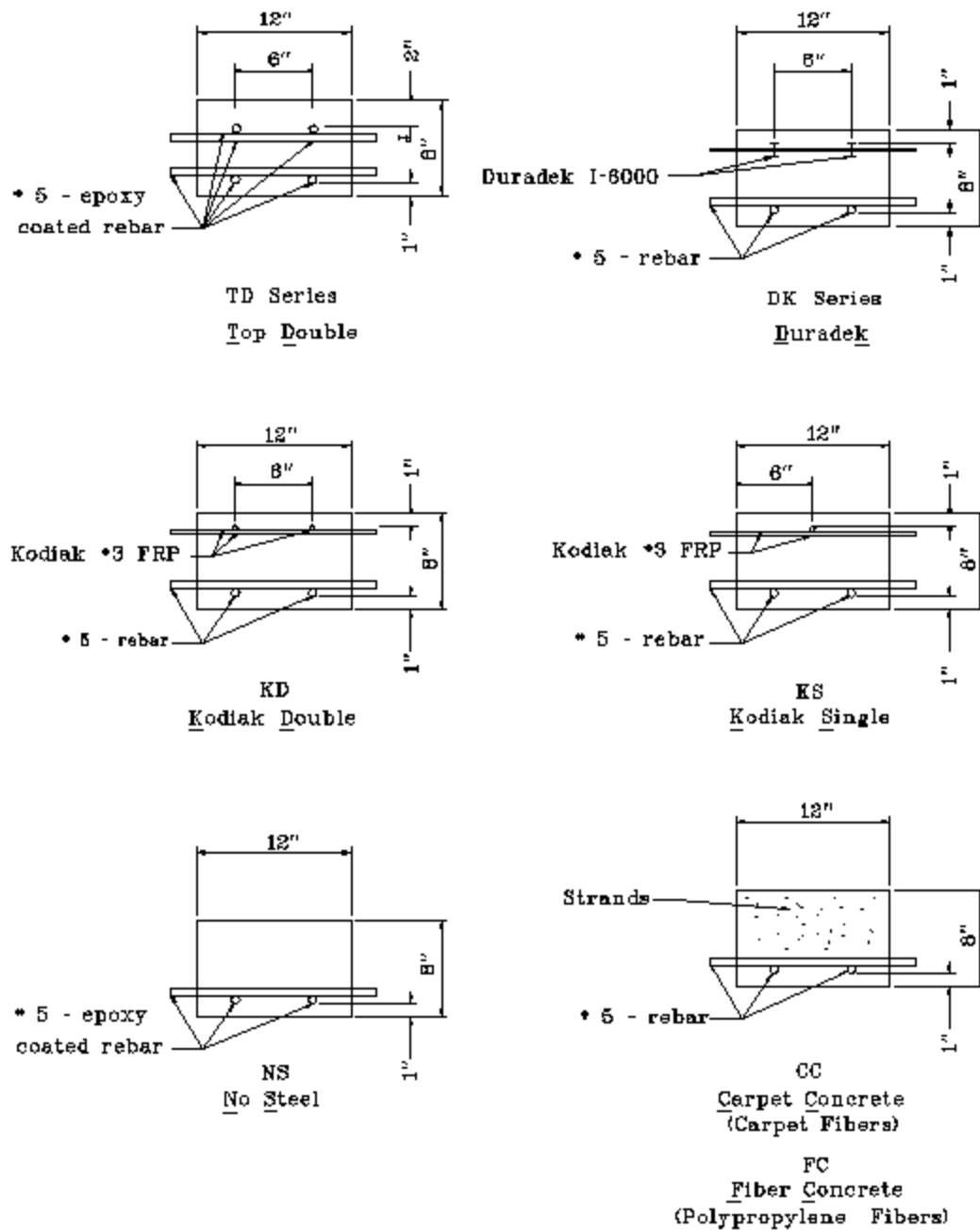
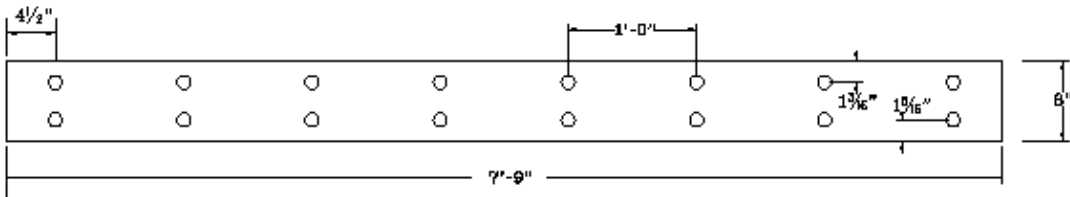
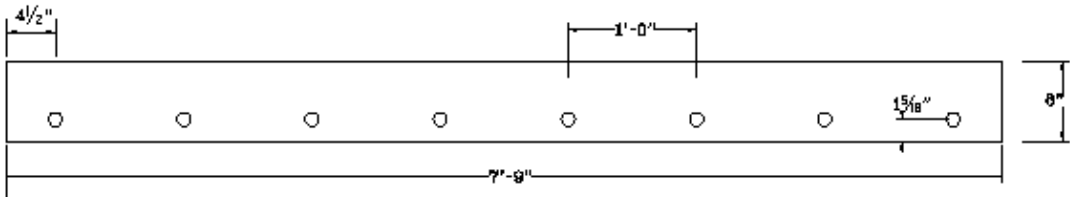


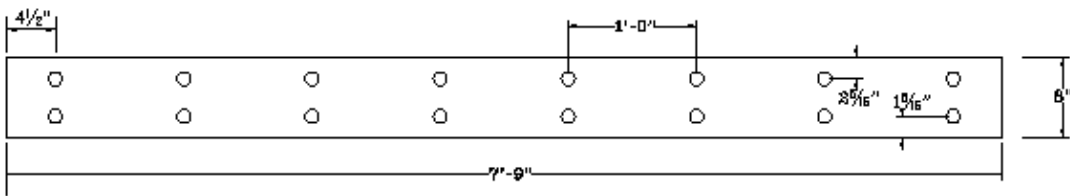
Figure 4.4 Cross Section of Beams



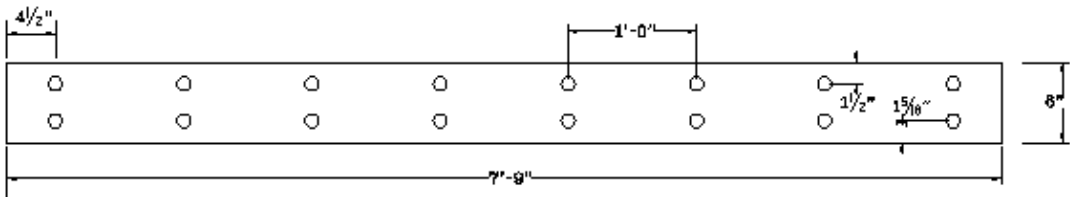
a) Side view of KS and KD series of beams



b) Side view of NS, FC, and CC series of beams



c) Side view of TD series of beams



d) Side view of DK series of beams

Figure 4.5 Side view of different beam configurations

4.3 BEAM SETUP

Figure 4.6 is a photo showing the test setup. Figure 4.7 is a schematic of the test setup. The center to center span length of the test spans is seven feet five inches. The center to center distance of points of applied load is eight inches. Three LDVT's were used to measure

deflections. The two LDVTs at each end were average and subtracted from the midspan deflection to obtain the actual deflection. An angle was used behind the beam connecting the two support beams to provide bracing to the supports.

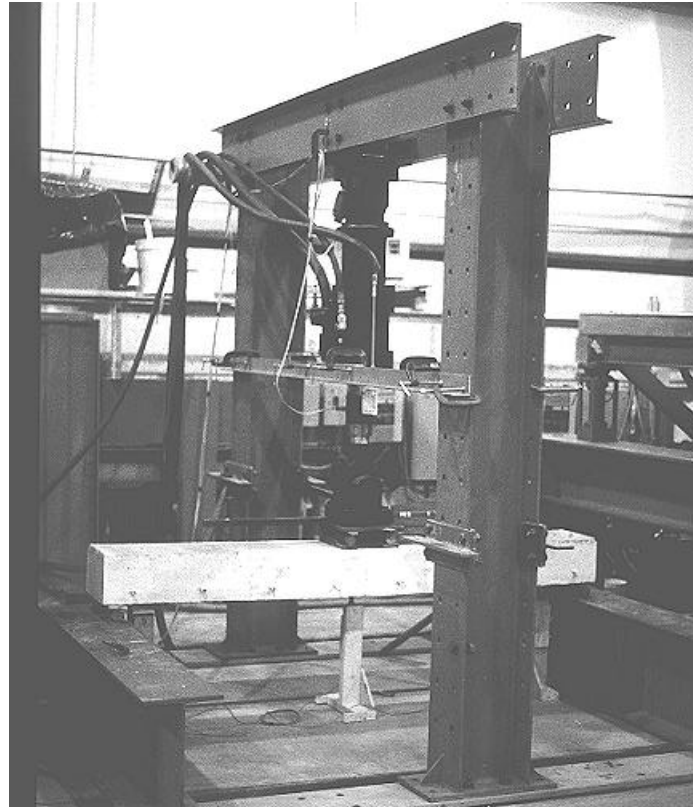


Figure 4.6 Test setup with beam in position.

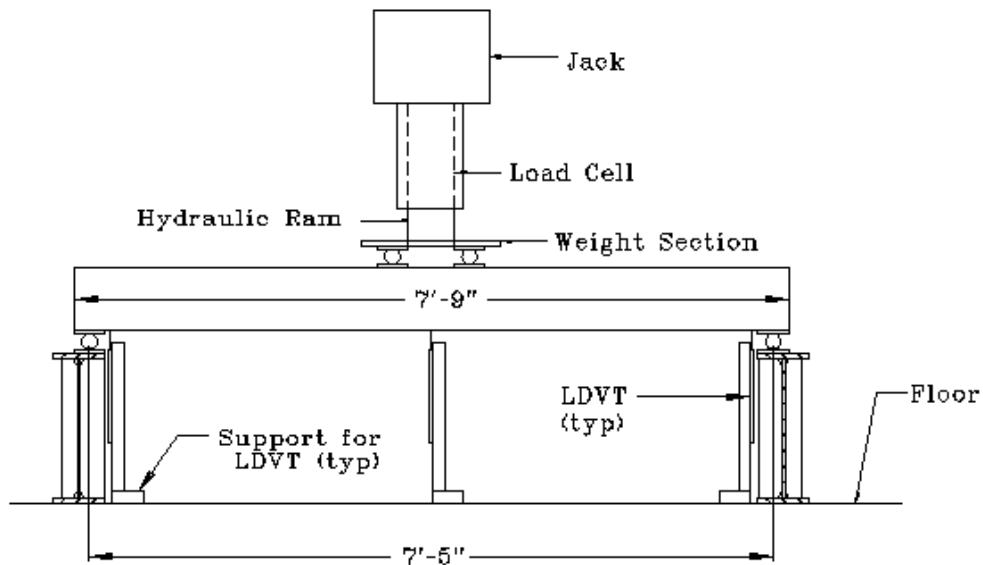


Figure 4.7 Beam load testing setup

The load capacity of the control beams, TD series, is rounded down to fifteen kips. A cyclic load pattern is shown in Table 4.2. The established pattern was chosen to allow for a beam test being completed in around eight hours. After working with the setup, the frequency of the ram was increase from one to two hertz. This enabled the option of testing two beams in just over an eight hour time frame.

Table 4.2 Cyclic tests load steps

Percent of Ultimate Load of Control Beams	Applied Load	Cycles
20	3.0	3,000
40	6.0	3,000
20	3.0	3,000
60	9.0	3,000
20	3.0	3,000
80	12.0	3,000
20	3.0	3,000

CHAPTER 5

EXPERIMENTAL RESULTS

5.1 INTRODUCTION

This chapter presents the measurements taken during the testing. Chapter 7 will present the conclusions of the testing. The testing phase was divided into two sections, first the control beams and the FRP #3 reinforcement beams, TD, KS, and KD series. The second phase was the remaining series of beams, DK, NS, CC, and FC. The first group of beams consisted of top reinforcement bars of steel and FRP that are round with surface deformations specifically designed for bonding to concrete. The second group of beams are the I-shape FRP member as reinforcement or no reinforcement in the top of the beams. The cracking pattern and load and deflections are examined and compared with the control beams, TD series.

5.2 CRACK PATTERNS

The sections to follow presents a comparison of the cracking pattern observed in the beams in this study. A scale drawing of the beams was prepared in a CAD program, Microstation, which is currently used by VDOT. These drawings have the location of the loads and support conditions shown. The round circles on the drawings depict the location of the transverse reinforcement used in the beams. Color slides of the beams are used to provide the crack

patterns. While looking through a hand slide viewer at the slides of each beam, the crack lines were placed as close as possible to the pattern observed for each particular beam.

Each series of beams is compared to the others in the group and then a comparison is made to the control beams, TD. Some beams will be singled out for problems that may have occurred during testing and invalidated the patterns observed.

5.2.1 TD Series

The crack patterns for this series of control beams are similar as can be seen in Figure 5.1. Beam TD2 shows more cracks than the others but it was overloaded to failure. Beam TD2 is will be ignored in the rest of the discussion. Beam TD3 was slightly underloaded; however the pattern resembles TD1. The first cracks formed were at the transverse reinforcement locations closest to the applied load. The cracks propagated from the tension face towards the compression zone. Additional cracks developed with increasing load application, progressing from the center of the span towards the ends of the beams. The cracks first appeared at the transverse reinforcement locations and then additional cracks formed between the transverse reinforcement. The cracks near the ends of the beams extend to or slightly above the transverse reinforcement in the test beams. The cracks near the center extend approximately the same distance towards the compression zone at the top of the beams.

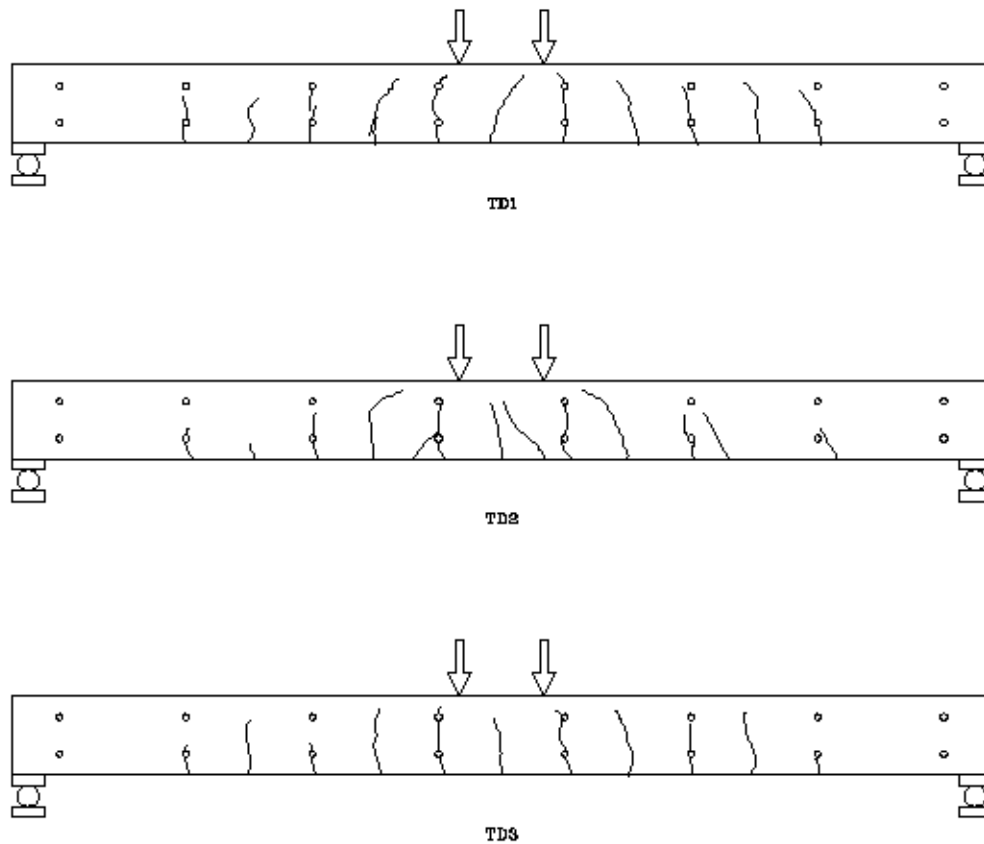


Figure 5.1 Schematic of crack patterns in the TD beam series

5.2.2 KS Series

The crack patterns for the KS series are shown in Figure 5.2. The cracks began near midspan at the transverse reinforcement. With an increasing load, the cracks progressed away from the midspan. The cracks near midspan extend to near the transverse reinforcement in the top of the beam. The cracks near the ends extend to almost the middle of the beam. Beam KS2 does differ from KS1 on the right end of the beam. There are double crack lines between the

transverse reinforcement. The lengths of the cracks do not differ by a great deal and where the double crack lines occur, the adjacent crack line is slightly shorter near midspan.

The crack pattern of the beam identified as KS1 resembles the crack pattern in the test beams, TD1 and TD3. The crack patterns away from midspan are at approximately the same height. The crack patterns near midspan get closer to the top of the section. The crack pattern of beam KS2 is somewhat different by having more cracks in the right half of the beam but the height of the cracks is nearly the same.

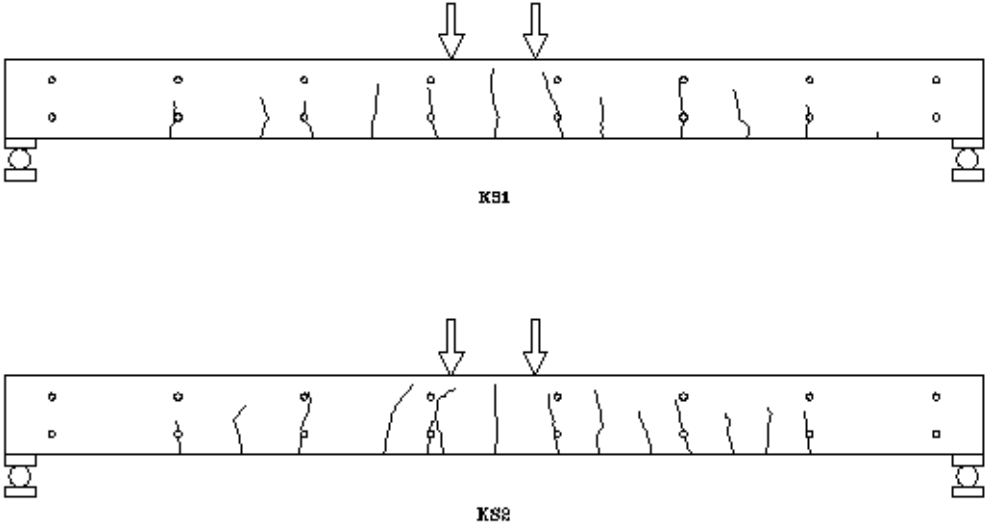


Figure 5.2 Schematic of crack patterns in the KS beam series

5.2.3 KD Series

Figure 5.3 shows the crack pattern of beams, KD1 and KD2. The KD series are somewhat different from each other in their crack pattern. Beam KD1 fell off the supports while being setup. The member had initial cracks when testing began. This explains the reason for the discrepancy in the crack pattern. The height of the cracks when maximum load was applied is nearly the same. Beam KD2 will be used for comparison with the control beams.

Cracking pattern of control beams and KD2 are nearly identical. The missing crack at the second transverse reinforcing bar is the only difference in the displayed patterns.

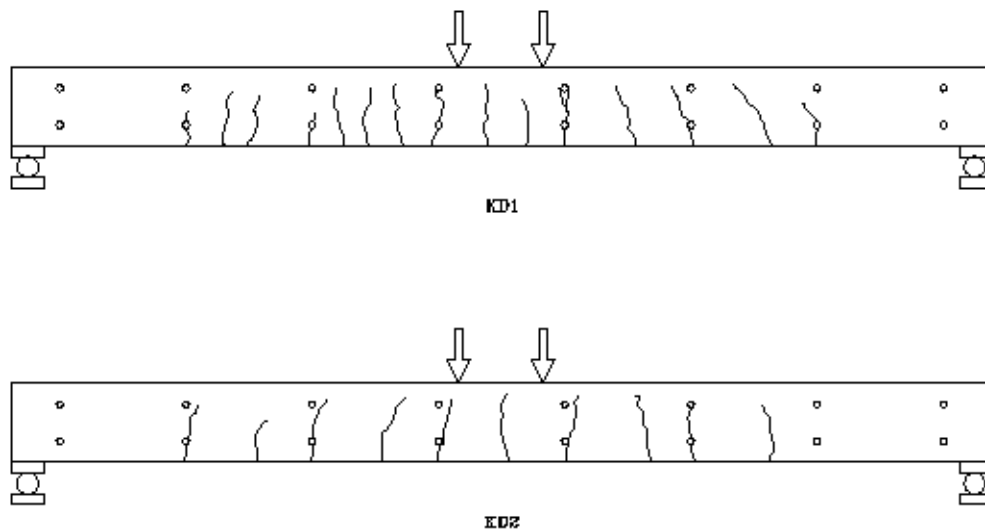


Figure 5.3 Schematic of crack patterns in the KD beam series

5.2.4 DK Series

Figure 5.4 shows the crack pattern for the DK series of beams. The cracks began near midspan at the transverse reinforcement. With an increasing load, the cracks progressed away from the midspan towards the supports. The cracks near midspan extend to the transverse reinforcement in the top of the beam. The cracks near the ends extend to almost the middle of the beam. Beam DK1 and DK2 show similar patterns of cracking. Beam DK2 does display some additional cracks that cross other vertical cracks.

The cracks in these specimens go higher than the cracks in the control beams. Near midspan the crack height is close to the same. The control beams' cracks are taller at midspan and shorter near the supports; the DK beams display a tall crack of nearly the same height from quarter point to three-quarter point.

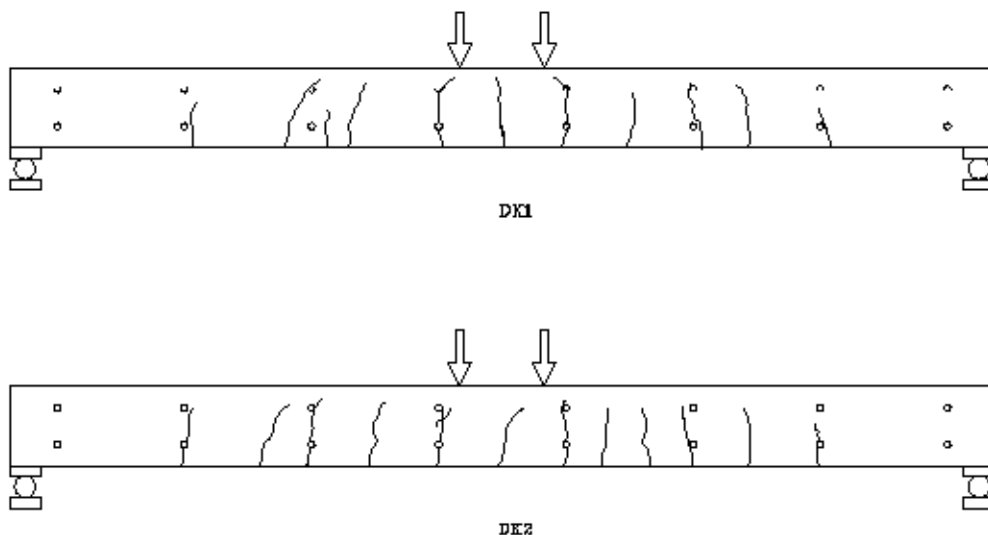


Figure 5.4 Schematic of crack patterns in the DK beam series

5.2.5 NS Series

Figure 5.5 is a schematic of the NS beams. The height and number of cracks are nearly identical for the two beams. The location of the cracks is within the same general area. The cracks progressed from the transverse reinforcement near the middle of the beam to the supports. Additional cracks between the transverse reinforcement were formed with an increase in load. There are two additional cracks at midspan of the test specimens.

There are two differences between these beams and the control beams. First, the cracks in the NS beams are somewhat higher than the control beams. Second, the midspan has two cracks between the loads in the NS beams and only one in the control beams, TD.

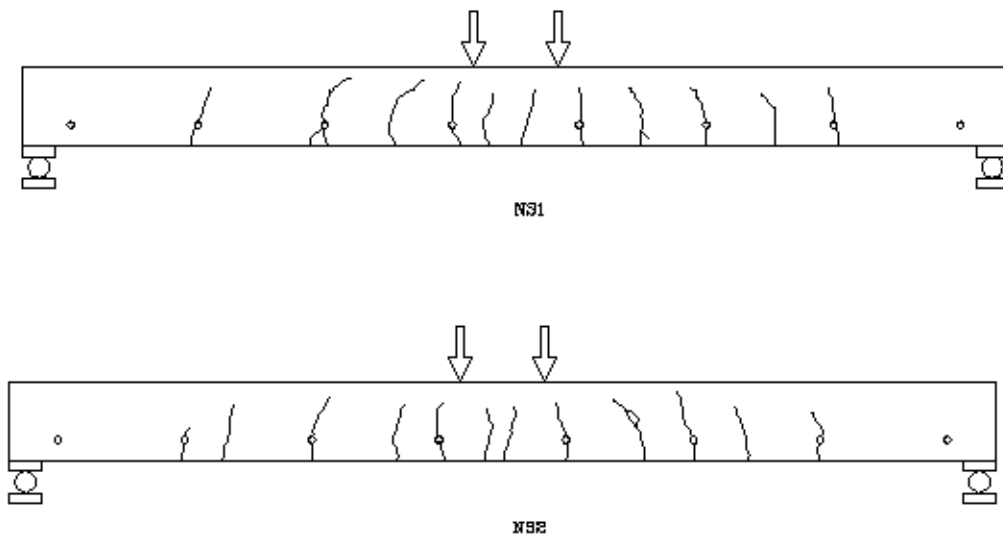


Figure 5.5 Schematic of crack patterns in the NS beam series

5.2.6 FC Series

Figure 5.6 shows the crack pattern in the FC test beams. These beams are the ones that contain the polypropylene fibers. The beams display a crack pattern similar to each other, with one crack not occurring in sample FC2 near the right support. The height, number, and location of the cracks compare favorably with each other.

These beams compare fairly close to the control beams. The height and location of the cracks are nearly identical.

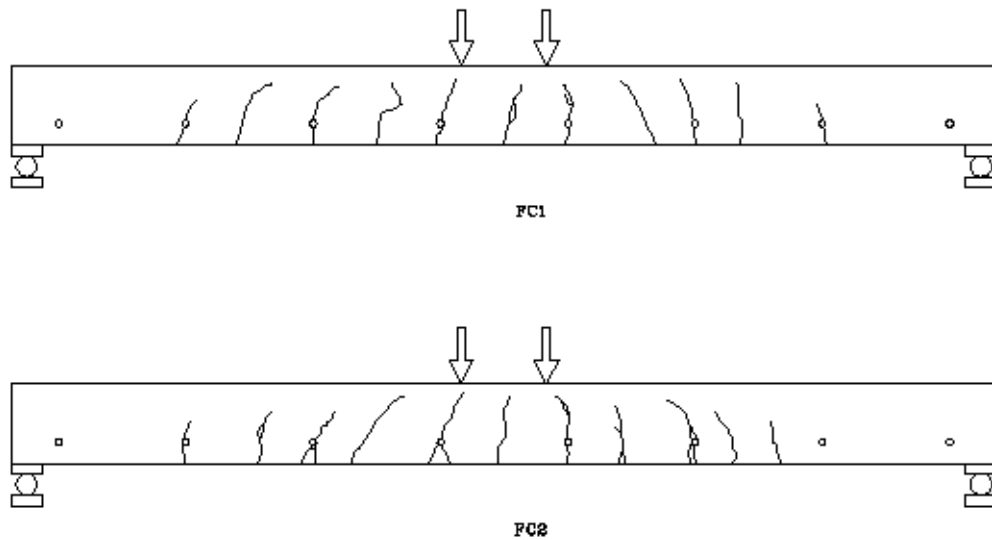


Figure 5.6 Schematic of crack patterns in the FC beam series

5.2.7 CC Series

Figure 5.7 is a schematic of the crack pattern for the CC beams. Here, again the two beams display a similar crack height and location pattern. The crack patterns in these beams resemble each other more than any other series of beams. Not only are the cracks at the same locations, the cracks travel paths are nearly identical. There is a split crack just left of midspan in both specimens. The curvature towards the center of the beam is extremely close to each other at several locations in the beams.

There is one difference between these beams and the control beams. The cracks in the CC beams are somewhat higher than the control beams.

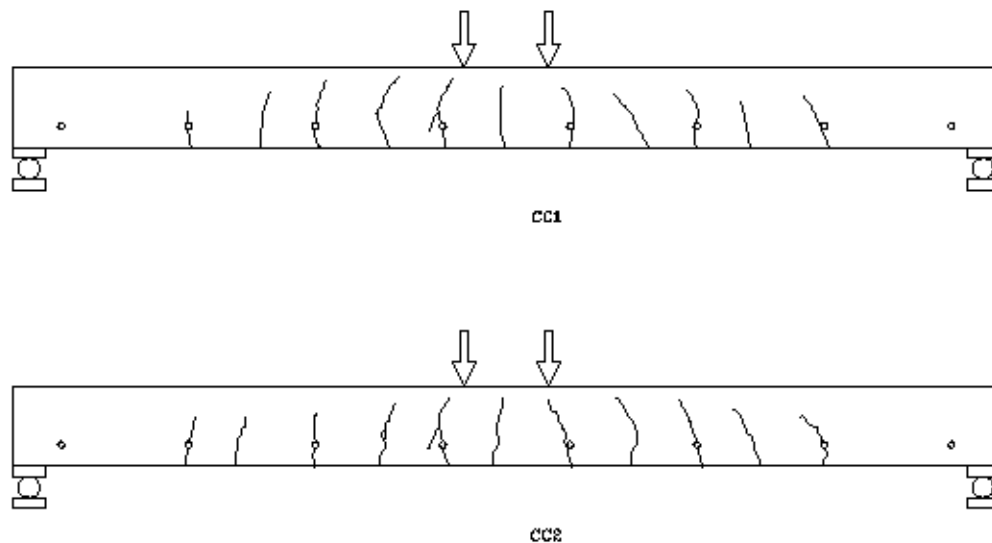


Figure 5.7 Schematic of crack patterns in the CC beam series

5.3 LOAD-DEFLECTION

The deflection calculations are determined by using equations in the fourteenth edition of *AASHTO Standard Specifications for Highway Bridges (1989)* and the beam deflection equations from *AISC Manual of Steel Construction (1994)*. Beam diagrams and formulas used from AISC are simple beam - two equal concentrated loads symmetrically placed for the applied loads

$$\Delta_{\max} = \frac{Pa(3l^2 - 4a^2)}{24EI}$$

and simple beam - uniformly distributed load for the self weight of the test beam

$$\Delta_{\max} = \frac{5wl^4}{384EI}$$

The concrete's modulus of elasticity, E_c is taken as

$$33w^{1.5} \sqrt{f'_c} \quad \text{AASHTO Sec. 8.7.1}$$

where $w = 145$ pcf.

The effective moment of inertia, I_e , is dependent on the cracking moment, applied moment, gross section moment of inertia and cracking moment of inertia. The equation for moment of inertia is

AASHTO (8-1)

$$I_e = \left(\frac{M_{cr}}{M_a} \right)^3 I_g + \left[1 - \left(\frac{M_{cr}}{M_a} \right)^3 \right] I_{cr} \leq I_g$$

where

$$M_{cr} = f_r I_g / y_t \quad \text{AASHTO (8-2)}$$

where f_r is the modulus of rupture given by

$$f_r = 7.5 \sqrt{f'_c} \quad \text{AASHTO Sec. 8.15.2.1.1}$$

The factor normally applied to the modulus of rupture is 7.5 as in the given equation; however, due to the high concrete test strengths and cracks occurring during the first cycle, the value of 6.0 was substituted and the equation used is

$$f_r = 6.0 \sqrt{f_c'}$$

The applied moment, M_a , is obtained from standard equations and is dependent on applied load and location of that load. The gross section moment of inertia for a rectangular concrete section is given by

$$I_g = \frac{1}{12}bh^3$$

and the cracking moment of inertia, I_{cr} , is determined by the use of transform sections properties. Table 5.1 list the material and section property values which are not dependent on the applied load. The gross moment of inertia and the cracking moment of the TD beams is greater than the other beams specimens as can be seen in Table 5.1. Table 5.2 shows the maximum load capacity of the different test beams along with the ratio of applied load to maximum capacity. Applied loads were determine based on the control test specimens capacity, TD, which was rounded to fifteen kips. Test were performed at twenty, forty, sixty, and eighty percent of the fifteen kips. The capacity of the beams excluding the control beam, TD, are close to each other. However, the capacity of these beams are nearly equal to the maximum applied load of twelve kips.

Table 5.1 Non-Load Related Terms for Equations

	TD	KS	KD	DK	NS	FC	CC
f_c' (psi)	7,026	6,448	6,448	6,448	6,448	6,395	6,156
E_c (ksi)	4,830	4,630	4,630	4,630	4,630	4,610	4,520
I_g (in⁴)	547	539	540	539	539	539	540
I_{cr} (in⁴)	113	116	116	116	116	116	118
M_{cr} (in-lb)	68,772	64,923	65,043	64,923	64,923	64,653	63,558
f_r (psi)	502.9	481.8	481.8	481.8	481.8	479.8	470.8

Table 5.2 Maximum Load Capacity and Percentage of Applied Load

	TD	KS	KD	DK	NS	FC	CC
P_{max} (kips)	15.1	12.1	12.1	12.3	12.7	12.1	12.1
<u>3</u> P_{max}	19.9%	24.8%	24.8%	24.4%	23.6%	24.8%	24.8%
<u>6</u> P_{max}	39.7%	49.6%	49.6%	48.8%	47.2%	49.6%	49.6%
<u>9</u> P_{max}	59.6%	74.4%	74.4%	73.2%	70.9%	74.4%	74.4%
<u>12</u> P_{max}	79.5%	99.2%	99.2%	97.6%	94.5%	99.2%	99.2%

A typical load-deflection diagram showing the cyclic pattern of the applied loads is shown in Figure 5.8. The load cycles one, two, four, and six which represent loads of three, six, nine and twelve kips respectively, can be distinguished from the diagram. The alternate cycles which are

the three kips load is hidden in the last three cycle patterns. The hidden three cycles does seem to show in a color plot that permanent set has taken place once the higher load has been reached.

Typical Cyclic Load-Deflection

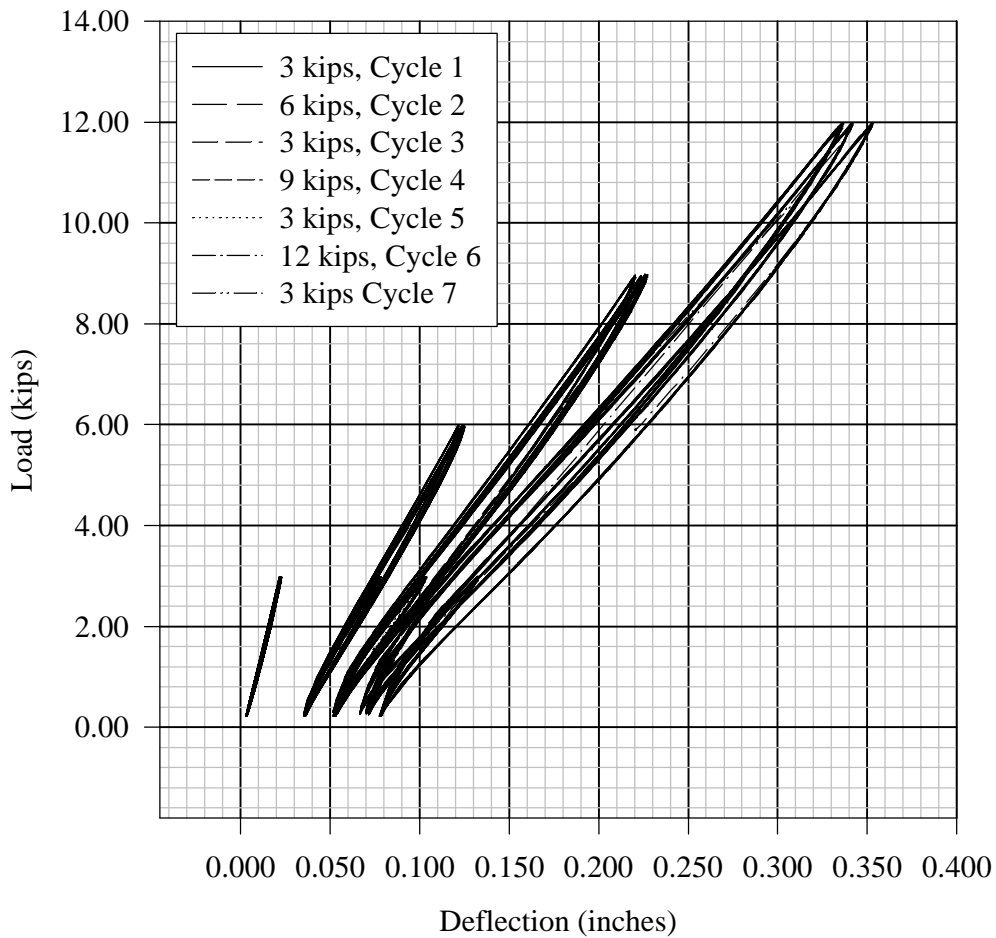
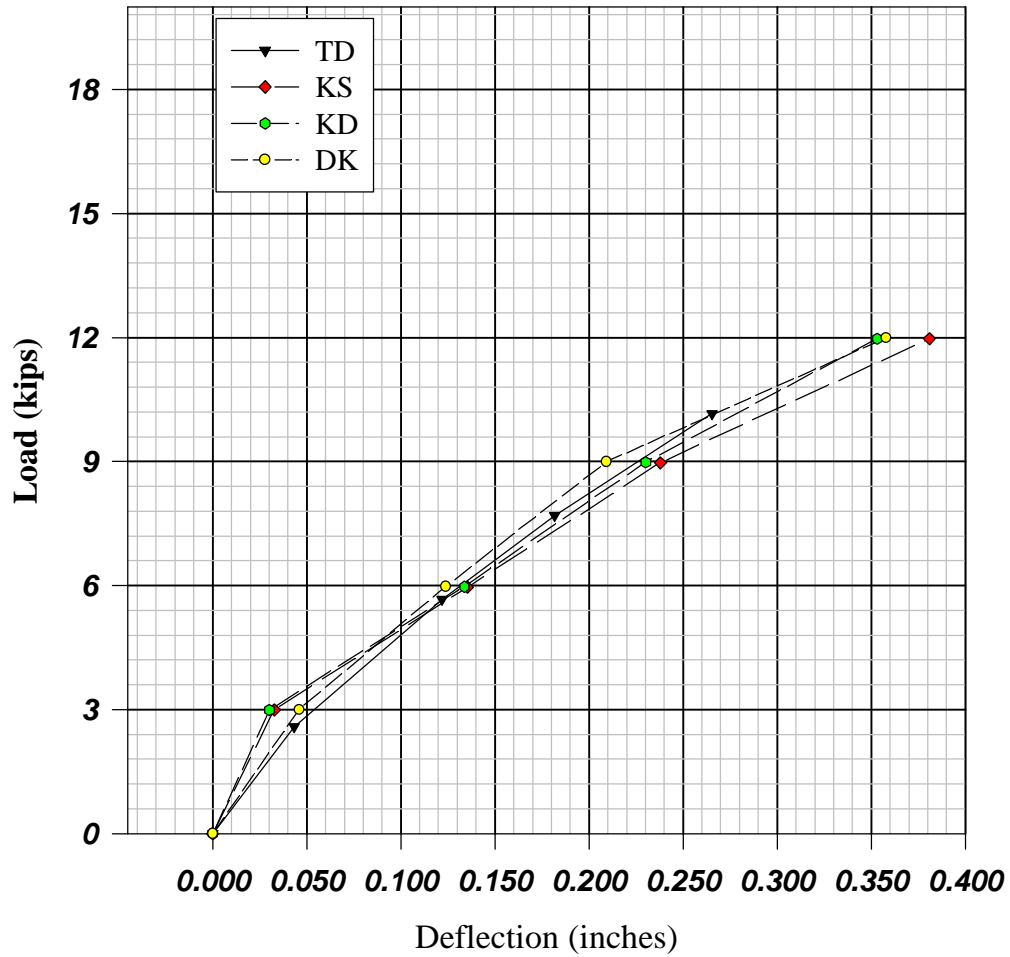


Figure 5.8 Typical Cyclic Load-Deflection Diagram.

In Figure 5.9, a plot of load versus deflection for beams with top reinforcement, beam TD deflects less than the others. The beam was not loaded to the full twelve kips, however, with

linear interpolation, the deflection is less than the other beams and shown in a chart later in this paper. The order of increasing deflection is TD, KD, DK, and KS at maximum load that was expected. In Figure 5.10, a plot of load versus deflection for beams without top reinforcement and the control beam, TD; beam TD deflects less than the others. The beam was not loaded to the full twelve kips, however, with linear interpolation, the deflection is less than the other beams and shown in a chart later in this paper. The order of increasing deflection is TD, NS, FC, and CC at maximum load that was somewhat of a surprise. It was expected that the beams FC and CC would deflect less than beam NS with CC less than FC due to a higher fiber content.

Load-Deflection



Figure

5.9 Load versus deflection for beams with top reinforcement, TD, KS, KD and DK.

Load-Deflection

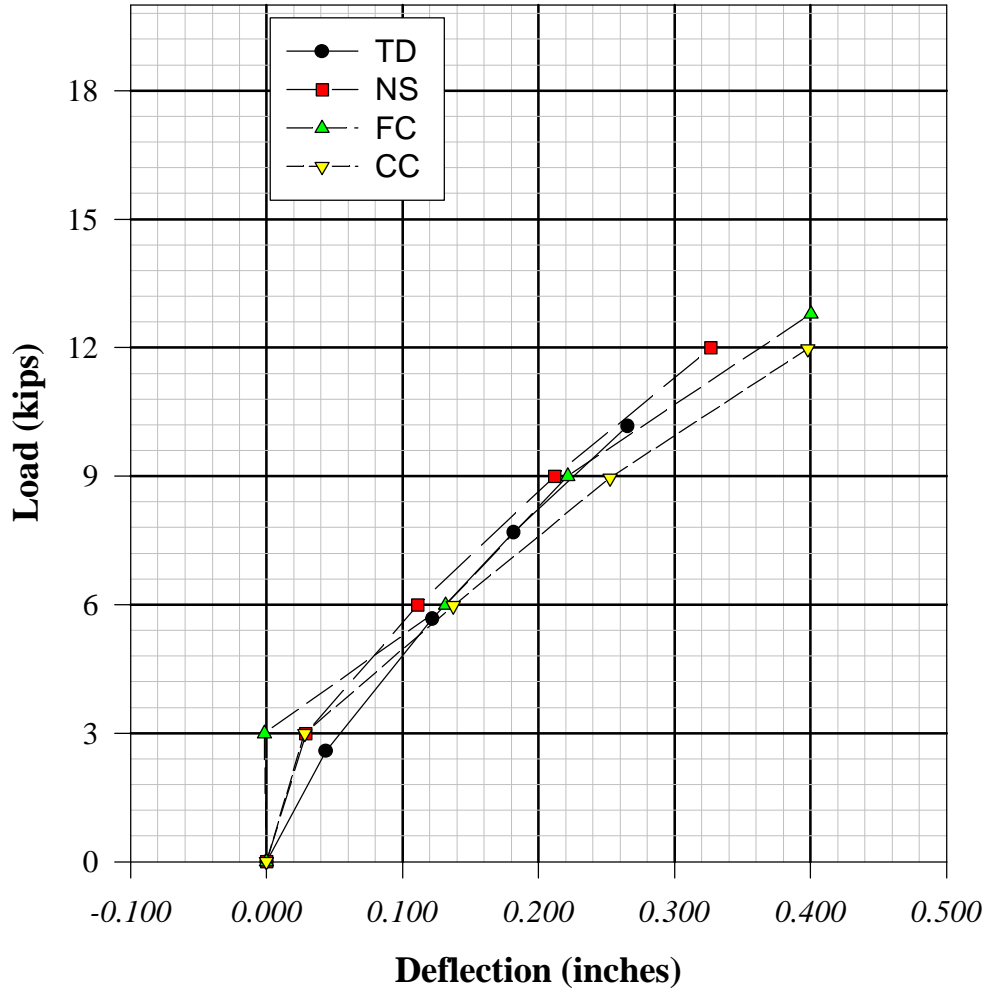
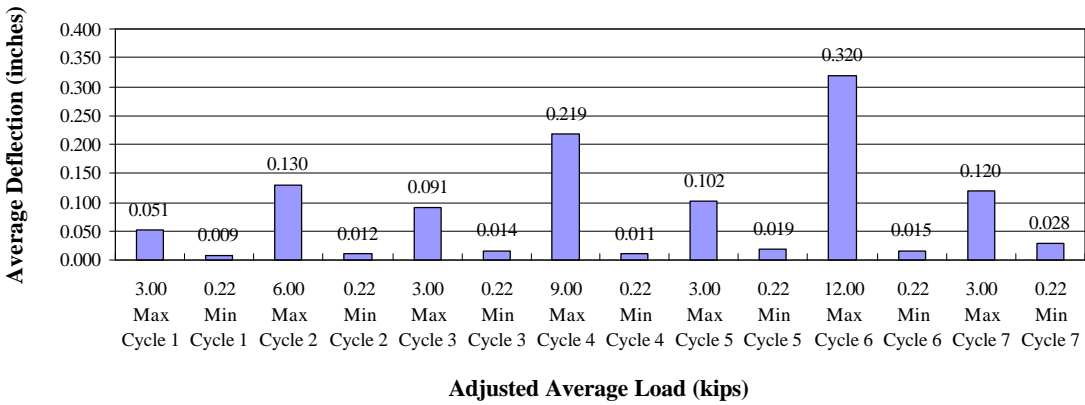


Figure 5.10 Load versus deflection for control beams and beams without top reinforcement, TD, NS, FC, and CC.

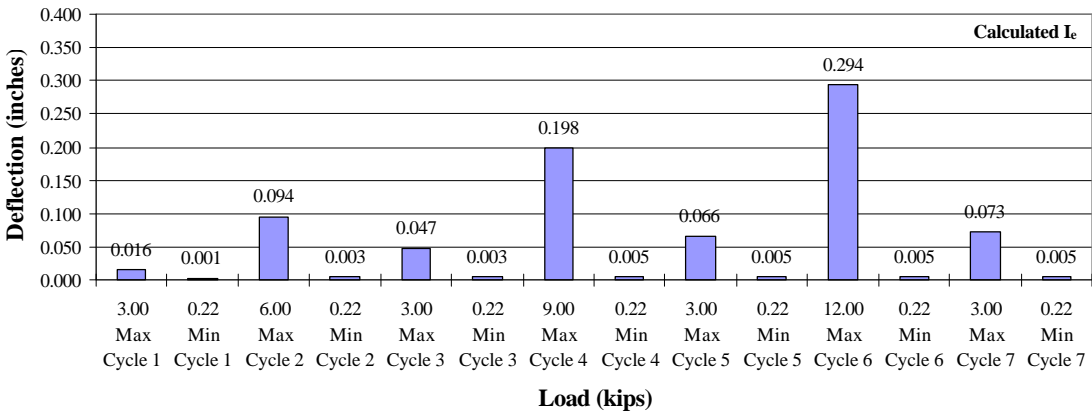
5.3.1 TD Series

Beam TD was loaded according to the cycle pattern determined and described earlier. At the initial three kip loading, the deflection was 0.051 of an inch. At the next cycle, six kip loading, 0.130 of an inch was obtained. During the second three kip loading, the maximum deflection was 0.091, a fifty percent increase from the initial three kip loading. At cycle four, nine kip loading, the deflection increased to 0.219 of an inch, nearly double the six kip load deflection. At the third three kip loading, cycle five the deflection increased slightly over the previously three kip loading. At the maximum loading of twelve kips, cycle six, the deflection increased to 0.320 of an inch, a fifty percent increase from the nine kip loading. At the last three kip cycle, the deflection in the member was 0.120 of an inch. Figure 5.11.1 shows the deflection progression due to the cyclic loading pattern established. The top chart is the linearly adjusted deflections for exact loading values. The middle chart presents the deflections based on the calculated effective moment of inertia. The calculated values underestimated the actual deflections. The bottom chart uses an effective moment of inertia equal to the cracking moment of inertia. The bottom chart shows that the expected deflection is high for loading below capacity and increases to approximately the actual as the load approaches the member capacity. The bottom chart provides the best representation of maximum deflection, that is with I_e equal to I_{cr} . The permanent deflection set in the beams was not predicted.

Adjusted Average Load-Deflections at Various Cycles for TD



Predicted Load-Deflections at Various Cycles for TD



Predicted Load-Deflections at Various Cycles for TD

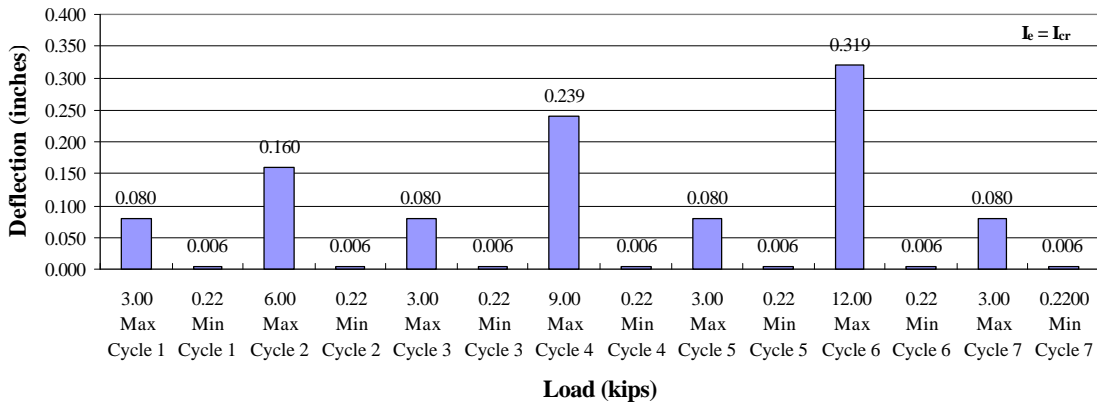


Figure 5.11.1 Chart of average and predicted load-deflection values for the minimum and maximum applied loads at each cycle for the TD beams.

5.3.2 KS Series

The KS beams were loaded in the same pattern as the control beams, TD. The initial deflection with a three kip load is less than in the TD series. Once additional loads were applied, the deflections in the KS series are greater than the control beams. At each increase in cycles, the difference in the same load applied to the TD beams is greater. The permanent deflection set into the beams is also greater than in the TD beams. The deflection in the KS beams is shown in the top chart in Figure 5.11.2. The predicted deflection using the calculated effective moment of inertia is less than actual. This is shown in the middle chart of Figure 5.11.2. The predicted deflection using the effective moment of inertia equal to the cracking moment of inertia is working until the twelve kip load is obtained. This is shown in the bottom chart of Figure 5.11.2. The twelve kip load is approximately ninety-nine percent of the calculated beam capacity. The actual deflection being greater than calculated is probably the result of variation of beam properties from those determined. The permanent deflection set in the beams was not predicted.

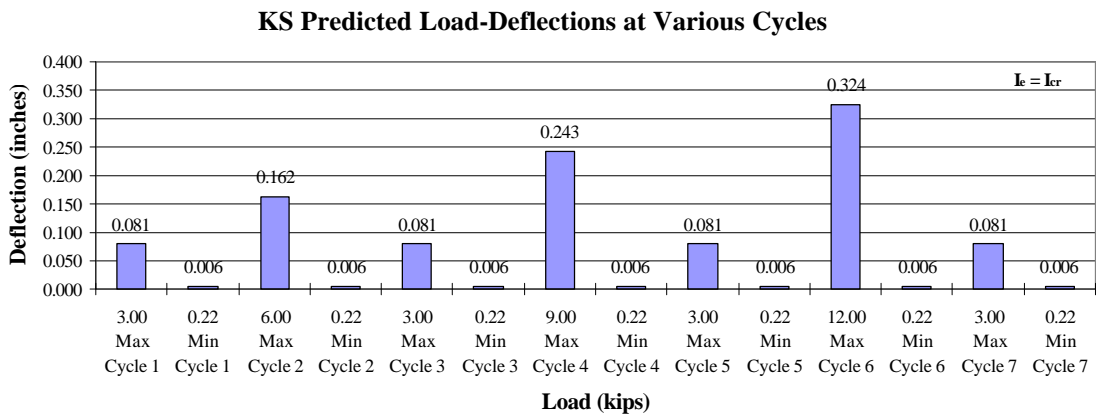
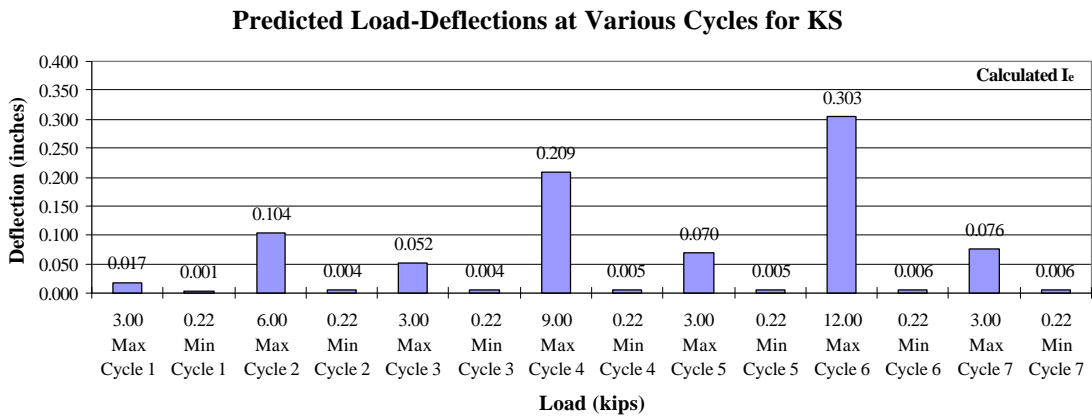
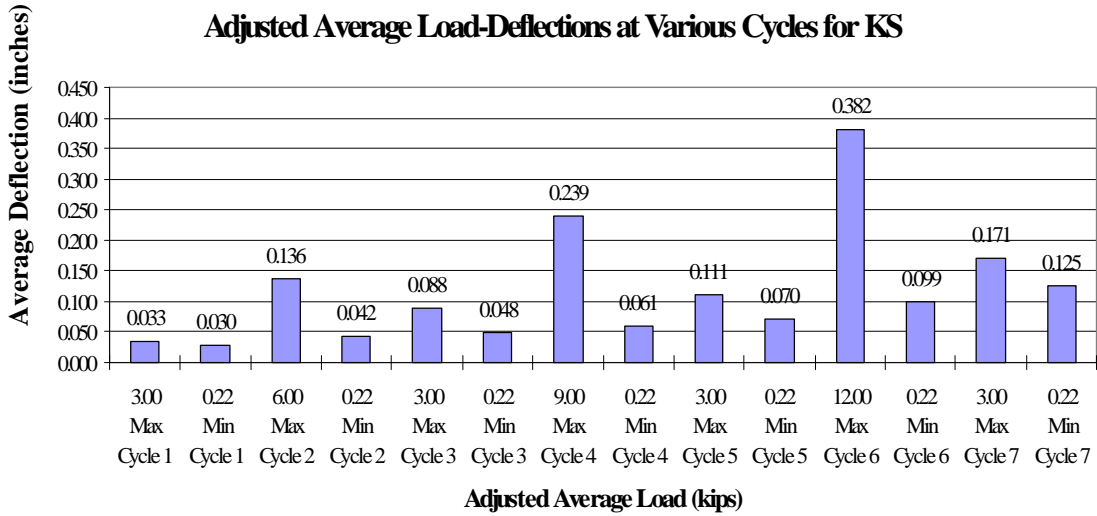


Figure 5.11.2 Chart of average load-deflection values for the minimum and maximum applied loads at each cycle for the KS beams.

5.3.3 KD Series

The KD beams were loaded in the same pattern as the control beams, TD. The initial deflection with a three kip load is less than in the TD series. Once additional loads were applied, the deflections in the KD series are greater than the control beams. At each increase in cycles, the difference in the same load applied to the TD beams is greater. The difference is less than that in the KS series. This difference is expected due to the additional FRP reinforcement bar in the top mat of reinforcement. The permanent deflection set into the beams is also greater than in the TD beams. The deflection in the KD beams is shown in the top chart in Figure 5.11.3. The predicted deflection using the calculated effective moment of inertia is less than actual and matches that for the KS series. This is shown in the middle chart of Figure 5.11.3. The predicted deflection using the effective moment of inertia equal to the cracking moment of inertia is working until the twelve kip load is obtained. This is shown in the bottom chart of Figure 5.11.3. The twelve kip load is approximately ninety-nine percent of the calculated beam capacity. The actual deflection being greater than calculated is probably the result of variation of beam properties from those determined. The permanent deflection set in the KD beam was not predicted.

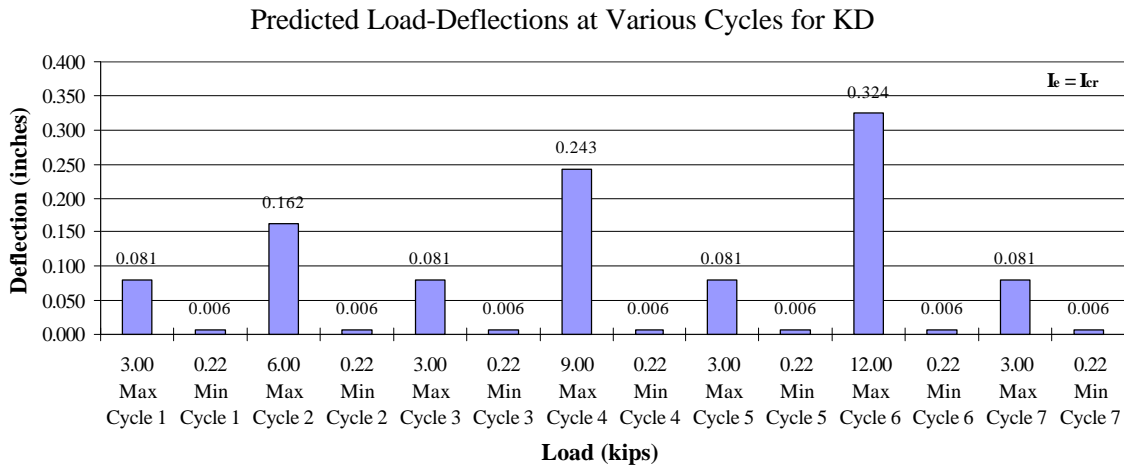
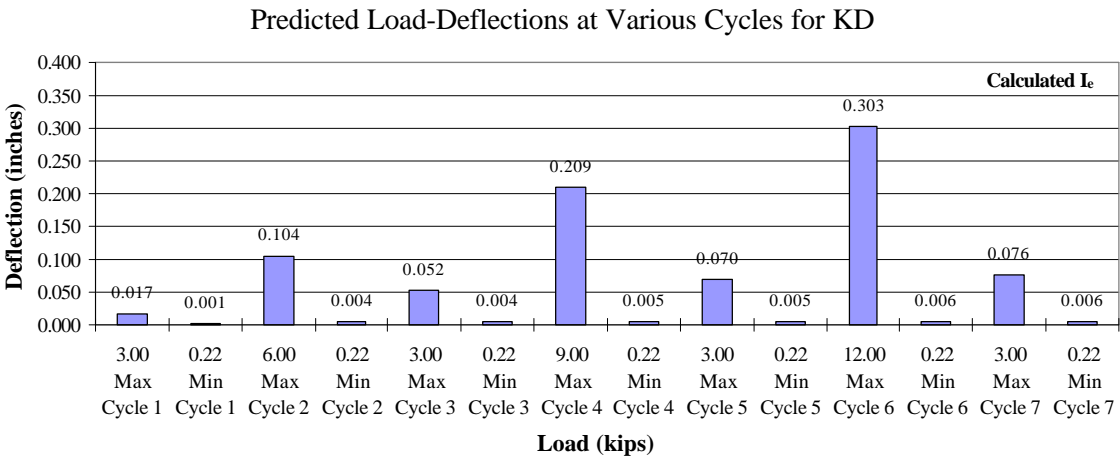
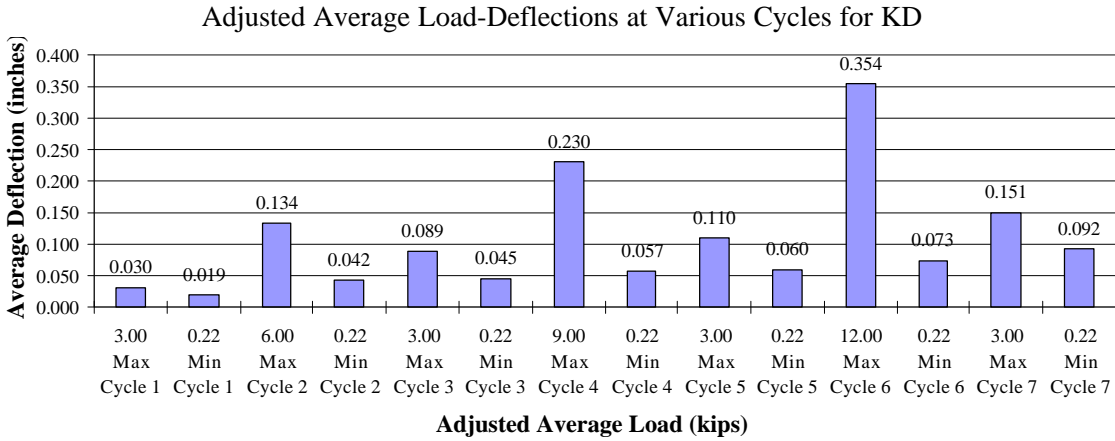


Figure 5.11.3 Chart of average load-deflection values for the minimum and maximum applied loads at each cycle for the KD beams.

5.3.4 DK Series

The DK beams were loaded in the same pattern as the control beams, TD. The deflection up to twelve kip load is less than in the TD series. At twelve kips, the deflections in the DK series are greater than the control beams. At each increase in cycles, the difference in the same load applied to the TD beams diminishes until DK deflects more than the control beams. The permanent deflection does not seem to be consistent. This can be attributed to the LVDT during the testing failing to work properly. The deflection in the DK beams is shown in the top chart in Figure 5.11.4. The predicted deflection using the calculated effective moment of inertia is less than or equal to the actual. This is shown in the middle chart of Figure 5.11.4. The predicted deflection using the effective moment of inertia equal to the cracking moment of inertia is working until the twelve kip load is obtained. This is shown in the bottom chart of Figure 5.11.4. The twelve kip load is at approximately ninety-eight percent of the calculated beam capacity. The actual deflection being greater than calculated is probably the result of variation of beam properties from those determined. Again, the permanent deflection set in the beam was not predicted.

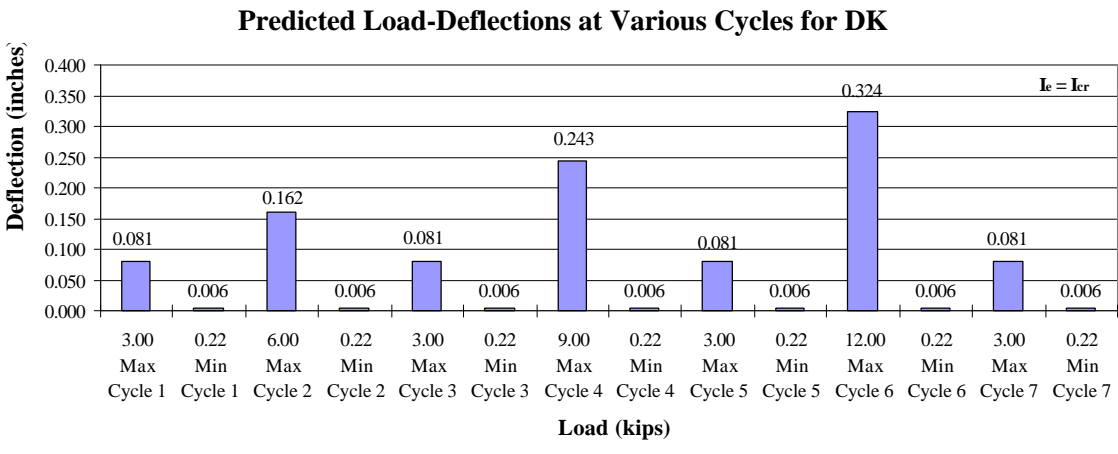
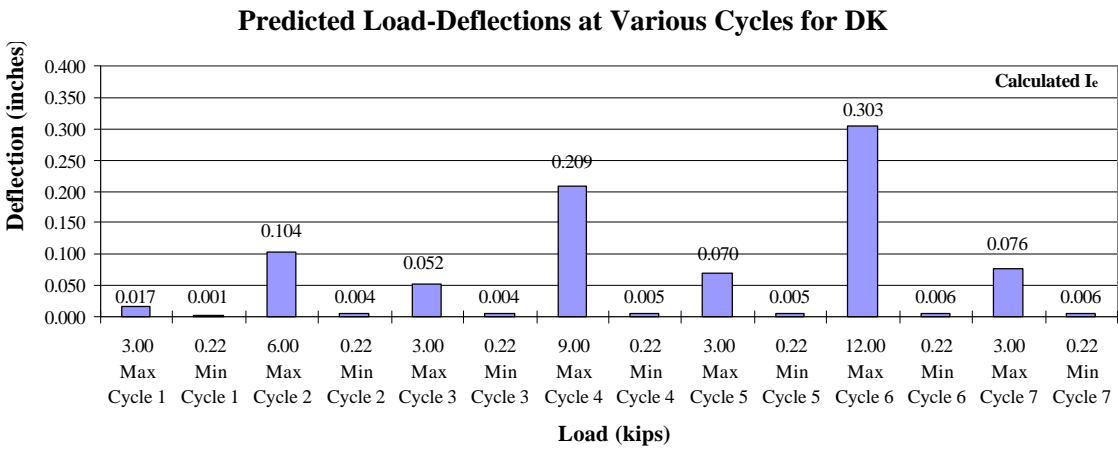
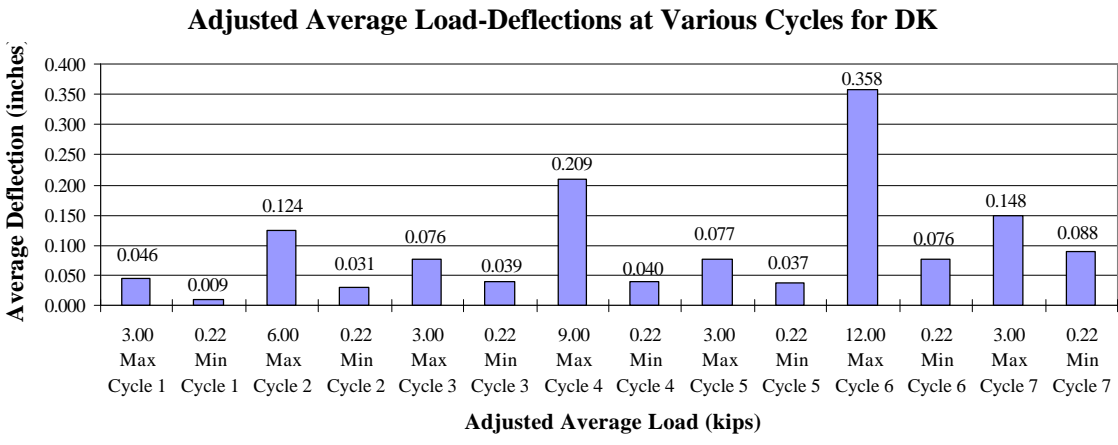
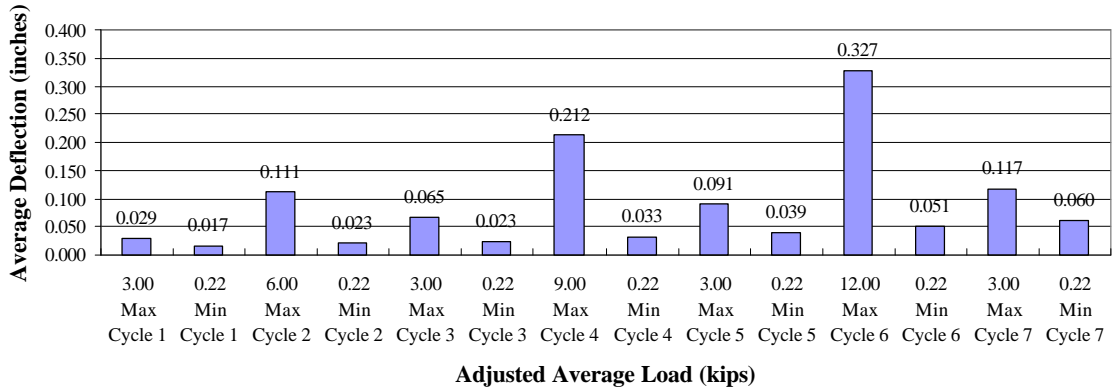


Figure 5.11.4 Chart of average load-deflection values for the minimum and maximum applied loads at each cycle for the DK beams.

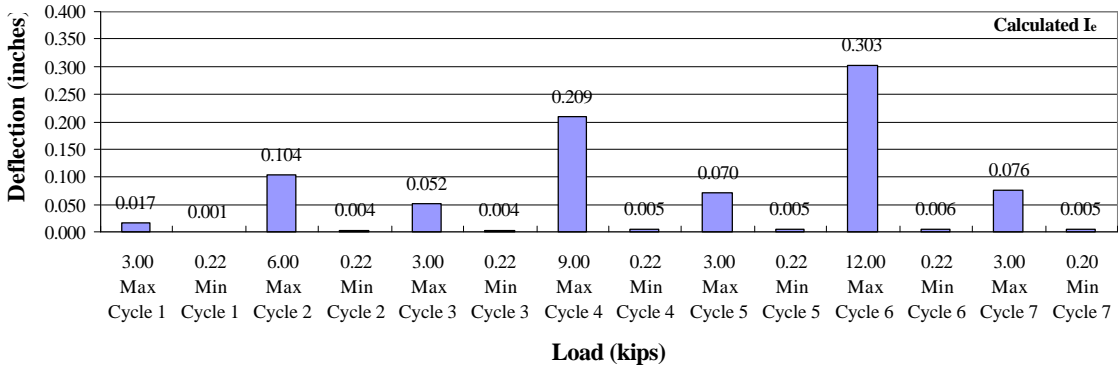
5.3.5 NS Series

The NS beams were loaded in the same pattern as the control beams, TD. The deflection up to twelve kip load is less than in the TD series. At twelve kips, the deflections in the NS series are greater than the control beams. At each increase in cycles, the difference in the same load applied to the TD beams diminishes until NS deflects more than the control beams. The deflections are not much different than the control beams, TD. The permanent deflection does not seem to be consistent. The deflection in the NS beams is shown in the top chart in Figure 5.11.5. The predicted deflection using the calculated effective moment of inertia is less than the actual deflections; however, the difference is not that great. This is shown in the middle chart of Figure 5.11.5. The predicted deflection using the effective moment of inertia equal to the cracking moment of inertia is conservative up to the twelve kip load. At the twelve kip loading, the predicted deflection is accurate. This is shown in the bottom chart of Figure 5.11.5. The twelve kip load is ninety-five percent of the calculated beam capacity. These deflections in this beam were the most accurately predictable.

Adjusted Average Load-Deflections at Various Cycles for NS



Predicted Load-Deflections at Various Cycles for NS



Predicted Load-Deflections at Various Cycles for NS

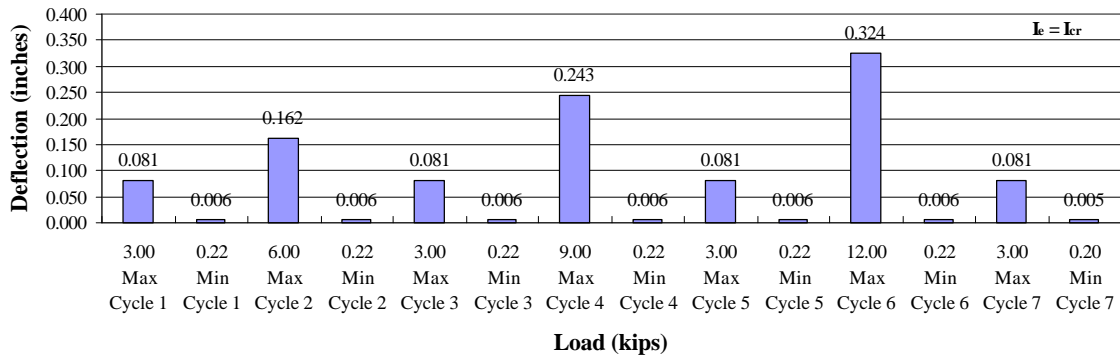


Figure 5.11.5 Chart of average load-deflection values for the minimum and maximum applied loads at each cycle for the NS beams.

5.3.6 FC Series

The FC beams were loaded in the same pattern as the control beams, TD. The deflection up to twelve kip load is similar to the TD series. At the initial three kip loading, the deflection is negative. This is attributed to either the beam rocking due to being slightly out of square or to the LVDT failure to work properly. At twelve kips, the deflections in the FC series are greater than the control beams. At each increase in cycles, the difference in the same load applied to the TD beams diminishes until FC deflects more than the control beams. The deflection in the FC beams is shown in the top chart in Figure 5.11.6. The predicted deflection using the calculated effective moment of inertia is less than the actual deflections; however, the difference is not that great. This is shown in the middle chart of Figure 5.11.6. The predicted deflection using the effective moment of inertia equal to the cracking moment of inertia is conservative up to the twelve kip load. The deflection at twelve kips is 0.050 of an inch more than predicted with effective moment of inertia equalling the cracking moment of inertia. This is shown in the bottom chart of Figure 5.11.6. The twelve kip load is ninety-nine percent of the calculated beam capacity.

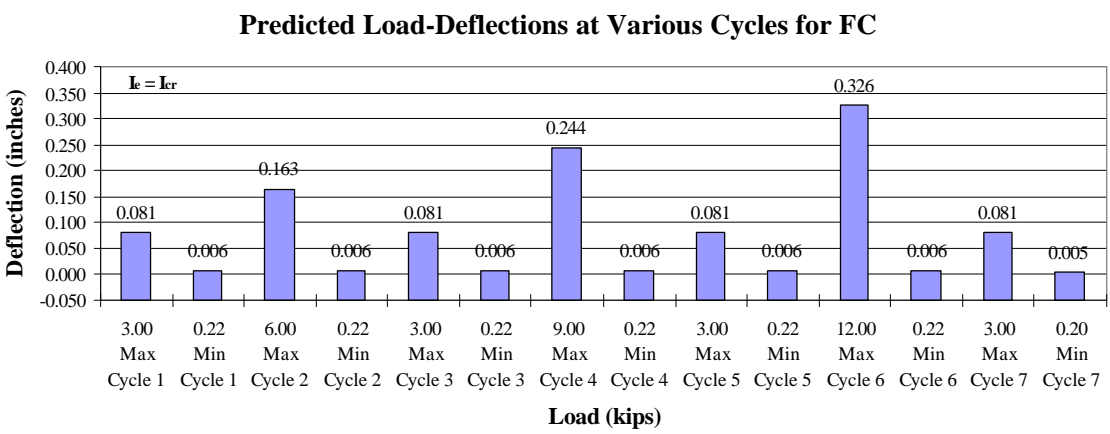
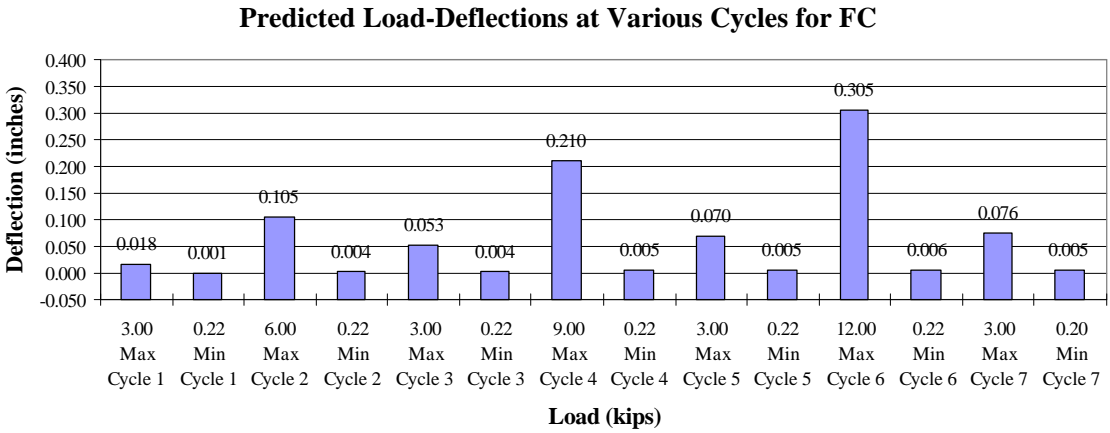
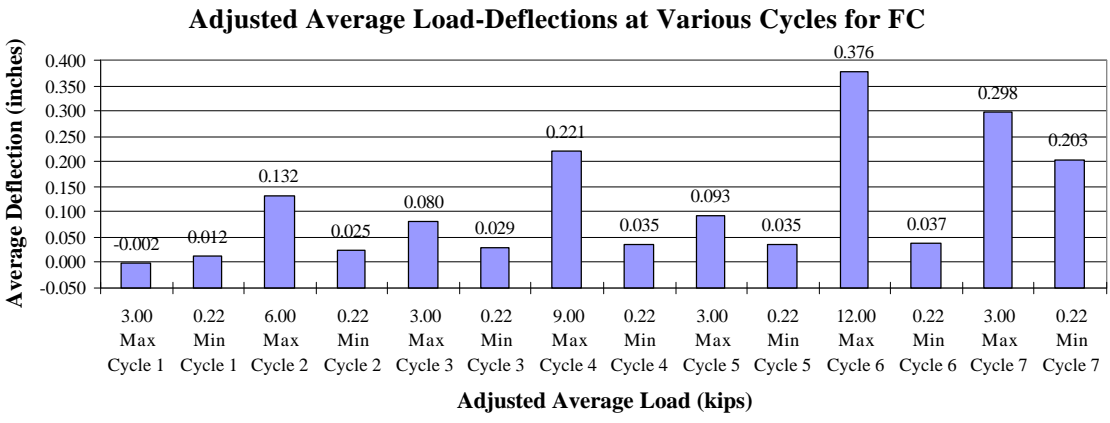


Figure 5.11.6 Chart of average load-deflection values for the minimum and maximum applied loads at each cycle for the FC beams.

5.3.7 CC Series

The CC beams were loaded in the same pattern as the control beams, TD. At the other loading cycles, the deflection in the CC beams is greater than in the control beams. At maximum load of twelve kips, the deflection in the CC series is the most deflection that occurred. At each increase in cycles, the difference in the same load applied to the TD beams increases. The permanent deflection does not seem to be consistent. The deflection in the CC beams is shown in the top chart in Figure 5.11.7. The predicted deflection using the calculated effective moment of inertia is less than the actual deflections and the accuracy is diminishing. This is shown in the middle chart of Figure 5.11.7. The predicted deflection using the effective moment of inertia equal to the cracking moment of inertia is conservative up to the six kip load. After the six kip load cycle, the predicted deflection is slightly low at nine kips and 0.072 of an inch low at the twelve kip load. The prediction is nearly twenty percent low. This is shown in the bottom chart of Figure 5.11.7. The twelve kip load is ninety-nine percent of the calculated beam capacity. The deflection at twelve kips of 0.400 inches is the greatest among the tested beams. The predicted deflection is also the worse with an error of 0.072 inches.

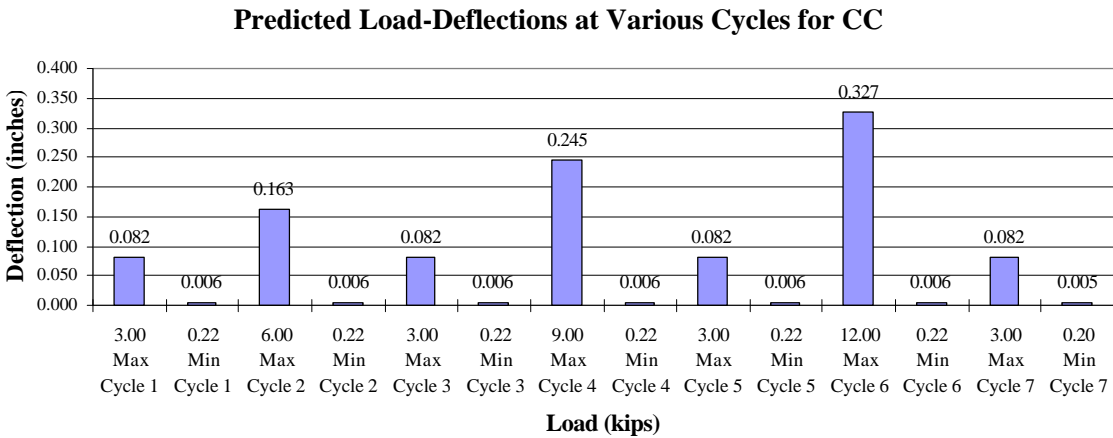
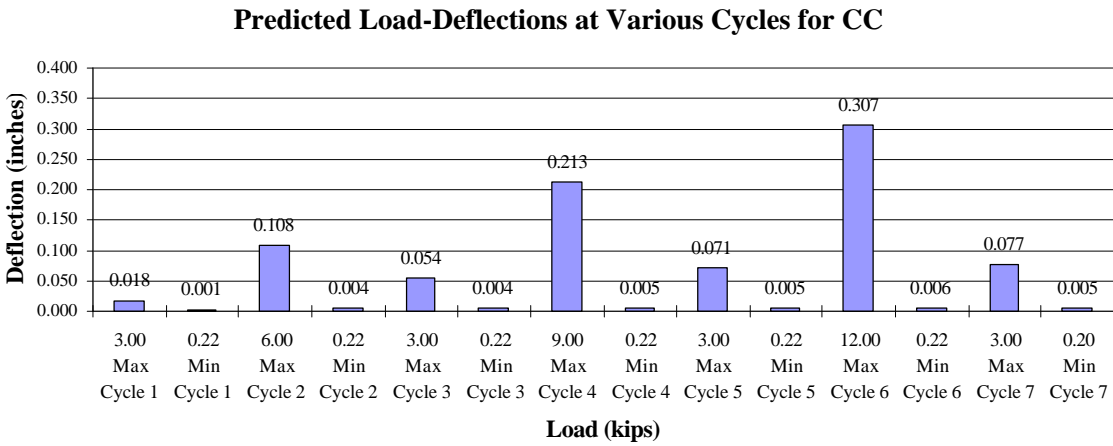
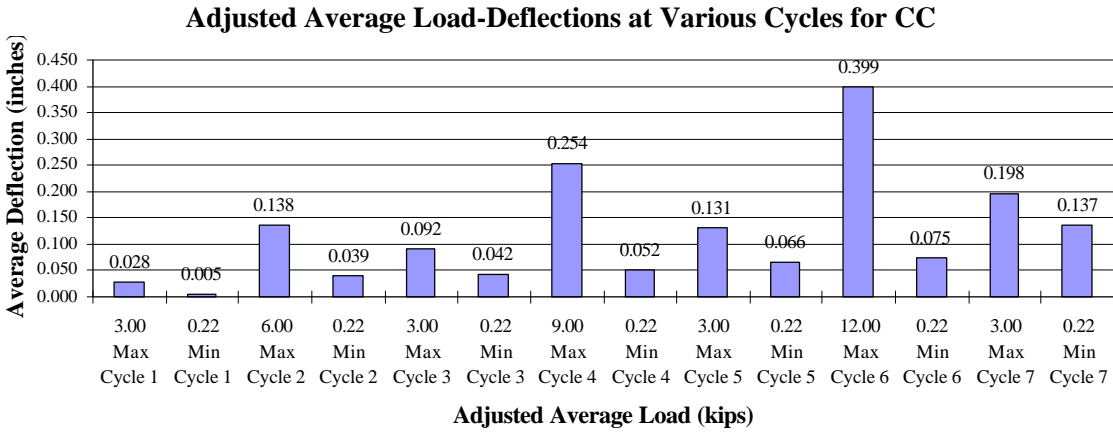


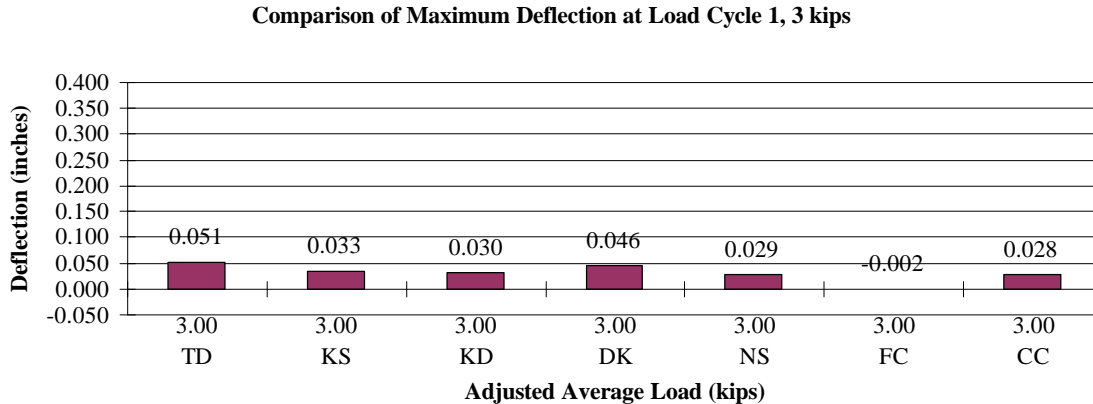
Figure 5.11.7 Chart of average load-deflection values for the minimum and maximum applied loads at each cycle for the CC beams.

5.4 Deflection By Cycle

The maximum deflection over each of the seven cycles will be examined. The changes and similarities will be discussed.

5.4.1 Cycle 1: 3 kips

Figure 5.12.1 displays the maximum deflection at the initial three kip loading cycle. The control beam, TD and beam DK had similar deflections. Beams KS, KD, NS and CC had deflections that are sixty percent less. This is surprising considering the concrete strength was lower resulting in a lower modulus of elasticity. The deflection in beam FC is negative due to fabrication of beam or the LVDT.



Figure

5.12.1 Load cycle 1 deflection of all beams.

5.4.2 Cycle 2: 6 kips

The deflection at six kips, or load cycle 2, is nearly the same for all beams. The Duradek beam, DK, and NS beam have a deflection slightly less than the others. The deflection for the six

kips load is approximately an eighth of an inch. This is shown in Figure 5.12.2. The sequence of highest deflection to lowest is TD, DK, KS, KD, NS, CC, and FC.

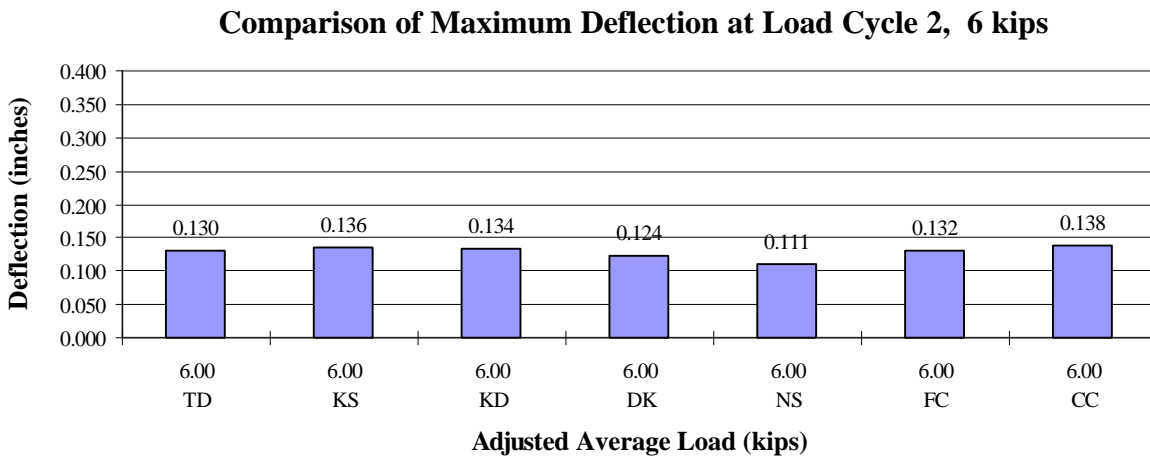


Figure 5.12.2 Load cycle 2 deflection of all beams.

5.4.3 Cycle 3: 3 kips

At load cycle three, the deflection is greater than at the initial three kip loading. The deflection is fifty to seventy-five percent of the deflection at the previous cycle. This ranges from nearly twice to four times the first three kip loading. The deflection for beams, TD, KS, KD, and CC are nearly the same. Beams DK and FC are closely matched. Beam NS has the lowest deflection whereas the highest deflection belongs to the carpet fiber beam. The order of the deflection is CC, TD, KD, KS, FC, DK, and NS. Figure 5.12.3 shows the comparisons of the third load cycle.

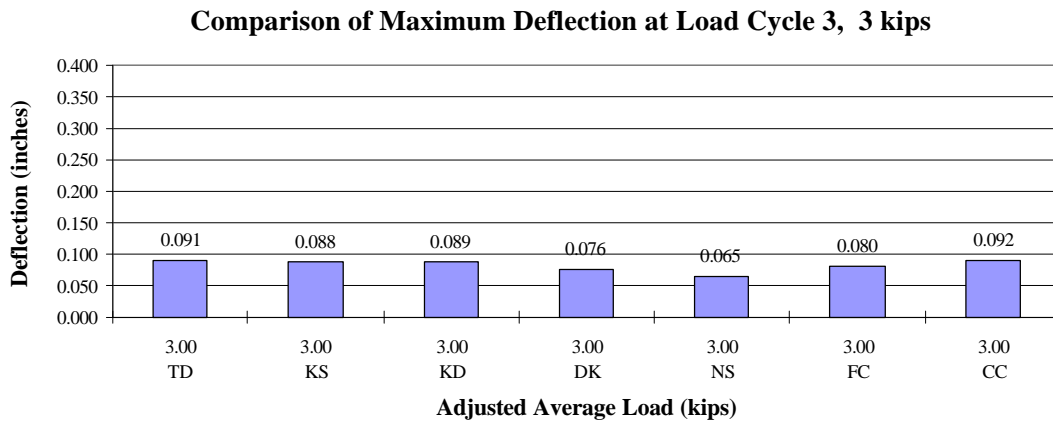


Figure 5.12.3 Load cycle 3 deflection of all beams.

5.4.4 Cycle 4: 9 kips

At nine kips, the deflections nearly double the six kip loading cycle. The average deflection is just under a quarter of an inch. The deflections at this higher load is not as close as they were at the six kip loading. The greatest deflection goes the beam containing carpet fibers, 0.254 inches. This is followed by KS, KD, FC, TD, NS and DK beams, respectively. The kodiak reinforced FRP beams and the polypropylene fiber beams now deflect more than the control beam, TD. Figure 5.12.4 Compares the deflection at load cycle, 4.

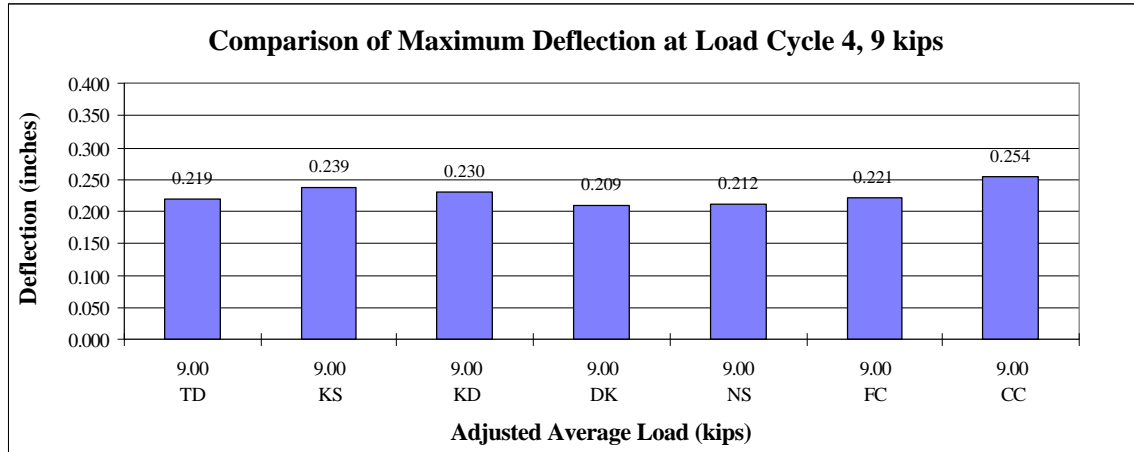


Figure 5.12.4 Load cycle 4 deflection of all beams.

5.4.5 Cycle 5: 3 kips

Load cycle 5 is the third three kip loading cycle. The deflection is greater than cycle three, three kip loading. The increase is not as much as it was from cycle one to cycle three. The order of deflections from highest is CC, KS, KD, TD, FC, NS, and finally DK. Beam CC deflects fifty percent of the nine kip loading deflection. The order of deflection remains the same as for the nine kip load. Beam TD, KS and KD are close to the same deflection with TD being the least. Beams FC and NS are similar in deflection measurements. Figure 5.12.5 shows the deflection of load cycle 5.

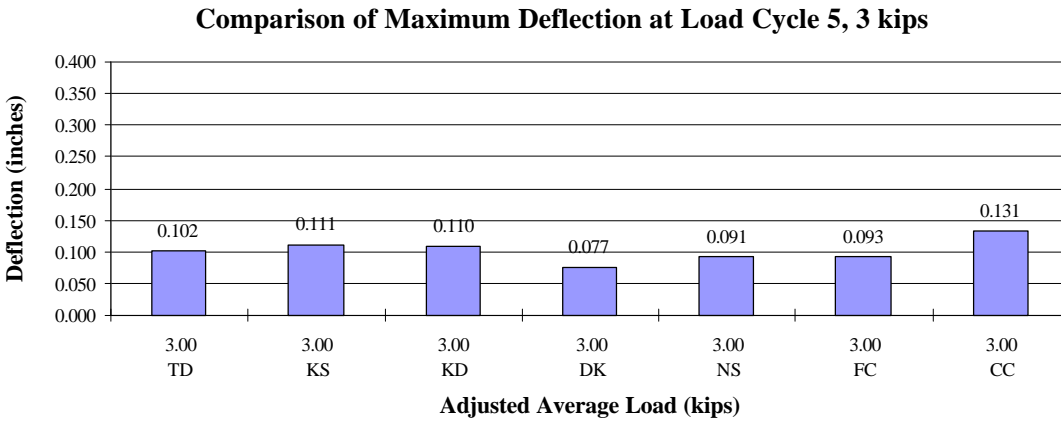


Figure 5.12.5 Load cycle 5 deflection of all beams.

5.4.6 Cycle 6: 12 kips

The maximum load cycle of twelve kips is cycle six. This was essentially capacity for all beams except the control beam, TD. This deflection showed the largest discrepancies from the predicted results. The maximum deflection, 0.399 inches, occurs at this load cycle and remains with beam CC. Beam CC is followed not too far back with beams with one kodiak #3 FRP bar in the top with a deflection of 0.382 inches. The other beams in order of highest deflection are FC, DK, KD, NS and finally, TD. The advantage of steel reinforcement is seen with beam TD last, 0.320 inches, but NS not too much greater at 0.327 inches. Figure 5.12.6 shows the maximum deflection that occurred in each of the beams.

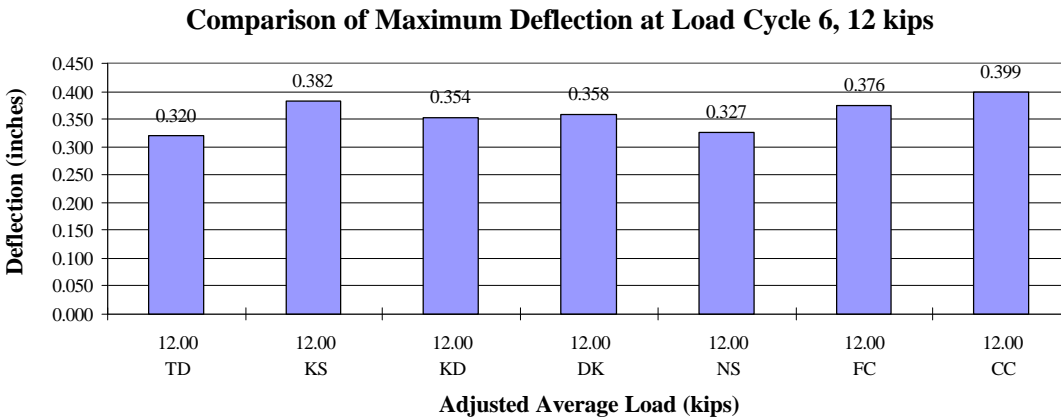


Figure 5.12.6 Load cycle 6 deflection of all beams.

5.4.7 Cycle 7: 3 kips

Figure 5.12.7 shows the deflection during the last cycle of loading. The maximum deflection is shown as beam FC. This seems high compared to the previous deflection. The other beam, CC, with polypropylene fibers is next with a deflection of 0.198 inches. The FRP beams are next in order of deflection. The steel only beams, NS and TD, are last. The deflection in the control beam, TD is 0.120 inches. This is only slightly higher than the NS beam and the deflection from the previous three kip loading cycle.

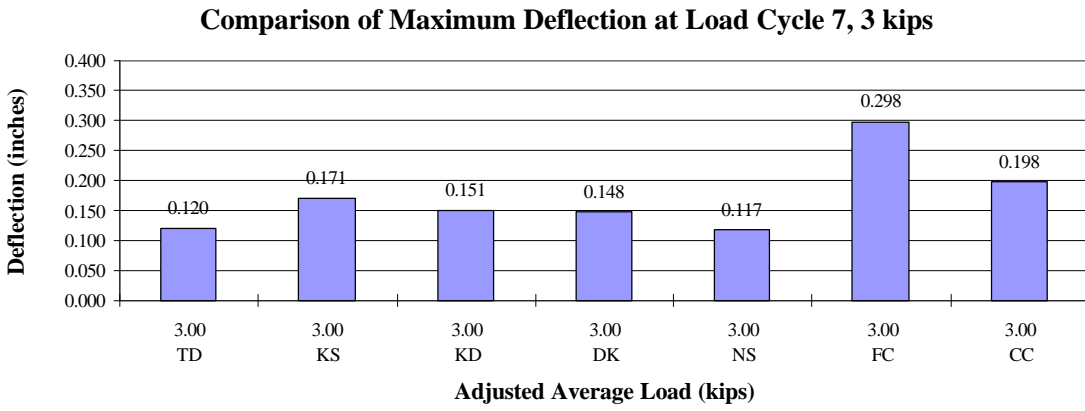


Figure 5.12.7 Load cycle 7 deflection of all beams.

CHAPTER 6

DESIGN OF BRIDGE DECKS

6.1 INTRODUCTION

This chapter uses the information gathered from this study and additional references to design a concrete bridge deck incorporating FRP reinforcement. It provides a design of a typical concrete bridge deck using standard steel reinforcement and then FRP reinforcement is used as the top mat of reinforcement. The Allowable Stress Design (ASD) and Load and Resistance Factor Design (LRFD) methods are both used to design the concrete bridge deck. A comparison of the results is presented.

6.2 DESIGN OF A BRIDGE DECK

The transverse section of the bridge deck to be designed is shown in Figure 6.1. The design will be for two traffic lanes and HS20-44 loading. For both reinforcement materials, steel and FRP, the same bridge section will be used. The beam spacing, eight feet, was chosen due to the fact it is similar to the one in this study and it is fairly common of bridges currently in use. The concrete strength, f_c' of 4,000 psi, is used for both materials. Since AASHTO Section 8.3.3 specifies that maximum f_y must be equal to or less than 60,000 psi and also because the ultimate of both materials, steel and FRP, is around 100,000 psi, the design will meet AASHTO specification for limiting reinforcement strength, f_y , as 60,000 psi.

The weight of plain concrete, w_c , is taken as 145 pcf. A future wearing surface (FWS) of fifteen pounds per square foot is assumed. Twenty pounds per square foot is assumed to provide for construction loads (CT). The deck has a half-inch integral wearing surface that does not participate in the design strength of the section. The modulus of elasticity of steel is taken as 29,000,000 psi.

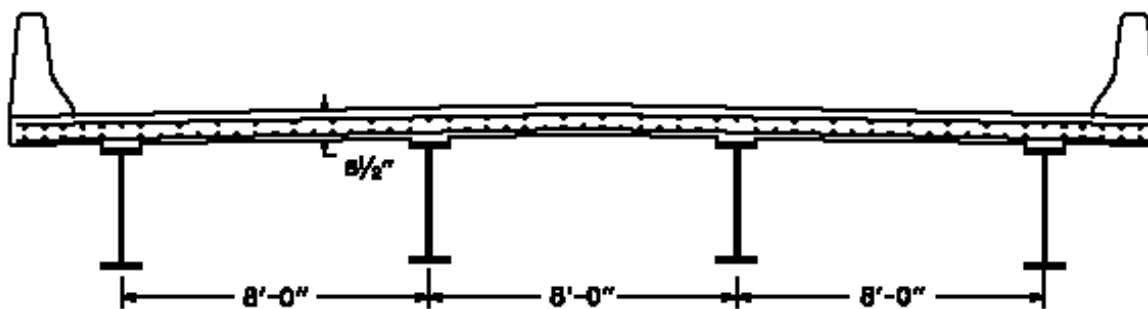


Figure 6.1 Proposed transverse section of bridge design

6.2.1 Steel Reinforcement

6.2.1.1 Allowable Stress Design Method (ASD) -- The design of this slab will use allowable stress (working stress) method. AASHTO Sec. 8.15.2.1 specifies the allowable concrete stress is $0.40f_c'$; which for f_c' equal to 4,000 psi is 1,600 psi. AASHTO Sec. 8.15.2.2 specifies that the allowable reinforcement stress is 24,000 psi for Grade 60 reinforcement. The beam is assumed to have a 12 in. flange width. The effective span length needs to be determined. For slab supported on steel stringers and continuous over more than two longitudinal supports, the effective span length, S , is given by

$$S = \text{c-c beams} - \frac{1}{2} \text{ top flange width}$$

$$= 96 \text{ in.} - \frac{1}{2} (12 \text{ in.}) = 90 \text{ in. or } 7.5 \text{ ft.}$$

The applied loads and moments are required. Dead load is

Concrete	8.5 in. (1 ft/12 in) 1.0 ft.(150 pcf) =	106.25 plf
FWS	15 psf (1 ft) =	15.00
CT	20 psf (1 ft.)	<u>20.00</u>

$$DL = 141.25 \text{ say } 145 \text{ plf}$$

$$M_{DL} = \frac{wS^2}{10} = \frac{0.145(7.5)^2}{10} = 0.82 \text{ k-ft.}$$

The live load is required. AASHTO Sec. 3.24.3.1 specifies that the live load moment formula for span continuous over more than two supports without impact is

$$M_{LL} = 0.8 \left(\frac{S+2}{32} \right) P$$

where S is in feet, P is wheel load in kips, and M_{LL} is in kip-ft. Impact is 30% for spans two feet to twenty-four feet; the range for which the equation is valid. For HS20 loading, P is sixteen kips, the load applied to one wheel. Thus, live load moment plus impact, M_{LL+I} is

$$M_{LL+I} = 0.8 \left(\frac{7.5+2}{32} \right) 16(1.30)$$

$$= 4.94 \text{ k-ft.}$$

The total bending moment is the sum of dead load and live load moment that is

$$M_T = M_{DL} + M_{LL+I} = 0.82 + 4.94 = 5.76 \text{ k-ft.}$$

Determining the required effective depth of concrete to carry this moment is the next step.

Using

$$E_s = 29,000,000 \text{ psi}$$

$$E_c = 33w^{1.5}(f_c')^{0.5}$$

$$= 3,644,147 \sim 3,644,000 \text{ psi}$$

the modular ratio can be taken as

$$n = \frac{E_s}{E_c} = 7.96 \sim 8.$$

Assume design constants, k and j , are equal to 0.375 and 0.875 as an initial estimate. Determine the minimum depth of concrete by using

$$d = \sqrt{\frac{2M_T}{kjbfc'}}$$

Substituting in the equation above yields

$$d = \sqrt{\frac{2(5760 \text{ ft} - \text{lb})(12 \text{ in} / \text{ft})}{0.375(0.875)(12 \text{ in})(1600 \text{ psi})}}$$

$$= 4.68 \text{ in.}$$

Determine the minimum deck thickness by adding the minimum cover for the reinforcement.

Minimum top and bottom reinforcement cover is two inches and one inch, respectively, per AASHTO Sec. 8.22.1. The distance from top of deck slab to centroid of top reinforcement is

$$0.5 + 2.0 + \frac{1}{2} * d_b = 2.8125 \text{ in.}$$

where 0.5 inch being an integral wearing surface.. The distance from bottom of deck slab to centroid of bottom reinforcement is

$$1.0 + \frac{1}{2} * d_b = 1.3125 \text{ in.}$$

Minimum depth of slab is

$$2.8125 + 4.68 = 7.6125 \text{ in.}$$

Use t_s equal to 8.5 inches to give a design section equivalent to test beams with an additional 0.5 inch integral wearing surface.

For positive moment regions,

$$\text{actual } d = 8.5 \text{ in.} - 1.3125 \text{ in.} - 0.5 = 6.6875 \text{ in.},$$

$$d' = 2.8125 \text{ in.} - 0.5 \text{ in.} = 2.3125 \text{ in.},$$

and

$$t_s = 8.0 \text{ in.} + \frac{1}{2} \text{ in.} \text{ integral wearing surface.}$$

For negative moment regions,

$$\text{actual } d = 8.5 \text{ in.} - 2.8125 \text{ in.} = 5.6875 \text{ in.},$$

and

$$d' = 1.3125 \text{ in.}$$

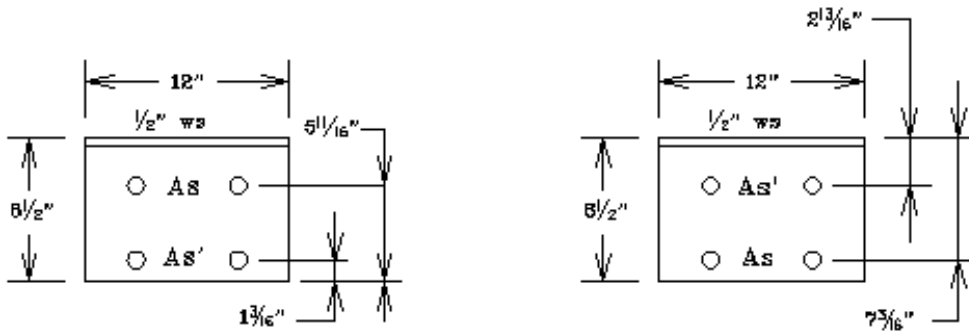
The same moment is applied in the positive and negative moment regions of the deck. This results in the negative moment region controlling the area of steel required due to a lower value of d .

Determine the required deck reinforcement by using

$$A_s = \frac{M_T}{f_s d} = \frac{5760 \text{ ft} - \text{lb}(12 \text{ in} / \text{ft})}{24000 \text{ psi}(0.875)(5.6875 \text{ in})} = 0.579 \text{ in}^2$$

Try #5 bars @ 6 in. , $A_s = 0.62 \text{ in}^2$ per foot.

Figure 6.2 shows the design sections. The section capacity of the negative moment region will govern due to the smaller moment arm.



a) Section over Beam, Negative Moment Region b) Section between Beam, Positive Moment Region

Figure 6.2 Section of deck design a) over support and b) at midspan.

Determine steel ratios, ρ and ρ'

$$r = \frac{A_s}{bd} \qquad r' = \frac{A_s'}{bd}$$

where

$$A_s = A_s' = 0.62 \text{ in}^2/\text{ft.}$$

The steel ratios are identical for top and bottom reinforcement

$$r = r' = \frac{0.62 \text{ in}^2}{(12 \text{ in})(5.6875 \text{ in})}$$

$$= 0.009084.$$

Determine the design constant, k . The constant, k , is different for a tension reinforced section and a doubly reinforced section (Everard, 1993). Both will be examined. For tension reinforced section,

$$k = \sqrt{2nr + (nr)^2} - nr$$

which gives

$$k = \sqrt{2(8)(0.009084) + (8 * 0.009084)^2} - (8)(0.009084) = 0.315.$$

For doubly reinforced section,

$$k = \sqrt{[nr + (2n - 1)r']^2 + 2[nr + (2n - 1)r' \frac{d'}{d}] - [nr + (2n - 1)r']}$$

which gives

$$k = \sqrt{[8(0.009084) + (2(8) - 1)0.009084]^2 + 2[8(0.009084) + (2(8) - 1)(0.009084) \left(\frac{1.3125}{5.6875} \right)] - [8(0.009084) + (2(8) - 1)0.009084]} = 0.293.$$

With k now determined, the neutral axis, kd can be located. For tension reinforcement only,

$$\text{N.A.} = kd = (0.315)(5.6875 \text{ in.}) = 1.794 \text{ in.}$$

For double reinforcement,

$$\text{N.A.} = kd = (0.293)(5.6875 \text{ in.}) = 1.666 \text{ in.}$$

With the neutral axis located, the stresses in the concrete and reinforcement can be determined and then the moment capacity of the section.

Figure 6.3 shows the section and the representative linear stress diagram. The compression area of steel is ignored for a singly reinforced section. This lowers the neutral axis due to higher stress in the concrete required. For tension reinforced section, set

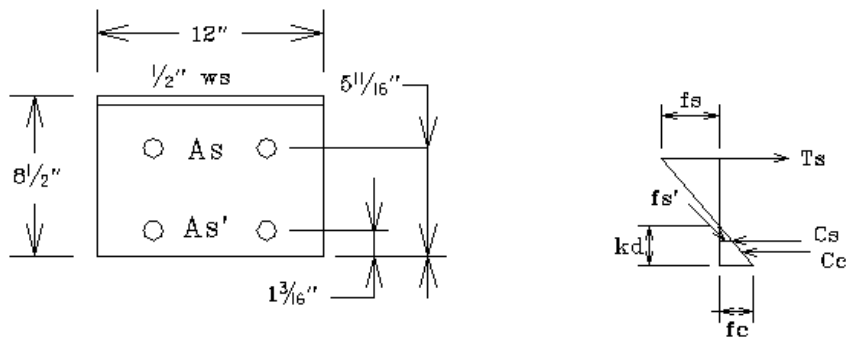
$$f_s = 24,000 \text{ psi}$$

$$f_c = \frac{f_s k}{n(1 - k)} \leq 0.40 f'_c$$

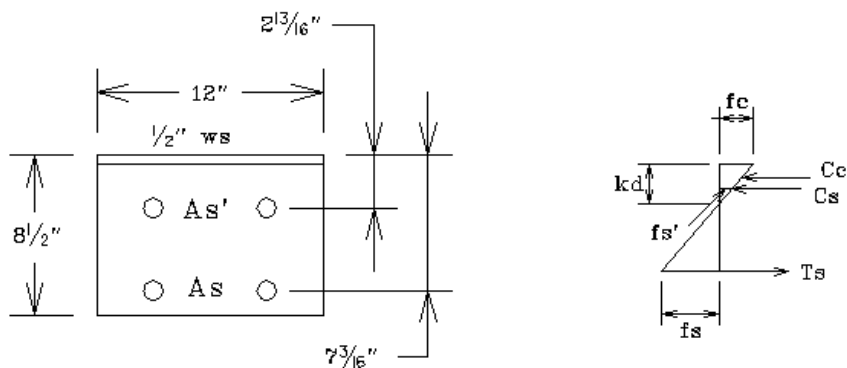
$$C_c = \frac{1}{2}f_c b k d$$

$$T_s = A_s f_s$$

$$M_n = T_s(d - k d) + C_c(k d - k d / 3)$$



a) Section over Beam, Negative Moment Region



b) Section between Beam, Positive Moment Region

Fig. 6.3 Stress diagrams for a) negative and b) positive moment region.

Substituting example variables

$$f_c = \frac{(24,000 \text{ psi})(0.315436)}{8(1 - 0.315436)} = 1,382 \text{ psi} < 0.40f_c' = 1,600 \text{ psi}$$

If f_c had been greater than allowable then it would be necessary to set f_c equal to 1,600 psi and determine f_s .

$$C_c = \frac{1}{2} (1,382 \text{ psi})(12 \text{ in})(1.794 \text{ in}) = 14,880 \text{ lbs.}$$

$$T_s = (0.62 \text{ in}^2)(24,000 \text{ psi}) = 14,880 \text{ lbs.}$$

$$C_c = T_s = 14,880 \text{ lbs.}$$

$$M_n = (14,880 \text{ lbs})(5.6875 - 1.794)(\text{in}) + (14,880 \text{ lbs})(1.794 - 1.794/3)(\text{in})$$

$$M_n = 75,731 \text{ in-lb} = 6,310 \text{ ft-lb} > 5,760 \text{ ft-lb needed.}$$

For doubly reinforced section, set

$$f_s = 24,000 \text{ psi}$$

$$f_c = \frac{f_s k}{n(1-k)} \leq 0.40 f'_c$$

$$f'_c = 2nf_c \frac{k - \frac{d'}{d}}{k}$$

$$C_c = \frac{1}{2} f_c b k d$$

$$C_s = A_s' f'_s$$

$$T_s = A_s f_s$$

$$M_n = T_s(d-kd) + C_c(kd-kd/3) + C_s(kd-d')$$

Substituting example variables

$$f_c = \frac{(24,000 \text{ psi})(0.292952)}{8(1-0.292952)} = 1,243 \text{ psi} < 0.40 f'_c = 1,600 \text{ psi} \quad \text{OK}$$

If f_c had been greater than allowable then it here again it would be necessary to set f_c equal to 1,600 psi and determine f_s and f'_s .

$$f'_s = 2(8)(1,243 \text{ psi}) \frac{0.293 - \frac{1.3125 \text{ in}}{5.6875 \text{ in}}}{0.293}$$

$$= 4,221 \text{ psi}$$

$$C_c = \frac{1}{2} (1,243 \text{ psi})(12 \text{ in})(1.666 \text{ in})$$

$$= 12,425 \text{ lbs}$$

$$\begin{aligned}
C_s &= 0.62 \text{ in}^2 (4,221 \text{ psi}) \\
&= 2,617 \text{ lbs} \\
T_s &= (0.62 \text{ in}^2)(24,000 \text{ psi}) \\
&= 14,880 \text{ lbs} \\
C_c + C_s &\approx T_s \\
12,425 + 2,617 &\approx 14,880 \\
15,042 &\approx 14,880 \text{ lbs}
\end{aligned}$$

The difference is due to round off. This produces a moment

$$\begin{aligned}
M_n &= (14,880 \text{ lbs})(5.6875 - 1.666)(\text{in}) + (12,425 \text{ lbs})(1.666 - 1.666/3) (\text{in}) \\
&\quad + 2,617(1.666 - 1.3125) \\
M_n &= 74,565 \text{ in-lb} = 6,213 \text{ ft-lb} > 5,760 \text{ ft-lb needed.}
\end{aligned}$$

Distribution reinforcement provides for the lateral distribution of the concentrated wheel loads. It is placed perpendicular to the main reinforcement and placed in the bottom of the slab.

Distribution reinforcement is a percentage of the main reinforcement and is determined by

$$D = \frac{220}{\sqrt{S}} \leq 0.67 \quad \text{AASHTO Sec. 3.24.10.2.}$$

For S equal to 7.5 ft,

$$D = 0.80 > 0.67.$$

Distribution area of steel is thus 67 percent of the strength steel, which is

$$A_s(0.67) = 0.62(0.67) = 0.42 \text{ in}^2 \text{ per foot.}$$

Try # 4 @ 5.5 in. = 0.44 in² per foot.

Check deflection of the deck slab. Determine the gross transformed moment of inertia, I_{gt} , in the positive moment area. Using

$$A_c = bh = (12 \text{ in})(8 \text{ in}) = 96 \text{ in}^2$$

$$A'_{st} = (n-1)A'_s = (8-1)(0.62) = 4.34 \text{ in}^2$$

$$A_{st} = nA_s = 8(0.62) = 4.96 \text{ in}^2$$

In the forms below we can get the moment of inertia.

	A in²	y in	Ay in³
Concrete	96	4.0	384
Top	4.34	2.3125	10.0363
Bottom	4.96	6.6875	33.17
Σ	105.3		427.2063

$$y_t = \frac{\sum Ay}{\sum A} = \frac{427.2063}{105.3} = 4.0570 \text{ in.} \quad \bar{y} = (y - y_t)$$

	A in²	\bar{y} in	$A\bar{y}^2$ in⁴	I_x in⁴
Concrete	96	-0.0570	0.3119	512
Top	4.34	-1.7445	13.2078	-
Bottom	4.96	2.6305	34.3209	-
Σ			47.8406	512

$$I_{gt} = A\bar{y}^2 + I_x = 559.8406 \cong 560 \text{ in}^4 .$$

Determine the gross transformed moment of inertia, $I_{g,,}$, for the negative moment area.

	A in²	y in	Ay in³
Concrete	96	4.0	384
Top	4.34	1.3125	5.69625
Bottom	4.96	5.6875	28.21
Σ	105.3		417.90625

$$y_t = \frac{\sum Ay}{\sum A} = \frac{417.90625}{105.3} = 3.9687 \text{ in.}$$

$$\bar{y} = (y - y_t)$$

	A in²	\bar{y} in	A \bar{y}^2 in⁴	I_x in⁴
Concrete	96	0.0313	0.0941	512
Top	4.34	-2.6562	30.6204	
Bottom	4.96	1.7188	14.6532	
Σ			45.3677	512

$$I_{gt} = A \bar{y}^2 + I_x = 557.3677 \cong 557 \text{ in}^4.$$

The moment of inertia is nearly identical for positive and negative moment region.

Determine the cracked moment of inertia, I_{cr} , for positive moment area. Assume neutral axis is above both rows of reinforcement which are in tension.

	A in²	y in.	Ay in³
Concrete	12c	c / 2	6c ²
Top	4.96	c - 2.3125	4.96c - 11.47
Bottom	4.96	c - 6.6875	4.96c - 33.17
Σ			6c ² + 9.92c - 44.64

Solving the quadratic for c yields

$$c = 2.0235 \text{ in.} < 2.3125 \text{ in. as assumed.}$$

Determine the moment of inertia by substituting in above table the value of c calculated above.

	A in²	\bar{y} in	$A\bar{y}^2$ in⁴	I_x in⁴
Concrete	24.282	1.0118	24.8584	8.2853
Top	4.96	-0.289	0.4143	-----
Bottom	4.96	-4.664	107.8944	-----
Σ			133.1671	8.2853

$$I_{cr} = Ay^2 + I_x = 141.4524 \cong 141 \text{ in}^4$$

Determine the cracked moment of inertia, I_{cr} , for negative moment area. Assume neutral axis both rows of reinforcement are in tension.

	Area in.	y in.	Ay^2 in⁴
Concrete	12c	c / 2	6c ²
Top	4.96	c - 1.3125	4.96c - 6.51
Bottom	4.96	c - 5.6875	4.96c - 28.21
Σ			6c ² + 9.92c - 34.72

Solving the quadratic for c yields

$c = 1.717 \text{ in.} > 1.3125 \text{ in.}$ Neutral axis is below the reinforcement. Compression reinforcement is present. Repeat calculations assuming neutral axis lies between the reinforcement.

	Area in ²	y in.	Ay ² in ⁴
Concrete	12c	c/2	6c ²
Top	4.34	c - 1.3125	4.34 c - 5.69625
Bottom	4.96	c - 5.6875	4.96c - 28.21
Σ			6c ² + 9.30c - 33.90625

Solving the quadratic for c yields

$$c = 2.5 \text{ in.} > 1.3125 \text{ in. as assumed; OK}$$

Determine the moment of inertia by substituting the calculated value for c in the form below.

	A in ²	\bar{y} in	A \bar{y}^2 in ⁴	I _x in ⁴
Concrete	30	1.25	46.8812	15.625
Top	4.34	1.1875	6.1201	----
Bottom	4.96	-3.1875	<u>50.3944</u>	----
Σ			103.3957	

$$I_{cr} = Ay^2 + I_x = 119.05207 \cong 119 \text{ in}^4.$$

Since the worse deflection should be with the effective moment of inertia equal to I_{cr}, the average I_{cr} [(141+119) / 2 = 130 in⁴] for the positive and negative region will be used.

Determine the deflection downward due to applied uniform and point loads, respectively,

$$\Delta_D = \frac{5wS^4}{384EI} = \frac{5(145 \text{ plf})(7.5 \text{ ft})^4 (1,728 \frac{\text{in}^3}{\text{ft}^3})}{384(3,644,000 \text{ psi})(130 \text{ in}^4)} = 0.0218 \text{ in.}$$

$$\Delta_{LL+I} = \frac{PS^3}{48EI} = \frac{20,800 \text{ lbs}(7.5 \text{ ft} * 12 \frac{\text{in}}{\text{ft}})^3}{48(3,644,000 \text{ psi})(130 \text{ in}^4)} = 0.6668 \text{ in.}$$

Determine the deflection upward due to resisting moment

$$\Delta_M = \frac{M S^2}{8EI} = \frac{5,760 \text{ ft-lbs} (7.5 \text{ ft} * 12 \frac{\text{in}}{\text{ft}})^2}{8(3,644,000 \text{ psi})(130 \text{ in}^4)} = 0.1477 \text{ in.}$$

This produces a total deflection of 0.0218 in. + 0.6668 in. – 0.1477 in. = 0.5409 in.

6.2.1.2 Load and Resistance Factor Design Method (LRFD) -- The same bridge deck section will be design by the LRFD procedure. This will show the differences in reinforcement and provide deflection criteria. The method of determining live load is different in the LRFD AASHTO. In order to have the same service load deflections, the load factors from building design shall be used. The design loads from ASD method will be used to obtain a design moment using

$$M_u = \phi M_n = 1.4M_D + 1.7M_{LL+I}$$

Where M_u is the ultimate moment and ϕM_n is the design moment.

This resolves into

$$M_u = 1.4(0.82) + 1.7(4.94) = 9.55 \text{ ft-kips.}$$

Estimating an area of steel by equation

$$A_s = \frac{M_u}{f_y j d}.$$

Substituting in previous values from the ASD analysis gives an area of steel, A_s , equal to 0.426 square inches per foot. #5 bars at 8 ½ in. spacing gives A_s equal to 0.438 sq. inches per foot. Checking the section capacity is next. For tension only section, determine a by

$$a = \frac{T_s}{0.85 f_c' b} = \frac{60,000 \text{ psi}(0.438 \text{ in}^2)}{0.85(4,000 \text{ psi})(12 \text{ in})} = 0.644 \text{ in.}$$

$$\begin{aligned} fM_n &= f A_s f_y \left(d - \frac{a}{2}\right) \\ &= 0.9(0.438 \text{ in}^2)(60,000 \text{ psi})(5.6875 - \frac{0.644}{2})(\text{in}) \frac{1 \text{ ft}}{12 \text{ in}} \\ &= 10.58 \text{ ft-kips.} \end{aligned}$$

For doubly reinforced section, we need to determine the stress in the top reinforcement. Assume the strain in the reinforcement is less than yield.

$$T_s = A_s f_y$$

$$T_s' = A_s' e_s' E_s \frac{d-c}{c}$$

$$C_c = 0.85 f_c' b \beta_1 c$$

Set C_c equal to $T_s' + T_s$. Substituting and inserting known values gives

$$\begin{aligned} 0.85 f_c' b \beta_1 c &= A_s' e_s' E_s \frac{d-c}{c} + A_s f_y \\ 0.85(4,000 \text{ psi})(12 \text{ in})0.85c &= (0.438 \text{ in}^2)(0.003)(29,000,000 \text{ psi}) \frac{5.6875 \text{ in} - c}{c} \\ &\quad + 0.438 \text{ in}^2 (60,000 \text{ psi}) \end{aligned}$$

Solving the equation for c gives $c = 1.042$ in. which is less than 1.3125 in. as assumed. Check the strain in the section

$$e_s' = 0.003 \frac{d'-c}{c} = 0.003 \frac{1.3125 - 1.042}{1.042} = 0.00078$$

$$f_s' = \epsilon_s' E_s = 22,580 \text{ psi} < 60,000 \text{ psi}$$

Solving for forces gives

$$T_s = 26,280 \text{ lbs}$$

$$T_s' = 9,890 \text{ lbs}$$

$$C_c = 36,150 \text{ lbs}$$

Using the calculated forces to obtain the nominal moment capacity of the section.

$$M_n = [(36,150 \text{ lbs})[1.042 - 0.8861(1/2)](\text{in.}) + (26,280 \text{ lbs})(5.6875 - 1.042) (\text{in.}) \\ + 9,890 \text{ lbs}(1.3125 - 1.042)(\text{in.})] (1 \text{ kip}/1000\text{lbs})$$

$$M_n = 160.3 \text{ in-k}$$

$$\phi M_n = 0.9(160.3) = 144.3 \text{ in-k} = 12.0 \text{ ft-k}$$

The gross transformed section moment of inertia can be calculated using the same procedure used in the ASD analysis. For this concrete section, the gross transformed moment of inertia is 546 in^4 . The averaged cracked moment of inertia is 100 in^4 which is obtained using procedures identical to the ASD analysis.

Using the equation for deflection from the ASD section, the deflection downward due to service loads:

$$\Delta_D = 0.0311 \text{ in.}$$

$$\Delta_{LL-H} = 0.9520 \text{ in.}$$

Determine the deflection upward due to resisting moment:

$$\Delta_M = 0.211 \text{ in.}$$

This produces a total deflection of $0.0311 \text{ in.} + 0.9520 \text{ in.} - 0.211 \text{ in.} = 0.772 \text{ in.}$

6.2.2 FRP Reinforcement

6.2.2.1 Allowable Stress Design Method (ASD) – Since corrosion is not a factor with FRP as top reinforcement, the minimum cover shall be assumed to be the same top and bottom. Even though this study used three-eighths diameter; five-eighths FRP will be considered as reinforcement in this example. According to IGI, the allowable tensile stress in their bars can be taken as

$$0.35f_{u,FRP}$$

which for a number five bar is 33.25ksi. For this example, the Kodiak rebar will be specified and the allowable stress will be taken as 24 ksi, the same allowable for steel reinforcement bars. Using this value permits the same amount of reinforcement to be used in the top and bottom of the concrete deck design. Also, it allows for the lower compressive strength of the FRP reinforcement.

The distance from concrete surface to center of the tension and compression reinforcement, d and d' , is 6.6875 and 1.3125 inches, respectively. To control deflection and provide for compressive failure design, the neutral axis will be located between the two mats of

reinforcement. As a starting point, the neutral axis will be lower than in the beams used in this study. The service load is taken as calculated in section 6.2.1.1, M equals 5,760 foot-lbs.

The design constant, k , is assumed to be 0.35. Setting c equal to kd equal to $0.35d$, we get

$$c = 0.35(6.6875 \text{ in.}) = 2.34 \text{ in. .}$$

Solving for the compression in the concrete,

$$\begin{aligned} C_c &= \frac{1}{2}f_cbc \\ &= \frac{1}{2}(1,600 \text{ psi})(12 \text{ in})(2.34 \text{ in}) \\ &= 22,464 \text{ lbs.} \end{aligned}$$

Considering tension reinforcement only, gives us

$$T = A_b f_s = C_c.$$

Substituting in f_s equal to 24,000 psi, we get A_b equals 0.936 square inches. Due to the assumption of the same bar size and equivalent allowable stress in steel and FRP, the area of reinforcement required is the same for both materials. Setting the #5 reinforcement to four inch spacing gives and actual area of reinforcement, A_b , equal to 0.93 square inches. Determine the maximum tension stress as by maximizing the concrete stress to 1,600 psi

$$f_s = \frac{n(1-k)f_c}{k}$$

For FRP, n is 2, which is less than the minimum value, 6, permitted for flexural design. Because the strength of FRP is taken equal to steel, n will be taken as 8 for tension reinforcement. Due to the lower compressive strength of the FRP reinforcement, the calculated n of 2 will be used for

compressive reinforcement. Substituting $k = 0.35$ and $n_{FRP} = 8$, f_s equals 23,771 psi which is less than 24,000 psi.

$$\begin{aligned} T_s &= A_b * f_a \\ &= (0.93 \text{ in}^2)(23,771 \text{ psi}) \\ &= 22,107 \text{ lbs} \end{aligned}$$

which approximately equals the concrete strength. Determining the singly reinforced moment capacity as

$$\begin{aligned} M_u &= T_s(d-kd/3) \\ &= (22,107 \text{ lb})(6.6875-2.34/3)(\text{in})(1 \text{ ft} / 12 \text{ in.}) \\ &= 10,883 \text{ ft-lb} \end{aligned}$$

Maintaining the neutral axis distance, kd equal to 2.34 inches, the stress in the FRP reinforcement can be taken as

$$f_{FRP} = 2nf_c \frac{k - \frac{d'}{d}}{k}$$

Substituting in terms, the stress in FRP reinforcement is 2,811 psi compression. To maintain the same kd more reinforcement is required. Lowering the spacing to 3.5 inches, the area of #5 reinforcement is 1.063 square inches.

The strengths can be taken as

$$\begin{aligned} C_c &= \frac{1}{2} f_c b k d \\ &= \frac{1}{2} (1,600 \text{ psi})(12 \text{ in})(2.34 \text{ in}) \\ &= 22,464 \text{ lbs.} \end{aligned}$$

$$\begin{aligned}
C_{FRP} &= A_{FRP}f_{FRP} \\
&= 1.063\text{in}^2(2,811 \text{ psi}) \\
&= 2,988 \text{ lbs.}
\end{aligned}$$

$$\begin{aligned}
T_s &= A_s f_s \\
&= 1.063 \text{ in}^2(23,771\text{psi}) \\
&= 25,269 \text{ lbs.}
\end{aligned}$$

Check $C_c + C_{FRP} = T_s$

$$22,464 + 2,988 = 25, 269$$

$$25,452 \cong 25,269 \text{ OK.}$$

The moment of inertia calculations follow the same procedure as illustrated in the steel ASD design. The values will be given here:

$$I_{gt} = 571 \text{ in}^4$$

$$I_{cr} = 193 \text{ in}^4 \text{ (positive) and } 93 \text{ in}^4 \text{ (negative) tension only steel.}$$

$$I_{cr} = 213 \text{ in}^4 \text{ (positive) and } 94 \text{ in}^4 \text{ (negative) doubly reinforced.}$$

The average cracked moment of inertia, I_{cr} , is 143 in^4 (tension only) and 153 in^4 (doubly reinforced). The equations for deflections are identical to those previously shown. Substituting these moment of inertia values for those previously used give the deflections shown in Table 6.1 for FRP ASD design.

6.2.2.2 Load Resistance Factor Design Method (LRFD) – The design of FRP reinforced deck will limit reinforcement yield to 60,000 psi as indicated in AASHTO. The value for c will be set equal to 1.3125 inches for the initial attempt. The compression strength of FRP

reinforcement is not as high as the tensile strength of FRP reinforcement. By setting the neutral axis as near as possible to the reinforcement, the added strength due to compression will be minimal and could be ignored.

Determine the compression in concrete as

$$\begin{aligned} C_c &= 0.85(4,000 \text{ psi})(12 \text{ in})(1.3125 \text{ in}) \\ &= 45,516 \text{ lbs.} \end{aligned}$$

Setting reinforcement tension equal to concrete compression and solving for area of reinforcement, gives an area of reinforcement equal to

$$45,415 \text{ lbs.} \div 60,000 \text{ psi} = 0.759 \text{ square inches.}$$

Number five bars at four one-half inches results in an area of reinforcement equal to 0.827 square inches. Working back to obtain the actual neutral axis results in 1.4302 inches that produces a low compression strength contribution which will be ignored.

$$\begin{aligned} T &= 0.827 \text{ in}^2(60,000 \text{ psi}) \\ &= 49,600 \text{ lbs.} \end{aligned}$$

$$\phi M_n = \phi T(d-a/2)$$

For $c = 1.4302 \text{ in.}$,

$$a = \beta_1 c = 0.85(1.4302) = 1.2157 \text{ in.}$$

$$\begin{aligned} \phi M_n &= 0.9(49,600 \text{ lbs.})(6.6875 - 1.2157/2)(\text{in})(1 \text{ ft}/ 12 \text{ in}) \\ &= 22,616 \text{ ft-lb.} \end{aligned}$$

Determine the transformed and cracked moment of inertia is the next step.

	Area in ²	y in.	Ay in ³
Concrete	96	4.0	384
Top	0.827	1.3125	1.0854
Bottom	6.616	6.6875	44.2445
Σ	105.3		429.3299

$$y_t = \frac{\sum Ay}{\sum A} = \frac{429.3299}{103.443} = 4.1504 \text{ in.} \quad \bar{y} = (y - y_t)$$

	A in ²	\bar{y} in	A \bar{y}^2 in ⁴	I _x in ⁴
Concrete	96	0.1504	2.1715	512
Top	0.827	-2.8379	6.6604	--
Bottom	6.616	2.5371	42.5864	--
Σ			51.4183	512

$$I_{gt} = A \bar{y}^2 + I_x \cong 563 \text{ in}^4$$

	Area in ²	y in.	Ay ² in ⁴
Concrete	12c	c/2	6c ²
Top	0.827	c - 1.3125	0.827c - 1.0854
Bottom	6.616	c - 6.6875	6.616c - 44.2445
Σ			6c ² + 7.443 - 45.3299

Solving the quadratic for c yields

$$c = 2.1975 \text{ in.} > 1.3125 \text{ in. as assumed; OK.}$$

Determine the moment of inertia by substituting in the calculated c value from above.

	A in²	\bar{y} in	$A \bar{y}^2$ in⁴	I_x in⁴
Concrete	26.37	1.0937	31.8354	10.6117
Top	0.827	0.885	0.6477	----
Bottom	6.616	-4.49	133.3792	----
Σ			165.8621	

$$I_{cr} = Ay^2 + I_x \cong 176 \text{ in}^4$$

	Area in²	y in.	Ay² in⁴
Concrete	12c	c/2	6c ²
Top	6.616	c - 1.3125	6.616c - 8.6835
Bottom	1.654	c - 6.6875	1.654c - 11.1611
Σ			6c ² + 8.27 - 19.7446

Solving the quadratic for c yields

$$c = 1.2514 \text{ in.} < 1.3125 \text{ in.} \text{ as assumed; OK}$$

Determine the moment of inertia by substituting the calculated c value from above.

	A in²	\bar{y} in	$A \bar{y}^2$ in⁴	I_x in⁴
Concrete	15.02	0.6257	5.8791	1.9597
Top	6.616	-0.0611	0.0247	----
Bottom	1.654	-5.4361	48.8777	----
Σ			54.7815	

$$I_{cr} = Ay^2 + I_x \cong 57 \text{ in}^4$$

Averaging the two cracking moments of inertia, I_{cr} , equals 116 in^4 .

Determine the deflection downward due to service loads by substituting this average value for previous ones:

$$\Delta_D = \frac{5wS^4}{384EI} = \frac{5(145\text{ plf})(7.5\text{ ft})^4 (1,728 \frac{\text{in}^3}{\text{ft}^3})}{384(3,644,000\text{ psi})(116\text{ in}^4)} = 0.0244\text{ in.}$$

$$\Delta_{LL+I} = \frac{PS^3}{48EI} = \frac{20,800\text{ lbs}(7.5\text{ ft} * 12 \frac{\text{in}}{\text{ft}})^3}{48(3,644,000\text{ psi})(116\text{ in}^4)} = 0.7468 \text{ in.}$$

Determine the deflection upward due to resisting moment:

$$\Delta_M = \frac{MS^2}{8EI} = \frac{5,760\text{ ft-lbs}(7.5\text{ ft} * 12 \frac{\text{in}}{\text{ft}})^2}{8(3,644,000\text{ psi})(116\text{ in}^4)} = 0.1655 \text{ in.}$$

This produces a total deflection of 0.0244 in. + 0.7468 in. – 0.1655 in. = 0.6057 in.

6.3 Comparison of Designs

Table 6.1 shows the moment of inertia, deflection, section capacity and applied loads, considering the reinforcement in the deck as either singly reinforced or doubly reinforced. The reinforcement was chosen such that the moment strength of a singly reinforced section was greater than the moments due to the applied loads. The section was then analyzed considering the top reinforcement as contributing to the capacity. In the case of FRP reinforcement and LRFD method, the neutral axis is located such that the top reinforcement does not contribute significantly to the capacity. In the case of FRP and ASD method, more reinforcement was required in a doubly reinforced section to maintain the neutral axis at the same location; this attributes to the different effective moment of inertia and deflections.

Table 6.1 Comparison of Concrete Bridge Design Methods

Material	Method		Bar Spacing	I	Deflections	Capacity	Applied Loads
			Inches	In ⁴	Inches	ft-kips	ft-kips
Steel	ASD	<i>Singly</i>	6.0	130	0.5409	6.31	5.76
		<i>Doubly</i>	--	--	--	6.21	--
	LRFD	<i>Singly</i>	8.5	91	0.772	10.58	9.55
		<i>Doubly</i>	--	--	--	12.00	--
FRP	ASD	<i>Singly</i>	4.0	143	.4917	10.88	5.76
		<i>Doubly</i>	3.5	153	.4596	12.23	--
	LRFD	<i>Singly</i>	4.5	116	.6057	22.62	9.55
		<i>Doubly</i>	--	--	--	--	--

Note that values not entered are the same as for singly reinforced sections.

The spacing of the reinforcement is less in the designs containing FRP reinforcement. The capacity of the FRP deck designs is nearly twice that required for loads. The spacing could probably be increased from these examples. This would lower the capacity some and let the deflections come closer to matching the steel only deck designs.

In the case of ASD design, approximately fifty percent more reinforcement is required. This has the result of an increase in material cost greater than fifty percent due to higher cost of #5 FRP reinforcement over that used in this study. In the case of LRFD design, the increase in material is nearly doubled with the same for cost expected.

CHAPTER 7

CONCLUSIONS AND RECOMMENDATIONS

7.1 CONCLUSIONS

To take advantage of the corrosion resistance of FRP bars, the cover was reduced. This resulted in a lower load capacity due to the closeness of the neutral axis and the top reinforcement. The top reinforcement contribution to strength is minimal. The additional yield stress in the epoxy-coated reinforcement over the non-coated reinforcement provided the majority of the difference in beam capacity. The beam NS capacity would be 12.1 kips also for 64,000 psi reinforcement.

There was a surprise in the results. It was expected that the beams with polypropylene fibers, FC and CC, would deflect less than the beam without any top reinforcement, NS. The beam expected to deflect the least here was CC due to its higher fiber content. At a seminar presented at Virginia Tech, the bond of polypropylene fibers and concrete was weak (Folillard, 1997). This study supports the theory that the bond between the polypropylene fibers and concrete is weak. The beam with carpet fibers deflected more than the beam with the polypropylene fiber from the concrete manufacturer due to the higher percentage of fibers used.

The crack patterns of the beams are similar. When determining the cracking moment of inertia, it was observed that the neutral axis of the beams is nearly the same. The cracked moment of inertia will need to be modified to accurately predict deflections in beams using FRP as reinforcement.

The beam without top reinforcement deflecting less than those containing the FRP bars was somewhat of a surprise. It was believed early on that the FRP reinforcement bars would help with deflection, but it was not believed that the FRP bars additional ductility would increase the deflection in the presence of steel reinforcement. The beams with steel reinforcement only deflected less than the other beams. The beams with FRP reinforcement bars deflect nearly the same with the beam with one kodiak #3 bar deflecting more than the other two beams as expected. The beam, KD, two kodiak #3 bars in the top, was chosen to design the bridge decks in chapter 6 due to its lower cost over the Duradek product of beam, DK and equivalent deflection.

Concrete bridge decks can be designed using this composite material. It does change the current design philosophy, slightly. The location of the neutral axis will require some control due to the different properties associated with the compressive and tensile strength of FRP reinforcement. The design of concrete bridge decks will require additional steel reinforcement when FRP reinforcement is used. This is necessary to control deflections. Using the equivalent size FRP reinforcement and steel reinforcement, #5, is higher cost than those in this study, #3. The material cost for a FRP-steel reinforced concrete bridge deck will be higher than the steel reinforced concrete bridge deck. The labor and shipping cost could possibly lower the cost. The biggest savings may be in the maintenance costs. If the material can reduce the number of maintenance expenditures over the life of the structure, it could offset the higher initial cost and be beneficial. The costs due to traffic control and interruption of service to the public will occur less frequently.

Using ASD and LRFD design procedures, concrete bridge decks utilizing FRP as reinforcement can be designed. The design procedures are not that much different than when steel reinforcement is used. The control of deflection is a major concern. There are some additional questions of bond strength, different compression and tension properties, material property uniformity from different manufacturers, and testing procedures and standards. Continue research and improvements will be needed to make FRP reinforcement a more desirable product.

The prediction of the permanent set in beams was not accurate. The previous loads' effective moment of inertia did not estimate the true deflection. There were some problems with the LVDT not working and beams not being level. The work should be repeated with improvements to setup and testing procedures.

The cost analysis for the beams in this study shows that the cost of FRP reinforcement material is approaching the cost of steel reinforcement. When the amount of material used for the design of concrete bridge decks is examined, the costs get further away. The extra material to offset the deflections increases costs. The initial higher cost over the future maintenance costs will need additional study.

7.2 RECOMMENDATIONS

The recommendations are separated into general recommendations and specific recommendations. The general recommendations are for FRP development, testing, and use. The specific area is meant as an outline of work that could be done to eventually provide design specifications and criteria.

7.2.1 General Recommendations

There is a need to improve the mechanical and chemical properties of FRP so their reactions can be predictable in a structure. ASTM needs to provide standard material properties testing methods. Research must continue to provide greater information in the transfer of forces in the fiber reinforced plastic concrete so that there is uniformity and predictability in the outcome. There needs to be an increase of the acceleration tests to determine the long term durability of the material. Design criterion needs to be implemented and tested to provide a future for this material.

A main area of expected use is in bridge decks. Because deflection is a major concern here, it would probably benefit FRP reinforcement development to provide FRP reinforcement in areas where deflection is not much of a concern. Concrete foundations would be one such area. There is contact with soil, deicing chemicals accumulate in the area, and deflection is less critical. Another location where additional information would be provided is using FRP in curbs, which is a gathering spot for road salt. Besides the benefit of testing the FRP reactions at such a hostile location, there is the ease at which the work could be redone in case something happens to the

curbing. A side benefit of increase field use of the FRP material would be an increase in production, quality testing, and companies producing FRP as reinforcement. With a large demand, procedures would become standardized quicker and cost would probably be lower.

7.2.2 Specific Recommendations

It is recommended that additional manufacturers of FRP bars be evaluated by testing the material properties. It is desirable to determine the bars' properties from the production inventory. The FRP bars should be evaluated to determine the bond strength with concrete, the modulus of elasticity, the yield strength, the ultimate strength. The testing program should narrow the available types to one (or two at most) individual brand of FRP reinforcing that can be cost competitive with reinforcing steel and be further tested.

After determining the best bar to use, test several concrete beams with the FRP. Some beams should have FRP bars as the top and bottom reinforcement. Some beams should have the FRP bars as the top reinforcement and steel reinforcing bars as the bottom reinforcement. The steel reinforcement should be of the type currently used, epoxy-coated and non-coated. The concrete should meet current design specifications and some specimens should have a low permeability. The beams should be tested as simply supported for positive and negative load using strain gauges on the reinforcement. Tests should include monotonic loading and cyclic loading. The test should determine the yield strength, the ultimate strength, deflections, cracking patterns, and failure load. From these tests, determine design equations which work from existing

equations currently used, equations developed by others and develop new formulas, where needed.

The next phase of testing should be to test beam samples that have been made composite with girders with fixed supports to determine actions in this manner. This would be a worse case analysis with the assumption that the bridge girders behaved as fixed supports.

Measure the strains in the reinforcement, steel and FRP, and concrete using strain gauges attached to the reinforcement and top of concrete at midspan and bottom of concrete near the supports. Tests should include monotonic loading and cyclic loading. The test should determine the yield strength, the ultimate strength, deflections, cracking patterns, and failure load. From these tests, determine the design equations which work from the existing design equations currently in use, the equations developed by others and develop new formulas, where needed. Also, previous equations can be verified and modified as needed.

Using available formulas and those derived for FRP as reinforcement, a small test floor should be designed and tested with loads to simulate truck loading on a bridge deck. Apply strain gauges to top of concrete slab. Tests should also include monotonic loading and cyclic loading. The test should determine the yield strength, the ultimate strength, deflections, cracking patterns, and failure load. From these tests, verify design equations that were used to design the slab. Modify the equations as needed, repeat until predicted results parallel actual results

Finally, an actual bridge should be built with gauges for monitoring and evaluating the structures' behavior. The bridge should be tested non-destructively before actual being placed in operation. The deflections and structures reactions should be evaluated to compare with the theoretical and actual values. Once traffic is placed on the structure, the bridge should be

monitored and evaluated. Afterwards, design procedures and formulas can be developed which will make bridges conform to an acceptable standard.

REFERENCES:

ACI Building Code Requirements for Reinforced Concrete, ACI 318-95 (1995),

American Concrete Institute, Detroit, MI.

ACI State-of-the-Art Report on Fiber Reinforced Plastic Reinforcement for Concrete Structures,

(1996), ACI Committee 440, American Concrete Institute, Detroit, MI.

AASHTO Standard Specifications for Highway Bridges, 14th edition, (1989), American

Association of State Highway and Transportation Officials, Washington, DC.

AASHTO LRFD Bridge Design Specifications, (1994), American Association of State Highway

and Transportation Officials, Washington, DC.

AISC Manual of Steel Construction, (1994), American Institute of Steel Construction, Chicago,

Ill.

Ahmad, Hasan and Dimitris C. Lagoudas, (1991), "Effective Elastic Properties of Fiber-Reinforced Concrete with Random Fibers," *Journal of Engineering Mechanics*, Vol. 117, No. 12,

pp. 2931-2938.

Allen, Peter, (1995), *Study of Fiberglass-Reinforced Plastic for Reinforcing Concrete Bridge Decks*, Thesis, Virginia Polytechnic Institute and State University, Blacksburg, VA.

ASTM D3916, “Standard Test Method for Tensile Properties of Pultruded Glass-Fiber-Reinforced Plastic Rod”.

ASTM A370, “Standard Test Methods and Definitions for Mechanical Testing of Steel Products”.

Bank, L.C. and A.S. Mossallam (1991), “Experimental Study of FRP Grating Reinforced Concrete Slabs,” *Advanced Composite Materials in Civil Engineering Structures*, ASCE, pp. 111-122.

Bank, L.C., Z. Xi, and E. Munley, (1992), “Tests of Full-Size Pultruded FRP Grating Reinforced Concrete Bridge Decks,” *Proceedings of the Materials Engineering Congress*, ASCE, pp. 618-631.

Bank, Lawrence C. and T. Russell Gentry, (1995). “Accelerated Test Methods to Determine the Long-Term Behavior of FRP Composite Structures: Environmental Effects”, *Journal of Reinforced Plastics and Composites*, Vol.14, No. 6, pp. 559-587.

Bedard, Claude, (1992). "Composite Reinforcing Bars: Assessing their use in Construction", *Concrete International: Design and Construction*, Vol. 14 No. 1, pp. 55-59.

Brown, Vicki L. and Charles L. Bartholomew, (1993). "FRP Reinforcing Bars in Reinforced Concrete Members," *ACI Materials Journal (American Concrete Institute)*, Vol. 90, No. 1, pp. 34-39.

"Deck Built Minus Top Steel," (1994), *Engineering News Record*, Vol. 232, No. 25, pp.18.

Erki, M.A. and S.H. Rizkalla, (1993). "Anchorages for FRP", *Concrete International: Design and Construction*, Vol. 15, No. 6, pp. 54-59.

Erki, M.A. and S.H. Rizkalla, (1993). "FRP Reinforcement for Concrete Structures", *Concrete International: Design and Construction*, Vol. 15, No. 6, pp. 48-53.

Everard, N.J., (1993), *Reinforced Concrete Design, 3rd edition, Schaum's Outline Series*, McGraw-Hill Inc., New York, NY.

EXTREN Design Manual, (1989), Morrison Molded Fiberglass Company, Bristol, VA.

Folillard, K., (1997), Seminar at Virginia Tech, W. R. Grace, Co.

GangaRao, H.V.S. and S.S. Faza (1991), "Bending and Bond Behavior and Design of Concrete Beams Reinforced with Fiber Reinforced Plastic Rebars," West Virginia University, Constructed Facilities Center.

Kodiak-Fiberglass-Reinforced Plastic Rebar, (1988), International Grating, Inc., Houston, TX.

Khalifa, Maghi A., Kuska, Sharon S. B., and Krieger, James, (1993). "Bridges Constructed Using Fiber Reinforced Plastics", *Concrete International: Design and Construction*, 15(6), 43-47.

Lamontagne, Ann and Michel Pigeon, (1995), "The Influence of Polypropylene Fibers and Aggregate Grading on the Properties of Dry-Mix Shotcrete," *Cement and Cement Research*, Vol. 25, No. 2, pp. 293-298.

Nanni, Antonio, (1993). "Flexural Behavior and Design of RC Members using FRP Reinforcement", *Journal of Structural Engineering*, 119(11), 3344-3359.

Nanni, A., Bakis, C.E., and Boothby, T.E., (1995). "Test Methods for FRP-Concrete Systems Subjected to Mechanical Loads: State of the Art Review", *Journal of Reinforced Plastics and Composites*, 14(6), 524-557.

Plevris, Nikolaos and Triantafillou, Thanasis C.,(1992). “Time-Dependent Behavior of RC Members Strengthened with FRP Laminates”, *Journal of Structural Engineering* 120(3), 1016-1042.

Saadatmanesh, H., (1994). “Fiber Composites for New and Existing Structures”, *ACI Structural Journal*, 91(3), 346-354.

Saadatmanesh, Hamid and Ehsani, Mohammad R., (1991). “RC Beams Strengthened with GFRP Plates. Experimental Study.”, *Journal of Structural Engineering*, 117(11), 3417-3433.

Soroushian, P., A. Khan, and J. Hsu, (1992), “Mechanical Properties of Concrete Materials Reinforced with Polypropylene or Polyethylene Fibers.”, *ACI Materials Journal* (American Concrete Institute), Vol. 89, No. 6, pp. 535-540.

Sotiropoulos, Sotiris N., H.V.S. GangaRao, and A.N.K. Mongi, (1994), “Theoretical and Experimental Evaluation of FRP Components and Systems”, *Journal of Structural Engineering*, Vol. 120, No. 2, pp. 464-485

Wei, An, Saadatmanesh, Hamid and Ehsani, Mohammad R., (1991), “RC Beams Strengthened with FRP Plates. II. "Analysis and Parametric study”, *Journal of Structural Engineering*, 117(11), 3434-3455.

APPENDICES

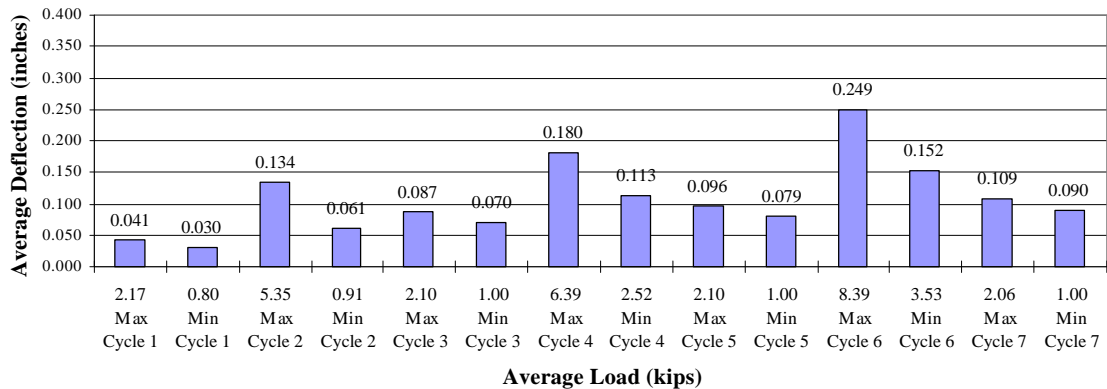
RECORDED LOAD-DEFLECTIONS

A.1 BEAM TD1

Recorded Loads and Deflections

	Load Kips	Near	Center	Far	True	Record
		Deflection inches	Deflection inches	Deflection inches	Deflection inches	
Max	2.1671	0.0294	0.0704	0.0289	0.0413	1
Min	0.8046	0.0156	0.0469	0.0183	0.0300	1
Max	5.3546	0.0597	0.1914	0.0561	0.1335	2
Min	0.9125	0.0240	0.0855	0.0253	0.0609	2
Max	2.1046	0.0381	0.1242	0.0368	0.0868	3
Min	1.0015	0.0251	0.0967	0.0276	0.0704	3
Max	6.3890	0.0747	0.2525	0.0695	0.1804	4
Min	2.5234	0.0433	0.1564	0.0445	0.1125	4
Max	2.1000	0.0406	0.1370	0.0405	0.0965	5
Min	0.9984	0.0278	0.1083	0.0311	0.0789	5
Max	8.3921	0.0949	0.3406	0.0889	0.2487	6
Min	3.5265	0.0579	0.2105	0.0583	0.1524	6
Max	2.0640	0.0428	0.1521	0.0440	0.1087	7
Min	0.9953	0.0304	0.1227	0.0347	0.0902	7

TD1 Average Load-Deflections at Various Cycles



A.2 BEAM TD2

TD2		Near	Center	Far	True	
	Load	Deflection	Deflection	Deflection	Deflection	Record
	Kips	inches	inches	inches	inches	
Max	0.0218	0.0015	0.0075	0.0103	0.0016	1
Min	-0.0812	-0.0015	-0.0078	-0.0040	-0.0051	1
Max	2.4156	0.0248	0.0883	0.0327	0.0596	2
Min	0.6843	0.0080	0.0080	0.0073	0.0004	2
Max	5.9984	0.0496	0.1831	0.1009	0.1079	3
Min	1.2484	0.0109	0.0624	0.0624	0.0258	3
Max	11.2530	0.1133	0.6209	0.1002	0.5142	4
Min	0.0406	-0.1506	-1.4953	-1.3861	-0.7270	4

Overloaded to Failure

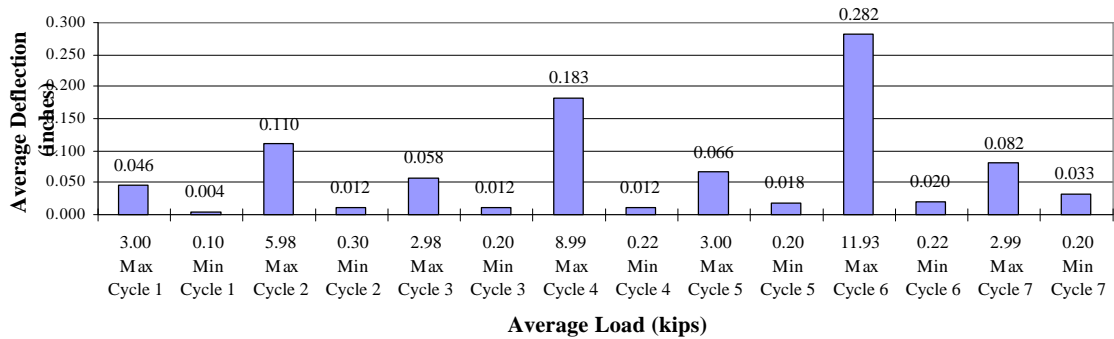
Data not used in any calculations or report due to beam failure

A.3 BEAM TD3

Recorded Loads and Deflections

TD3		Near	Center	Far	True	
	Load	Deflection	Deflection	Deflection	Deflection	Record
	Kips	inches	inches	inches	inches	
Max	2.9984	0.0352	0.0876	0.0488	0.0456	1
Min	0.0984	0.0037	0.0152	0.0179	0.0044	1
Max	5.9824	0.0570	0.1749	0.0723	0.1103	2
Min	0.2984	0.0117	0.0300	0.0252	0.0116	2
Max	2.9843	0.0382	0.1039	0.0541	0.0578	3
Min	0.1953	0.0100	0.0285	0.0236	0.0117	3
Max	8.9937	0.0762	0.2693	0.0964	0.1830	4
Min	0.2203	0.0110	0.0311	0.0273	0.0120	4
Max	2.9968	0.0395	0.1159	0.0596	0.0664	5
Min	0.1984	0.0105	0.0375	0.0287	0.0179	5
Max	11.9310	0.0981	0.3920	0.1218	0.2821	6
Min	0.2218	0.0320	0.0519	0.0322	0.0198	6
Max	2.9859	0.0422	0.1356	0.0653	0.0819	7
Min	0.1984	0.0120	0.0555	0.0335	0.0328	7

TD3 Average Load-Deflections at Various Cycles



A.4 BEAM KS1

KS1	Near	Center	Far	True		
Load	Deflectio	Deflectio	Deflectio	Deflectio	Recor	
	n	n	n	n	d	
Kips	inches	inches	inches	inches		
Ma x	2.9921	0.0265	0.0617	0.0319	0.0325	1
Min	0.1890	0.0045	0.0200	0.0081	0.0137	1
Ma x	5.8156	0.0499	0.1891	0.0543	0.1370	2
Min	0.3015	0.0106	0.0616	0.0151	0.0488	2
Ma x	Values for Record ? included in 3.				0.0000	?
Min				0.0000		?
Ma x	9.0390	0.0741	0.3066	0.0788	0.2302	3
Min	1.4984	0.0245	0.1182	0.0333	0.0893	3
Ma x	2.9921	0.0354	0.1527	0.0421	0.1140	4
Min	0.2796	0.0107	0.0800	0.0190	0.0652	4
Ma x	12.046	0.1004	0.4883	0.0969	0.3897	5
Min	2.7828	0.0440	0.2234	0.0470	0.1779	5
Ma x	2.0250	0.0361	0.1961	0.0413	0.1574	6
Min	0.0978	0.0255	0.1675	0.0328	0.1384	6

Note: After Inspection of data, it cannot be separated reliably, thus data will be ignored.

The recording was not performed in a consistent pattern and was short cycled where it is difficult to determine anything to be useful.

Note: After inspection of data, it cannot be separated reliably; thus data will be ignored. The recording of data was not performed in a consistent pattern and was short cycled. It is difficult to determine anything that can be useful.

A.5 BEAM KS2

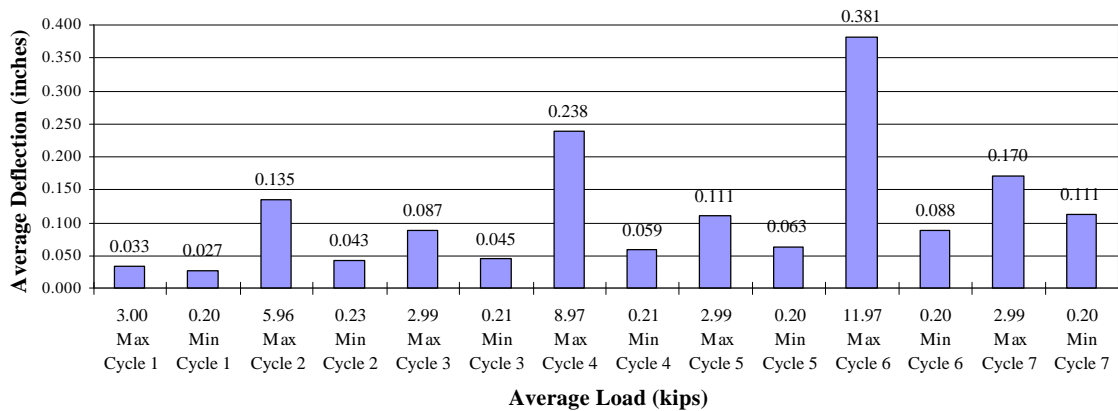
Recorded Loads and Deflections

KS2	Near Load	Center Deflecti on	Far Deflecti on	True Deflecti on	Reco rd	
Max	-	-2.2495	-2.2855	-2.2505	-0.0355	1
	51.200					0
Min	51.198	2.2495	2.2855	2.2504	0.0355	1
						0
Max	2.9796	0.0981	0.9400	0.0445	0.8687	2
Min	0.1953	0.4900	0.0345	0.0068	-0.2139	2
Max	-	-2.2495	-2.2855	-2.2505	-0.0355	3
	51.200					0
Min	51.198	2.2495	2.2855	2.2504	0.0355	3
						0
Max	2.9968	0.0433	0.0666	0.0243	0.0328	4
Min	0.1953	-0.0221	0.0102	-0.0105	0.0265	4
Max	5.9593	0.0809	0.2026	0.0535	0.1354	5
Min	0.2265	0.0155	0.0486	-0.0044	0.0431	5
Max	2.9921	0.0543	0.1325	0.0358	0.0875	6
Min	0.2078	0.0152	0.0517	-0.0021	0.0452	6
Max	8.9718	0.1107	0.3349	0.0833	0.2379	7
Min	0.2140	0.0236	0.0735	0.0057	0.0589	7
Max	2.9921	0.0614	0.1680	0.0532	0.1107	8
Min	0.1984	0.0243	0.0793	0.0083	0.0630	8
Max	11.973	0.1482	0.5142	0.1184	0.3809	9
						0
Min	0.1968	0.0432	0.1238	0.0278	0.0883	9
Max	2.9890	0.0759	0.2400	0.0641	0.1700	10
Min	0.1953	0.0378	0.1448	0.0291	0.1114	10

Beam Not Square.

First 3 Records used to balance deflections

KS2 Average Load-Deflections at Various Cycles

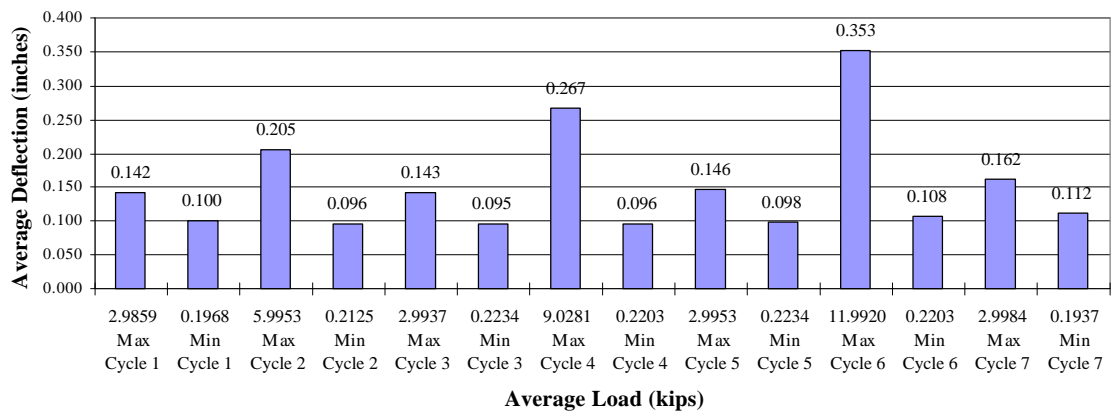


A.6 BEAM KD1

Recorded Loads and Deflections

KD1		Near	Center	Far	True	
	Load	Deflection	Deflection	Deflection	Deflection	Record
	Kips	inches	inches	inches	inches	
Max	2.9859	0.0566	0.1968	0.0532	0.1419	1
Min	0.1968	0.0232	0.1196	0.0159	0.1001	1
Max	5.9953	0.0828	0.2836	0.0754	0.2045	2
Min	0.2125	0.0240	0.1211	0.0267	0.0958	2
Max	2.9937	0.0582	0.2007	0.0574	0.1429	3
Min	0.2234	0.0236	0.1208	0.0271	0.0955	3
Max	9.0281	0.1072	0.3700	0.0980	0.2674	4
Min	0.2203	0.0251	0.1232	0.0299	0.0957	4
Max	2.9953	0.0597	0.2066	0.0621	0.1457	5
Min	0.2234	0.0252	0.1265	0.0320	0.0979	5
Max	11.9920	0.1223	0.4738	0.1198	0.3528	6
Min	0.2203	0.0170	0.1343	0.0360	0.1078	6
Max	2.9984	0.0497	0.2202	0.0671	0.1618	7
Min	0.1937	0.0146	0.1377	0.0364	0.1122	7

KD1 Average Load-Deflections at Various Cycles

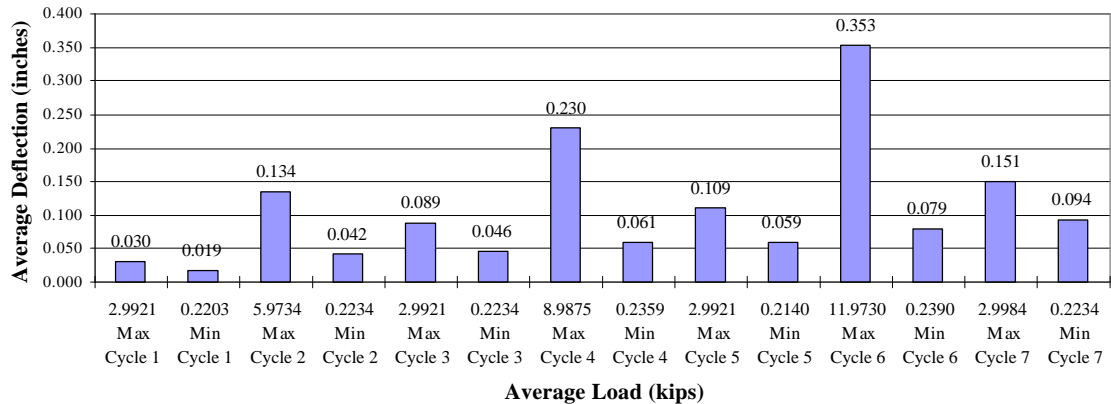


A.7 BEAM KD2

Recorded Loads and Deflections

KD2		Near	Center	Far	True	
	Load	Deflection	Deflection	Deflection	Deflection	Record
	Kips	inches	inches	inches	inches	
Max	2.9921	0.0375	0.0697	0.0416	0.0302	1
Min	0.2203	0.0044	0.0261	0.0105	0.0187	1
Max	5.9734	0.0715	0.2031	0.0671	0.1338	2
Min	0.2234	0.0247	0.0681	0.0267	0.0424	2
Max	2.9921	0.0471	0.1385	0.0518	0.0891	3
Min	0.2234	0.0244	0.0727	0.0296	0.0457	3
Max	8.9875	0.0893	0.3222	0.0949	0.2301	4
Min	0.2359	0.0276	0.0917	0.0346	0.0606	4
Max	2.9921	0.0520	0.1683	0.0657	0.1095	5
Min	0.2140	0.0278	0.0941	0.0430	0.0587	5
Max	11.9730	0.1180	0.4717	0.1192	0.3531	6
Min	0.2390	0.0319	0.1202	0.0499	0.0793	6
Max	2.9984	0.0580	0.2169	0.0738	0.1510	7
Min	0.2234	0.0338	0.1365	0.0518	0.0937	7

KD2 Average Load-Deflections at Various Cycles

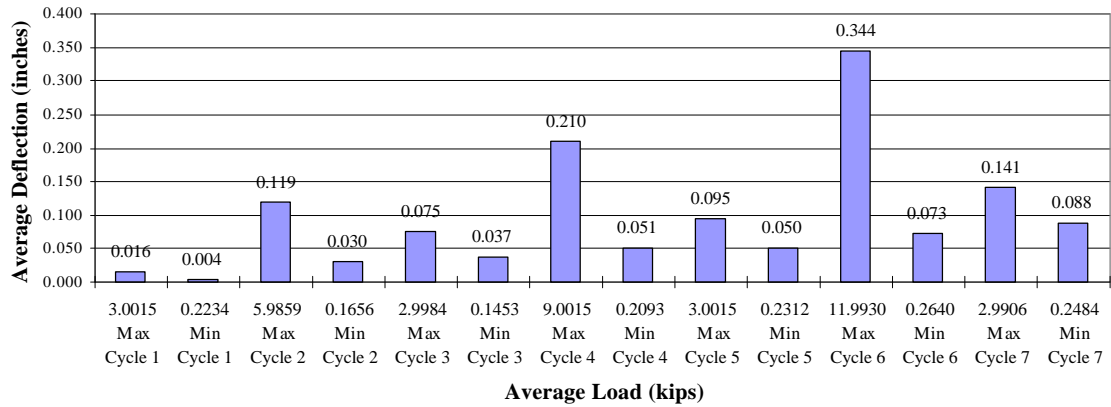


A.8 BEAM DK1

Recorded Loads and Deflections

DK1		Near	Center	Far	True	Record
	Load	Deflection	Deflection	Deflection	Deflection	
	Kips	inches	inches	inches	inches	
Max	3.0015	0.0271	0.0461	0.0323	0.0164	1
Min	0.2234	0.0021	0.0090	0.0074	0.0043	1
Max	5.9859	0.0592	0.1825	0.0677	0.1191	2
Min	0.1656	0.0083	0.0416	0.0150	0.0300	2
Max	2.9984	0.0380	0.1155	0.0432	0.0749	3
Min	0.1453	0.0159	0.0553	0.0208	0.0370	3
Max	9.0015	0.0812	0.2926	0.0848	0.2096	4
Min	0.2093	0.0241	0.0779	0.0304	0.0507	4
Max	3.0015	0.0506	0.1481	0.0558	0.0949	5
Min	0.2312	0.0302	0.0820	0.0342	0.0498	5
Max	11.9930	0.1073	0.4538	0.1124	0.3440	6
Min	0.2640	0.0370	0.1120	0.0405	0.0733	6
Max	2.9906	0.0614	0.2042	0.0658	0.1406	7
Min	0.2484	0.0413	0.1310	0.0440	0.0884	7

DK1 Average Load-Deflections at Various Cycles

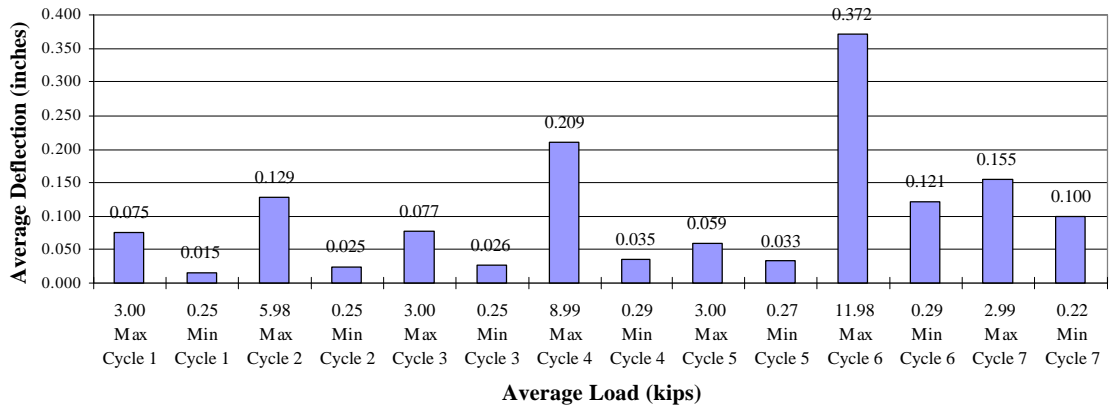


A.9 BEAM DK2

Recorded Loads and Deflections

DK2		Near	Center	Far	True	
	Load	Deflection	Deflection	Deflection	Deflection	Record
	Kips	inches	inches	inches	inches	
Max	2.9984	0.0100	0.0980	0.0353	0.0754	1
Min	0.2500	0.0083	0.0235	0.0086	0.0151	1
Max	5.9765	0.0671	0.1901	0.0558	0.1287	2
Min	0.2515	0.0133	0.0376	0.0124	0.0248	2
Max	2.9953	0.0463	0.1182	0.0364	0.0769	3
Min	0.2484	0.0163	0.0400	0.0120	0.0259	3
Max	8.9890	0.1281	0.3146	0.0831	0.2090	4
Min	0.2921	0.0333	0.0618	0.0195	0.0354	4
Max	3.0046	0.1315	0.1483	0.0478	0.0587	5
Min	0.2703	0.0424	0.0664	0.0248	0.0328	5
Max	11.9820	0.1567	0.5061	0.1122	0.3717	6
Min	0.2937	0.0661	0.1720	0.0352	0.1214	6
Max	2.9890	0.1063	0.2377	0.0592	0.1550	7
Min	0.2218	0.0586	0.1468	0.0360	0.0995	7

DK2 Average Load-Deflections at Various Cycles

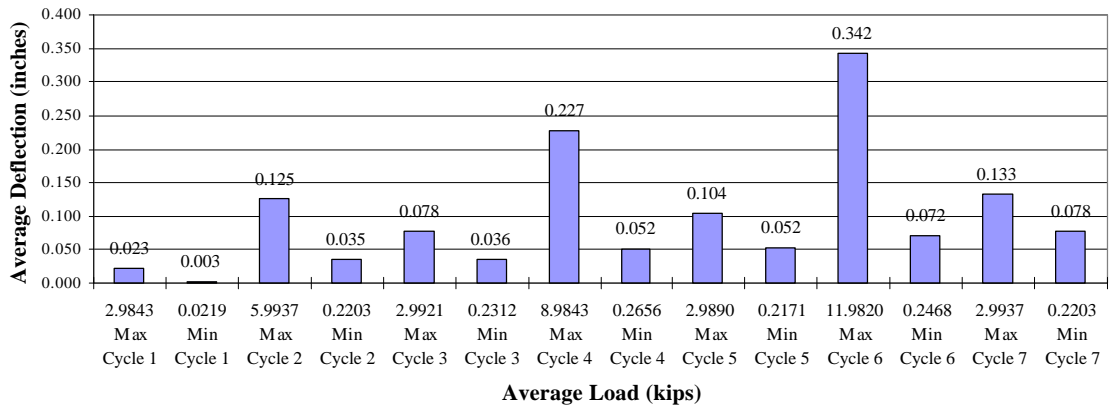


A.10 BEAM NS1

Recorded Loads and Deflections

NS1		Near	Center	Far	True	Record
	Load	Deflection	Deflection	Deflection	Deflection	
	Kips	inches	inches	inches	inches	
Max	2.9843	0.0300	0.0504	0.0252	0.0228	1
Min	0.0219	0.0049	0.0084	0.0056	0.0032	1
Max	5.9937	0.0652	0.1819	0.0484	0.1251	2
Min	0.2203	0.0141	0.0481	0.0116	0.0353	2
Max	2.9921	0.0443	0.1165	0.0326	0.0781	3
Min	0.2312	0.0192	0.0525	0.0131	0.0364	3
Max	8.9843	0.0994	0.3145	0.0753	0.2272	4
Min	0.2656	0.0330	0.0776	0.0186	0.0518	4
Max	2.9890	0.0597	0.1547	0.0421	0.1038	5
Min	0.2171	0.0361	0.0801	0.0197	0.0522	5
Max	11.9820	0.1322	0.4587	0.1013	0.3420	6
Min	0.2468	0.0419	0.1054	0.0256	0.0717	6
Max	2.9937	0.0627	0.1900	0.0511	0.1331	7
Min	0.2203	0.0427	0.1132	0.0276	0.0781	7

NS1 Average Load-Deflections at Various Cycles

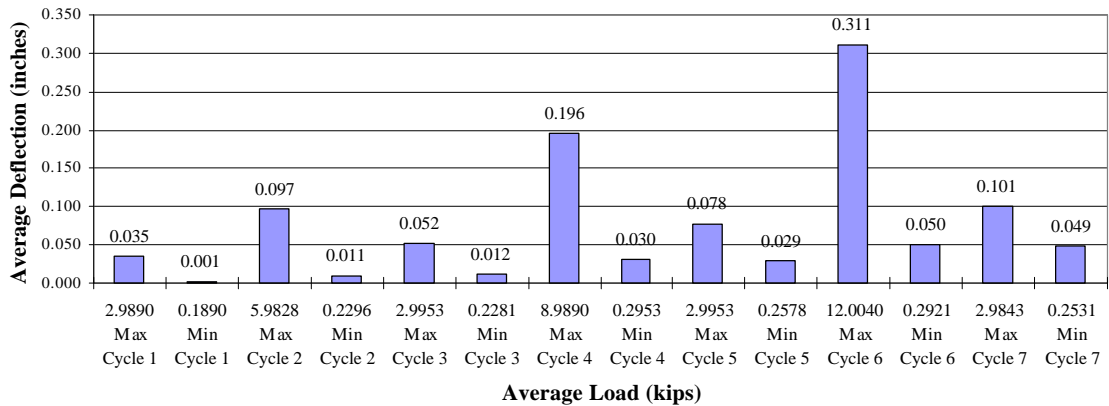


A.11 BEAM NS2

Recorded Loads and Deflections

NS2	Load	Near	Center	Far	True	Record
	Kips	Deflection inches	Deflection inches	Deflection inches	Deflection inches	
Max	2.9890	0.0188	0.0559	0.0232	0.0349	1
Min	0.1890	0.0030	0.0049	0.0040	0.0014	1
Max	5.9828	0.0359	0.1369	0.0431	0.0974	2
Min	0.2296	0.0063	0.0177	0.0081	0.0105	2
Max	2.9953	0.0218	0.0783	0.0300	0.0524	3
Min	0.2281	0.0061	0.0197	0.0101	0.0116	3
Max	8.9890	0.0532	0.2557	0.0657	0.1963	4
Min	0.2953	0.0070	0.0412	0.0146	0.0304	4
Max	2.9953	0.0245	0.1089	0.0374	0.0780	5
Min	0.2578	0.0078	0.0405	0.0157	0.0288	5
Max	12.0040	0.0832	0.3944	0.0833	0.3112	6
Min	0.2921	0.0192	0.0677	0.0162	0.0500	6
Max	2.9843	0.0365	0.1369	0.0360	0.1007	7
Min	0.2531	0.0199	0.0661	0.0152	0.0486	7

NS2 Average Load-Deflections at Various Cycles

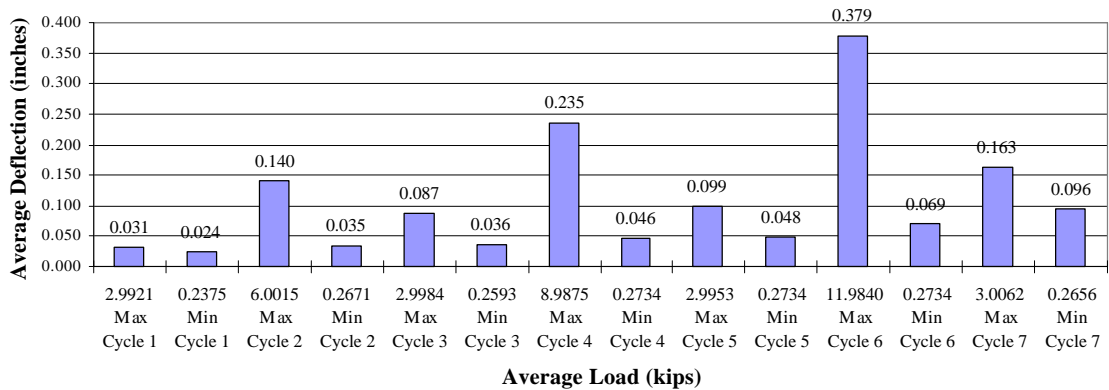


A.12 BEAM FC1

Recorded Loads and Deflections

FC1	Load	Near	Center	Far	True	Record
	Kips	Deflection inches	Deflection inches	Deflection inches	Deflection inches	
Max	2.9921	0.0256	0.0577	0.0286	0.0306	1
Min	0.2375	0.0102	0.0286	0.0000	0.0235	1
Max	6.0015	0.0477	0.2003	0.0722	0.1404	2
Min	0.2671	0.0151	0.0486	0.0129	0.0346	2
Max	2.9984	0.0343	0.1284	0.0486	0.0870	3
Min	0.2593	0.0159	0.0532	0.0191	0.0357	3
Max	8.9875	0.0836	0.3290	0.1054	0.2345	4
Min	0.2734	0.0245	0.0712	0.0254	0.0463	4
Max	2.9953	0.0613	0.1595	0.0596	0.0991	5
Min	0.2734	0.0267	0.0754	0.0291	0.0475	5
Max	11.9840	0.1091	0.5015	0.1359	0.3790	6
Min	0.2734	0.0372	0.1069	0.0382	0.0692	6
Max	3.0062	0.0554	0.2262	0.0715	0.1628	7
Min	0.2656	0.0338	0.1337	0.0424	0.0956	7

FC1 Average Load-Deflections at Various Cycles

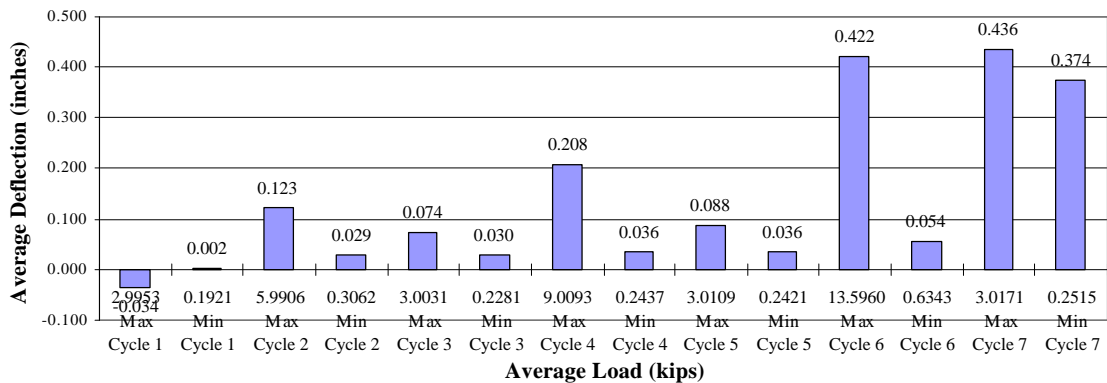


A.13 BEAM FC2

Recorded Loads and Deflections

FC2		Near	Center	Far	True	Record	<i>Adjusting of LDVT</i>
	Load	Deflection	Deflection	Deflection	Deflection		
	Kips	inches	inches	inches	inches		
Max	-51.2000	-2.2495	-2.2855	-2.2505	-0.0355	1	
Min	51.1980	2.2494	2.2855	2.2504	0.0356	1	
Max	2.9953	0.1200	0.0362	0.0208	-0.0342	2	
Min	0.1921	0.0002	0.0038	0.0044	0.0015	2	
Max	5.9906	0.0394	0.1637	0.0416	0.1232	3	
Min	0.3062	0.0061	0.0369	0.0092	0.0293	3	
Max	3.0031	0.0234	0.0991	0.0274	0.0737	4	
Min	0.2281	0.0074	0.0378	0.0090	0.0296	4	
Max	9.0093	0.0661	0.2730	0.0635	0.2082	5	
Min	0.2437	0.0121	0.0491	0.0144	0.0359	5	
Max	3.0109	0.0326	0.1212	0.0337	0.0881	6	
Min	0.2421	0.0146	0.0507	0.0155	0.0357	6	
Max	13.5960	0.1081	0.5277	0.1039	0.4217	7	
Min	0.6343	0.0228	0.0786	0.0258	0.0543	7	
Max	3.0171	0.0707	0.5021	0.0622	0.4357	8	
Min	0.2515	0.0526	0.4206	0.0404	0.3741	8	

FC2 Average Load-Deflections at Various Cycles

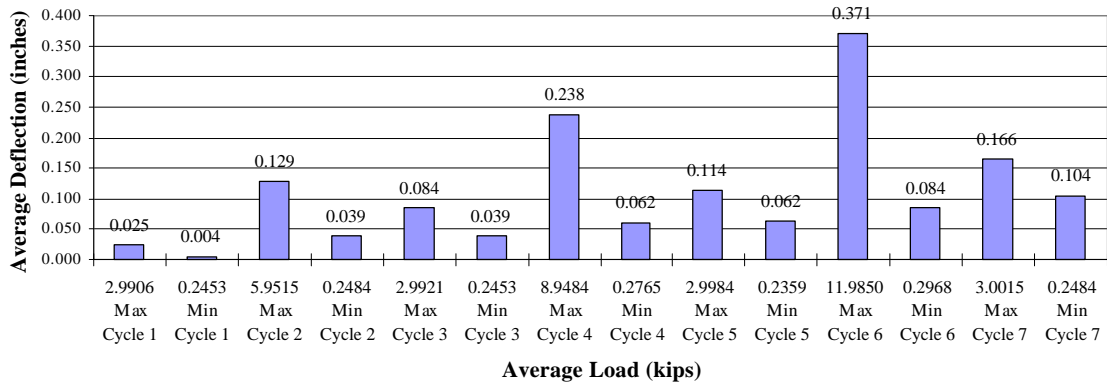


A.14 BEAM CC1

Recorded Loads and Deflections

CC1		Near	Center	Far	True	
	Load	Deflection	Deflection	Deflection	Deflection	Record
	Kips	inches	inches	inches	inches	
Max	2.9906	0.0201	0.0491	0.0273	0.0254	1
Min	0.2453	0.0050	0.0091	0.0059	0.0037	1
Max	5.9515	0.0394	0.1750	0.0535	0.1286	2
Min	0.2484	0.0107	0.0514	0.0144	0.0389	2
Max	2.9921	0.0279	0.1174	0.0392	0.0839	3
Min	0.2453	0.0124	0.0537	0.0169	0.0391	3
Max	8.9484	0.0512	0.3026	0.0774	0.2383	4
Min	0.2765	0.0075	0.0765	0.0221	0.0617	4
Max	2.9984	0.0249	0.1505	0.0473	0.1144	5
Min	0.2359	0.0085	0.0781	0.0237	0.0620	5
Max	11.9850	0.0770	0.4600	0.1001	0.3715	6
Min	0.2968	0.0166	0.1080	0.0309	0.0843	6
Max	3.0015	0.0360	0.2109	0.0548	0.1655	7
Min	0.2484	0.0199	0.1299	0.0312	0.1044	7

CC1 Average Load-Deflections at Various Cycles

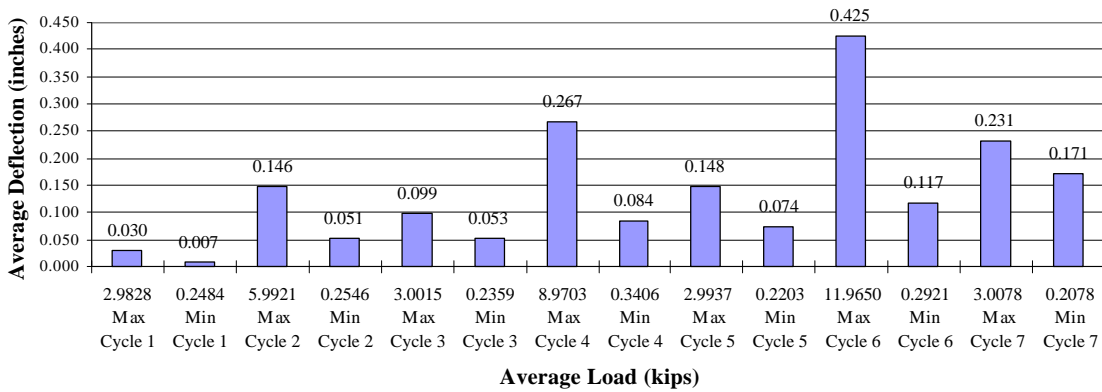


A.15 BEAM CC2

Recorded Loads and Deflections

CC2	Load	Near	Center	Far	True	Record
	Kips	Deflection	Deflection	Deflection	Deflection	
		inches	inches	inches	inches	
Max	2.9828	0.0221	0.0534	0.0243	0.0302	1
Min	0.2484	0.0063	0.0124	0.0043	0.0071	1
Max	5.9921	0.0534	0.1941	0.0427	0.1461	2
Min	0.2546	0.0157	0.0601	0.0021	0.0512	2
Max	3.0015	0.0370	0.1296	0.0236	0.0993	3
Min	0.2359	0.0199	0.0643	0.0024	0.0532	3
Max	8.9703	0.0775	0.3249	0.0392	0.2666	4
Min	0.3406	0.0260	0.0885	-0.0168	0.0839	4
Max	2.9937	0.0427	0.1711	0.0036	0.1480	5
Min	0.2203	0.0267	0.0963	0.0183	0.0738	5
Max	11.9650	0.0981	0.5107	0.0736	0.4249	6
Min	0.2921	0.0300	0.1263	-0.0122	0.1174	6
Max	3.0078	0.0457	0.2616	0.0160	0.2308	7
Min	0.2078	0.0323	0.1826	-0.0087	0.1708	7

CC2 Average Load-Deflections at Various Cycles



VITA

Curtis Barton Boyd, son of Curtis G. and Christine Boyd, was born on January 8, 1959, in Martinsville, Virginia. He grew up in Henry and Patrick Counties, graduating from John D. Bassett High School, Bassett, Virginia, in 1977. He graduated from Virginia Polytechnic Institute and State University, Blacksburg, Virginia, in 1982 with a Bachelor of Science in Civil Engineering. After working for five years as a general contractor, he was hired by the Virginia Department of Transportation (VDOT) as a Transportation Engineer in the Richmond District Structure and Bridge Office. After eight years with VDOT, he took a leave of absence and enrolled in the Structures Division of the Via Department of Civil Engineering at Virginia Polytechnic Institute and State University. He returned to the Richmond District Structure and Bridge Office of VDOT and graduated with a Master of Science in Civil Engineering in 1997.